PREPARATION AND CHARACTERISTICS OF ALUMINAS

by

KIM-OANH THI NGUYEN

B.S., Kansas State University, 1981

A MASTER'S THESIS

submitted in partial fulfillment of the
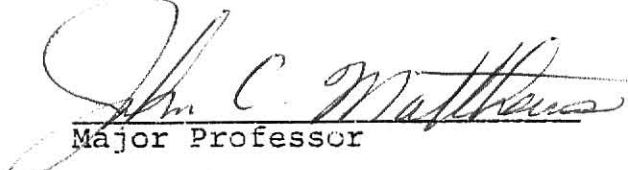
requirements for the degree

MASTER OF SCIENCE

Department of Chemical Engineering

KANSAS STATE UNIVERSITY
Manhattan, Kansas

1983

Approved by

Major Professor

TABLE OF CONTENTS

Page

LIST OF TABLES

LIST OF FIGURES

THIS BOOK
CONTAINS
NUMEROUS PAGES
WITH THE ORIGINAL
PRINTING BEING
SKEWED
DIFFERENTLY FROM
THE TOP OF THE
PAGE TO THE
BOTTOM.

THIS IS AS RECEIVED
FROM THE
CUSTOMER.

INTRODUCTION

Alumina is widely used in the process industry and over
50 million pounds of high surface area aluminas are produced
annually (1). Alumina is used as a catalyst in alcohol dehy-
drations and in the Claus process for conversion of hydrogen
sulfide to elemental sulfur.

$$2H_2S + SO_2 \longrightarrow 3S + 2H_2O$$

Alumina is used extensively as a catalyst support, for
example, in hydrodesulfization where the catalyst is sulfided
Co-Mo or Ni-Mo on alumina. Alumina serves both a catalyst and
a catalyst support in the process known as "catalyst reforming"
of petroleum naptha. A typical reforming reaction is the
transformation of n-heptane to toluene

$$C_7H_{16} \longrightarrow (C_6H_5) - CH_3 + 4H_2$$
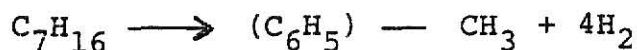
The catalyst for the dehydrogenation is Pt or Pt-Re and is dis-
persed as small crystallites on an alumina support. The alumina
is the catalyst of the isomerizations.

Three techniques for the production of alumina have been
described in the literature.

1. Precipitation from aqueous solution containing Al^{3+}
ions (2,3,4,5,6).

2. Pyrolysis of aluminum salts (4).

3. Reacting amalgamated aluminum with water (2).

When the precipitation method is used the first precipitate is gel-like. Depending on the conditions of the precipitation and subsequent aging temperature and durations many distinct compounds are discernible.

Among the first compounds in the dehydration sequence are three structures of aluminum trihydrate, $Al_2O_3 \cdot 3H_2O$ or $Al(OH)_3$. One structure (5) is denoted α and has the same X-Ray diffraction pattern and composition as the mineral gibbsite. A second structure is denoted β is called bayerite. A third structure (6) is called Norstrandite after its discoverer.

There are two crystalline forms of aluminum monohydrate, $Al_2O_3 \cdot H_2O$ or $AlO(OH)$. As indicated by the second formula the monohydrate is sometimes called aluminum oxide hydroxide. The two forms are α, also known as boehmite, and β which has the same X-ray diffraction pattern as the mineral diaspore.

Two structures that are important as catalysts and as catalysts supports are eta (η) and gamma (γ) alumina. These materials are obtained only after calcination at temperatures of approximately 600°C. Whereas the mono and trihydrates are highly crystalline, eta and gamma are only partially crystalline. Regardless of their history all aluminas revert to alpha (α), also known as corundum, when subjected to high, approximately 1200°C, temperatures. Of all the aluminas only alpha alumina is completely dehydrated and can correctly be given the chemical formula Al_2O_3. In addition to eta and gamma there are transition structures known as chi, delta, kappa and theta.

Emphasis in this work will be on beta trihydrate or bayerite, alpha monohydrate or boehmite as well as eta and gamma alumina. The simplest approach to a description of the various structures is to begin with the structure of alpha alumina. In alpha alumina the oxygen anions are hexagonal close packed. The Al^{3+} cations are located between the oxygen layers in the octahedral sites. To conserve electrical neutrality one in every three of the possible sites is vacant. A particular symmetry of occupied and vacant sites is observed (3).

The question that must be answered with the trihydrates is the location of the protons. The trihydrates are layer compounds and can be visualized as two closed packed lyaers of O^{2-} anions with the Al^{3+} cations located between the two layers as in alpha alumina. The hydrogens are then attached to every oxygen as shown schematically in Figure 1.1.

$$OH^- \diagdown_{} Al^{3+} \diagup^{OH^-} \quad OH^- \diagdown_{} Al^{3+} \diagup^{OH^-} \quad Al^{3+} \diagup^{OH^-}$$
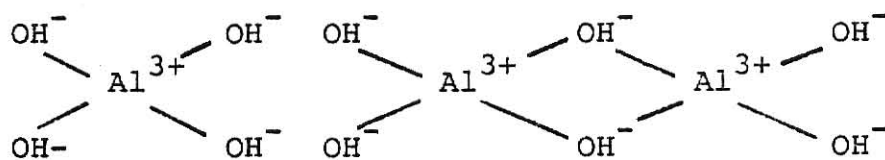
Figure 1.1. Schematic structure of trihydrates.

The trihydrates differ in the way the oxygen are stacked. In bayerite the stacking is 1,2,1,2,1, ...

In boehmite the hexagonal close packing of the oxygen ions changes to cubic close packing and the Al^{3+} ions are found both in octahedral and tetrahedral sites. The structure has been

illustrated by Gates, Katzer and Schuit (3) as shown in Figure 1.2.

The structure of eta and gamma are similar to that of the mineral spinel, $MgAl_2O_4$. In this structure the oxygens are packed face centered cubic. The unit cell requires 32 oxygen atoms yielding 32 octahedral sites and 64 tetrahedral sites. In $MgAl_2O_4$, the eight Mg^{2+} are in the tetrahedral sites and the sixteen Al^{3+} ions are in the octrahedral sites. Obviously not all sites are occupied.

To show the resemblance to the spinel structure eta and gamma alumina are sometimes written $(H_{\frac{1}{2}}Al_{\frac{1}{2}})$ Al_2O_4, where the $H_{\frac{1}{2}}Al_{\frac{1}{2}}$ has replaced Mg. This implies that some of the Al^{3+} ions are in the tetrahedral sites and this is believed to be the case. It further implies that the protons are in the tetrahedral sites. More likely, however, they are on the surface. This structure is consistent with the high surface area of eta and gamma alumina.

It should be noted that $(H_{\frac{1}{2}}Al_{\frac{1}{2}})$ Al_2O_4 can be written $Al_2O_3 \cdot \frac{1}{5}H_2O$. The extent of bound water in eta and gamma is such that if they are written $Al_2O_3 \cdot n\ H_2O$, n will be between zero and 0.6.

The difference between eta and gamma is that they have different ratios of Al^{3+} in the octahedral and tetrahedral sites and they have different symmetries of occupation. Eta alumina is the more acidic and this is believed to be due to it having relatively more of the Al^{3+} ions in the less shielded
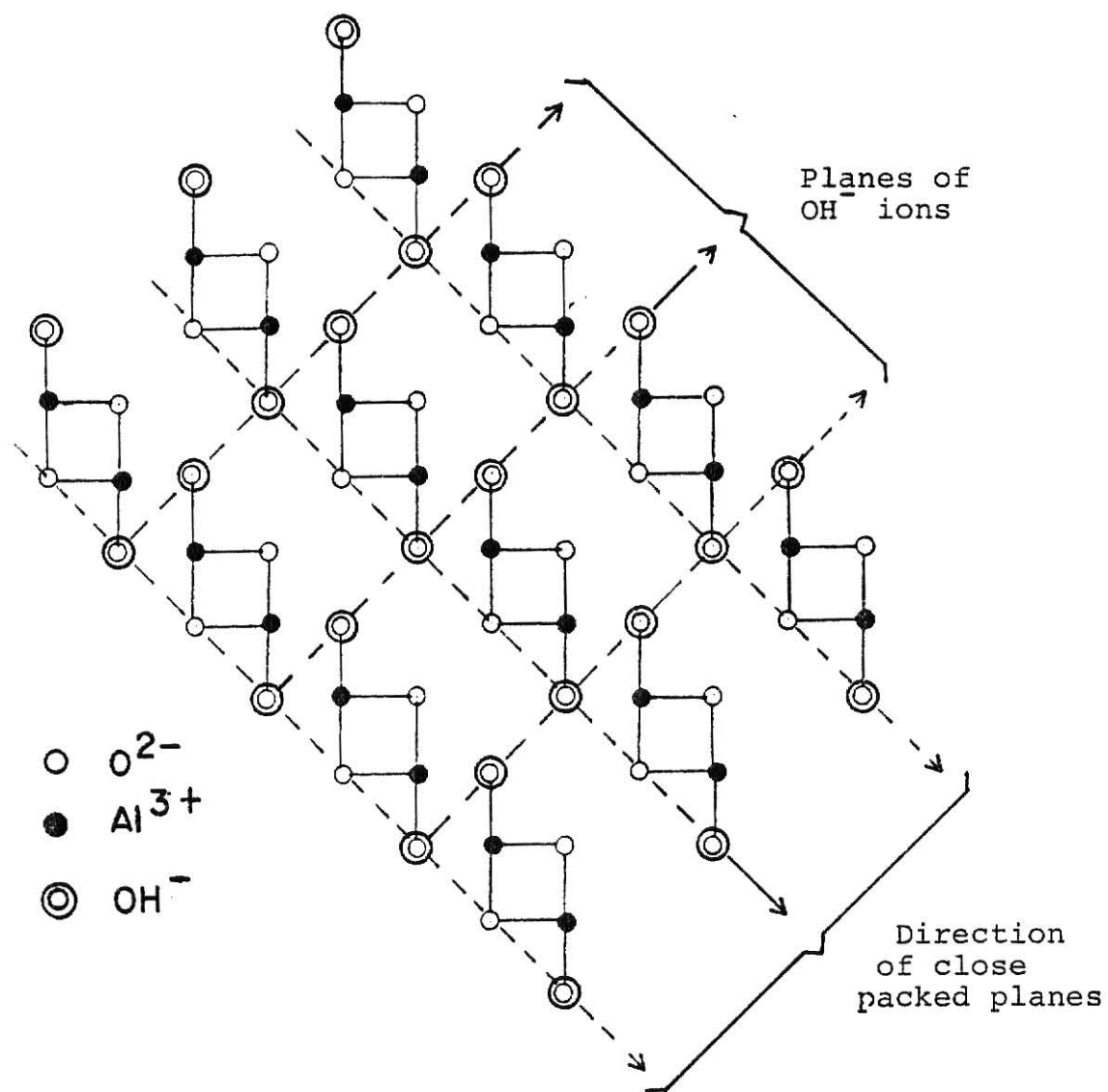
Figure 1.2. Schematic structure of boehmite.

Identification of the various aluminas is best done by
X-ray diffraction. Table 1.1 shows the accepted d spacings
and intensities for bayerite, boehmite, eta and gamma alumina.
Also shown are the values of 2θ which were calculated using
$n\lambda = 2d\sin\theta$ for Cu K α radiation. The wavelength, λ, of Cu K α
radiation is 1.542 A.

The diffraction patterns produced by the aluminas prepared
as a part of this work are shown in Figure 1.3 (bayerite),
Figure 1.4 (pseudoboehmite), Figure 1.5 (microcrystalline boeh-
mite), Figure 1.6 (eta alumina), and Figure 1.7 (gamma alumina).

X-ray diffraction analysis was done on equipment produced
by the Siemens Company. The runs were done with Cu Kα radia-
tion using a nickel filter at a voltage of 40 kV and a current
of 18 mA.

The purpose of this work was to prepare and identify the
different aluminas particularly eta and gamma. An additional
purpose was to modify the pore size of different aluminas.
This work will serve as a foundation for later work on the
effect of pore size distribution on the sintering of supported
metals.

The aluminas were identified by X-ray diffraction. Surface
area, pore volume and pore size distribution have been determined
by physical adsorption using a static glass apparatus with nitro-
gen as the adsorbent.

Chapter 2 of this thesis surveys various methods to pre-
pare aluminas with different pore sizes with the emphasis on

Table 1.1. X-ray diffraction patterns for aluminas (6).

Boehmite			Bayerite			Gamma			Eta		
d/n	2θ	I	d/n	2θ	I	d/n	2θ	I	d/n	2θ	I
6.11	14.50	100	4.72	18.8	100	2.70	33.2	2	4.60	19.3	4
3.16	28.21	65	4.36	20.4	70	2.41	37.3	6	2.80	32.0	2
2.35	38.37	53	3.19	28.0	25	2.28	39.5	6	2.40	37.5	6
1.98	45.83	6	3.08	29.0	1	2.18	41.4	2	2.27	39.7	3
1.86	48.98	32	2.69	33.3	3	2.09	43.3	1	1.97	46.1	8
1.85	49.26	27	2.45	36.7	3	1.98	45.8	10	1.52	61.0	2
1.77	51.65	6	2.34	38.5	6	1.95	46.6	6	1.40	66.8	10
1.66	55.28	13	2.28	39.5	3	1.54	60.1	2	1.21	79.2	1
1.53	60.65	6	2.21	40.8	67	1.39	67.4	10	1.14	85.1	2
1.45	64.10	16	2.14	42.2	3	1.14	85.1	3	1.03	96.9	1
1.43	65.06	9	2.06	44.0	2	1.04	95.7	1	0.99	102.3	1
1.41	66.19	1	1.97	46.1	3	1.00	100.9	1			
1.40	67.05	2	1.91	47.6	1						
1.38	67.76	6	1.83	49.8	1						
1.37	68.55	2	1.76	52.0	1						
1.31	71.98	15	1.71	53.6	26						
1.30	72.56	3	1.68	54.6	2						
1.22	78.09	1	1.64	56.1	1						
1.21	79.24	2	1.59	58.0	4						
1.18	81.76	3	1.67	59.2	2						
1.17	82.36	1	1.55	59.7	4						
1.16	83.22	3	1.52	61.0	1						
1.13	85.67	5	1.48	62.8	1						
1.09	89.83	1	1.47	63.3	1						
1.05	94.97	2	1.45	64.2	7						

bayerite, boehmite, eta and gamma alumina are presented.
Specific surface area, and pore size measurement techniques
are discussed in detail in Chapter 3. Isotherm of the aluminas
are also shown in this chapter. Some recommendations for
future work are given at the end of Chapter 3.

ILLEGIBLE DOCUMENT

THE FOLLOWING DOCUMENT(S) IS OF POOR LEGIBILITY IN THE ORIGINAL

THIS IS THE BEST COPY AVAILABLE

Figure 1.3.   X-Ray diffraction pattern of bayerite. 40 kV copper radiation with nickel filter.
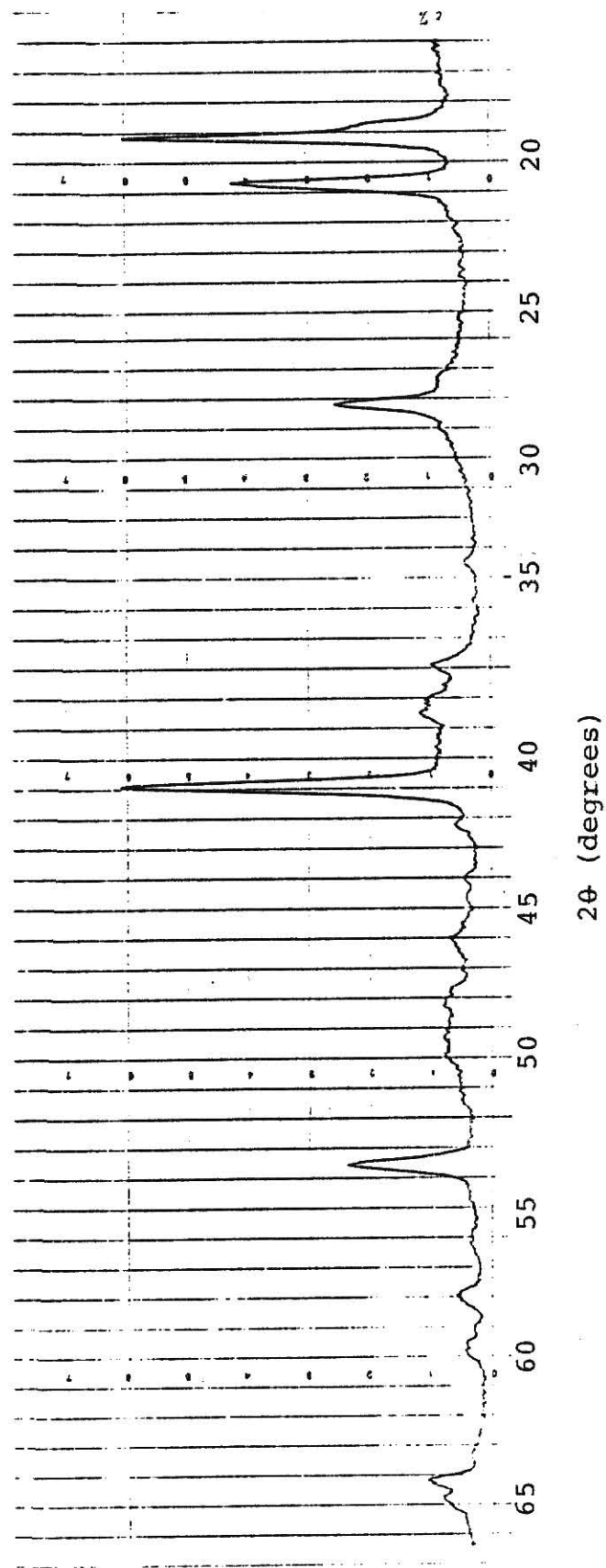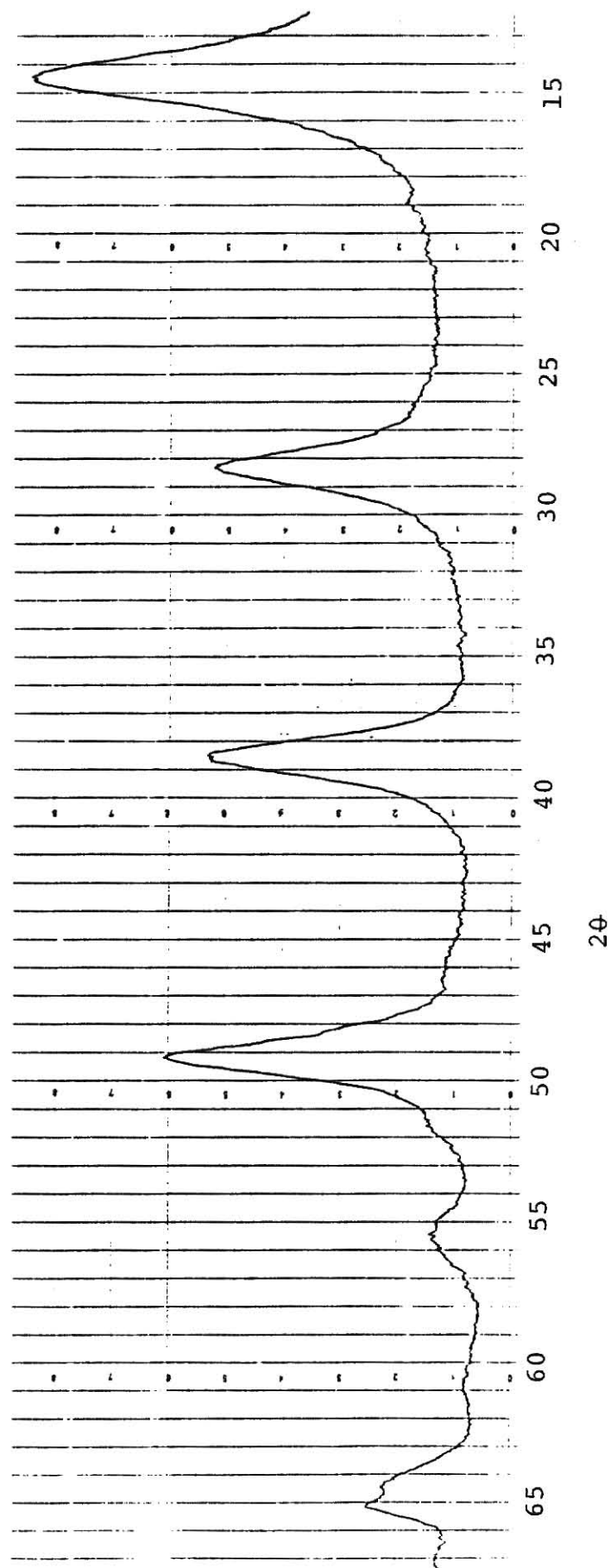
2θ (degrees)

Figure 1.4.   X-ray diffraction pattern of boehmite.
40 kV copper radiation with nickel filter.
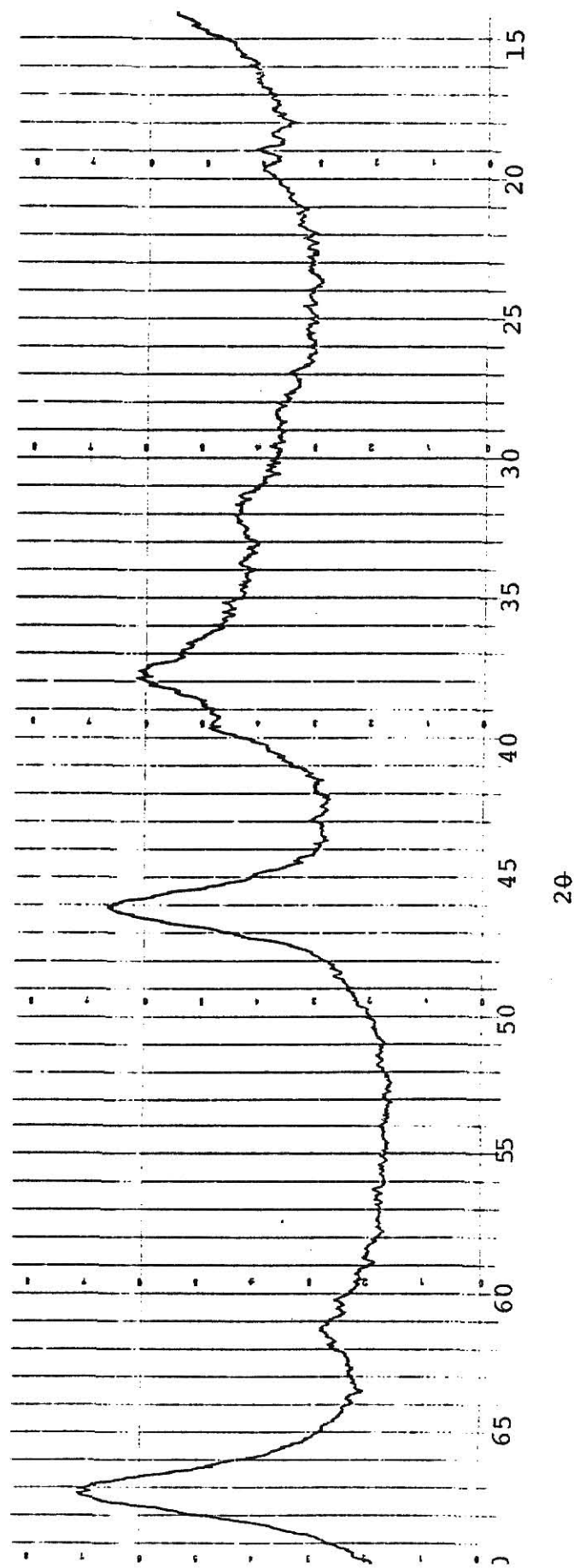
10

Figure 1.5.   X-ray diffraction pattern of eta alumina.
40 kV copper radiation with nickel filter.

11
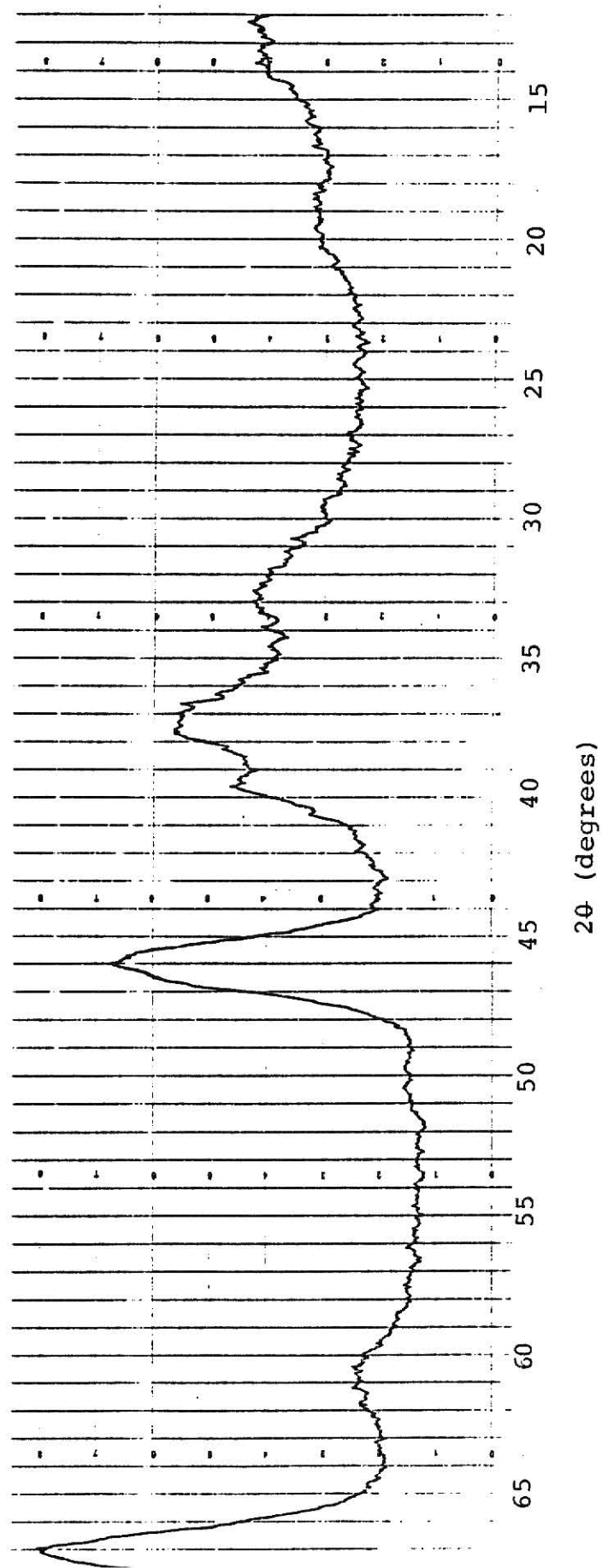
Figure 1.6. X-ray diffraction pattern of gamma alumina. 40 kV copper radiation with nickel filter.

2θ (degrees)

12

ALUMINA PREPARATION

This chapter deals with the preparation of bayerite, boehmite, and eta and gamma alumina. The literature on the preparation of eta and gamma alumina is large and often contradictory.

2.1 Bayerite

Bayerite for this work was prepared as follows:

100 grams of $Al(NO_3).9H_2O$ was dissolved in 175 ml of distilled water. This solution was slowly added to a 25 ml of concentrated (pH = 12.85) solution of NH_4OH. The pH was kept above 9.5 throughout the process. The resulting mixture was filtered with coarse filter paper under moderate vacuum and washed with 9 liters of water after standing in the mother liquor for 4 hours. The precipitation was then contacted with water for 12 hours. The solid product was then refiltered under moderate vacuum and aged at 120°C for 72 hours.

The diffraction pattern of this product is shown on Figure 1.3. The method given here is essentially that of MacIver et al. (7).

Summaries of the various methods by which bayerite has been prepared are given by Wefers and Bell (6) and by Lippens and Steggerda (8). Both reviews site a technique by Schmäh (9) as giving crystallographically pure bayerite. The Schmäh tech-

room temperature. Both reviews indicate that the purity and
crystallinity of bayerite prepared by methods other than that
of Schmäh are suspect.

2.2 Boehmite

Boehmite was prepared as follows:

227 grams of $Al(NO_3) \cdot 9H_2O$ was dissolved in 1000 ml of
water and brought to 80°C. The initial pH of this solution
was 1.35. 330 ml of concentrated NH_4OH was slowly added to
this solution maintaining the temperature at approximately 80°C.
The final pH was 8.0. The material was then aged at 80°C in
the mother liquor for 48 hours. It was then filtered using a
coarse filter paper and moderate vacuum and the solid was then
washed with 12 liters of distilled water and dried at 120°C
for 48 hours.

The X-ray diffraction for this material is shown on Figure
1.4. The procedure above is again due to MacIver et al. (7).

Figure 2.1 shows a plot of pH versus milliliters of NH_4OH
during preparation of boehmite. A tentative explanation of
this behavior is as follows. On dissolving the original alumi-
num nitrate compound dissociates. The hydroxyl ions are par-
tially associated with the aluminum ions while the hydrogen
ions and nitrate ions are completely dissociated, the original
pH is therefore low. As NH_4OH is added more of the hydroxyl
ions are associated with the aluminum ions and the pH rises
because of dilution. Ultimately, the aluminum ions cannot
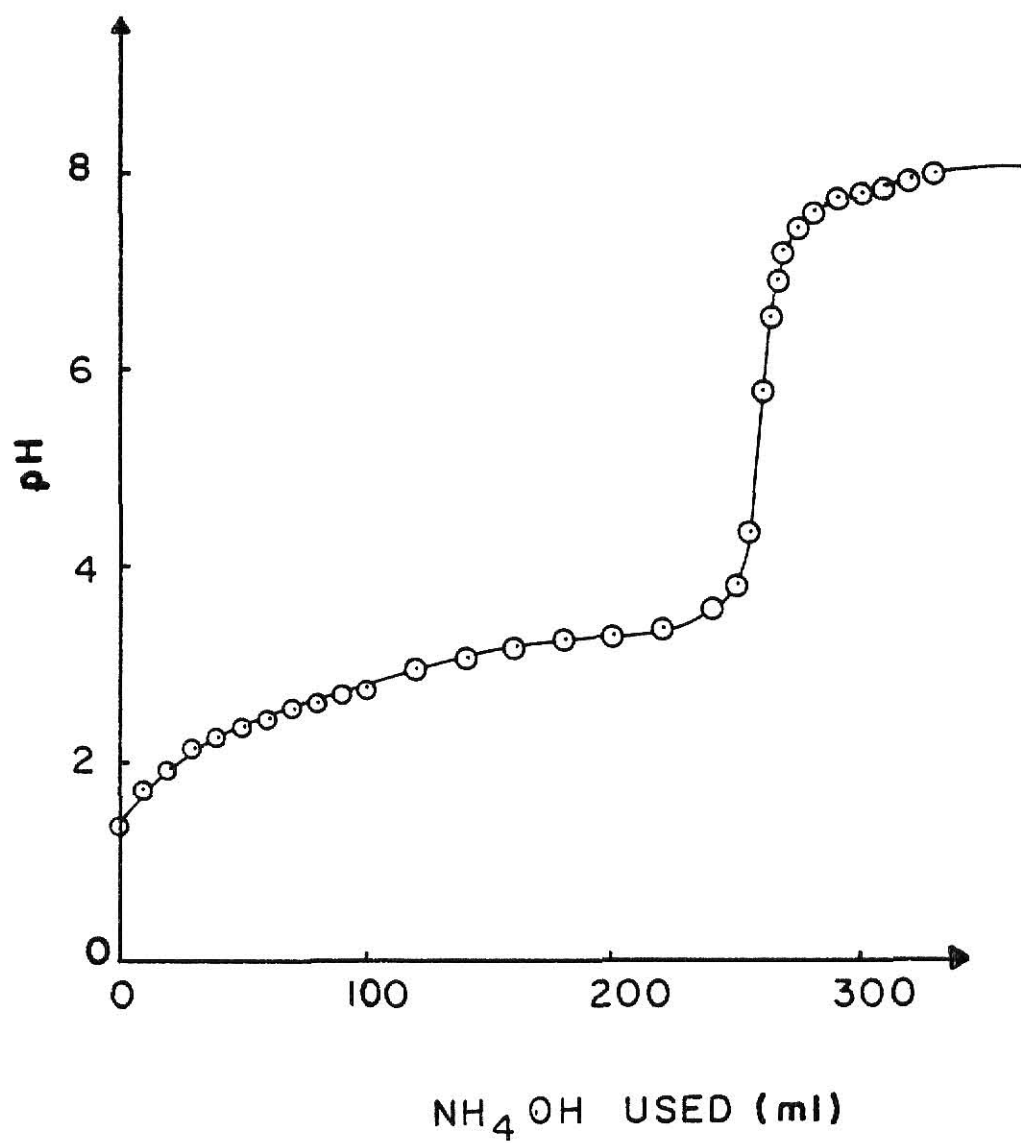accept more hydroxyl ions and the pH rises rapidly to 7 as the

Figure 2.1 pH versus ml of NH_4OH.

The continued but slower rise in pH as more NH_4OH is added is due to dilution. The nature of the compounds formed with the aluminum ions during this process is not known to this author; however, Wefers and Bell (6) show complexes such as $Al(H_2O)_6{}^{3+}$, $(Al(OH)(NO_3))^+H_2O$, $H_2OAl(OH)^{2+}$, $(AlOHO)_2 : HOH : (OHOAl)_2$, and $Al(OH)_4{}^-$.

As the NH_4OH is added the viscosity of the mixture also rises in a manner similar to the pH. The sharp rise in viscosity indicates significant polymerization. The behavior and appearance at this pH is that of a gel. Unlike the pH, viscosity will eventually decrease as more NH_4OH is added. No quantitative viscosity data were taken.

There are, in fact, two types of boehmite. One is called crystalline boehmite, the other is known as pseudoboehmite or gelantious boehmite. The diffraction pattern of pseudoboehmite, as described, though not presented by Lippens and Steggerda, consists of broad bands with spacings similar to the most intensive lines of well crystallized boehmite. The broad peaks shown on Figure 1.4 would seem to imply that boehmite produced by the method outlined by MacIver et al. (7) is pseudoboehmite.

Preparation of well crystallized boehmite, according to Lippens and Steggerda, can be accomplished by aging aluminum gel at a pH greater than 12 and at 80°C. Oomes (10) obtained well crystallized boehmite by aging pseudoboehmite in NaOH. Wefers and Bell (6) indicate that aging of pseudoboehmite at 300°C for 48 hours will convert it to crystallized boehmite.

in the preparation of gamma alumina, this additional aging was not performed. It was found that aging for 96 hours at 120°C was not sufficient to achieve the sharp peaks indicative of well crystallized boehmite.

2.3 Eta alumina

Eta alumina was prepared as follows:

The bayerite, prepared as the method above, was slowly brought to 300°C in a 14 hour period. The heated sample was immediately submitted to an oven preheated to 600°C and kept there for 24 hours. The diffraction pattern of this product is shown in Figure 1.5. The method given here is due to MacIver et al. (7).

Distinguishing eta and gamma alumina using the diffraction patterns is difficult. According to R. E. Van Norstrand (11), two criteria to distinguish between eta and gamma alumina can be summarized as:

1. In the eta pattern, there is a sharp spike on a broad base at $2\theta = 19.3°$; but only a broad line is observed in the gamma pattern.

2. There are two peaks that somewhat overlap with each other to produce a broad peak with a hump for gamma alumina, while, for the case of eta alumina, there is only one peak at $2\theta = 45.9°$.

As shown in Figures 2.2 and 2.3, the sample H3 can be designated as eta alumina since it satisfies the above criteria.
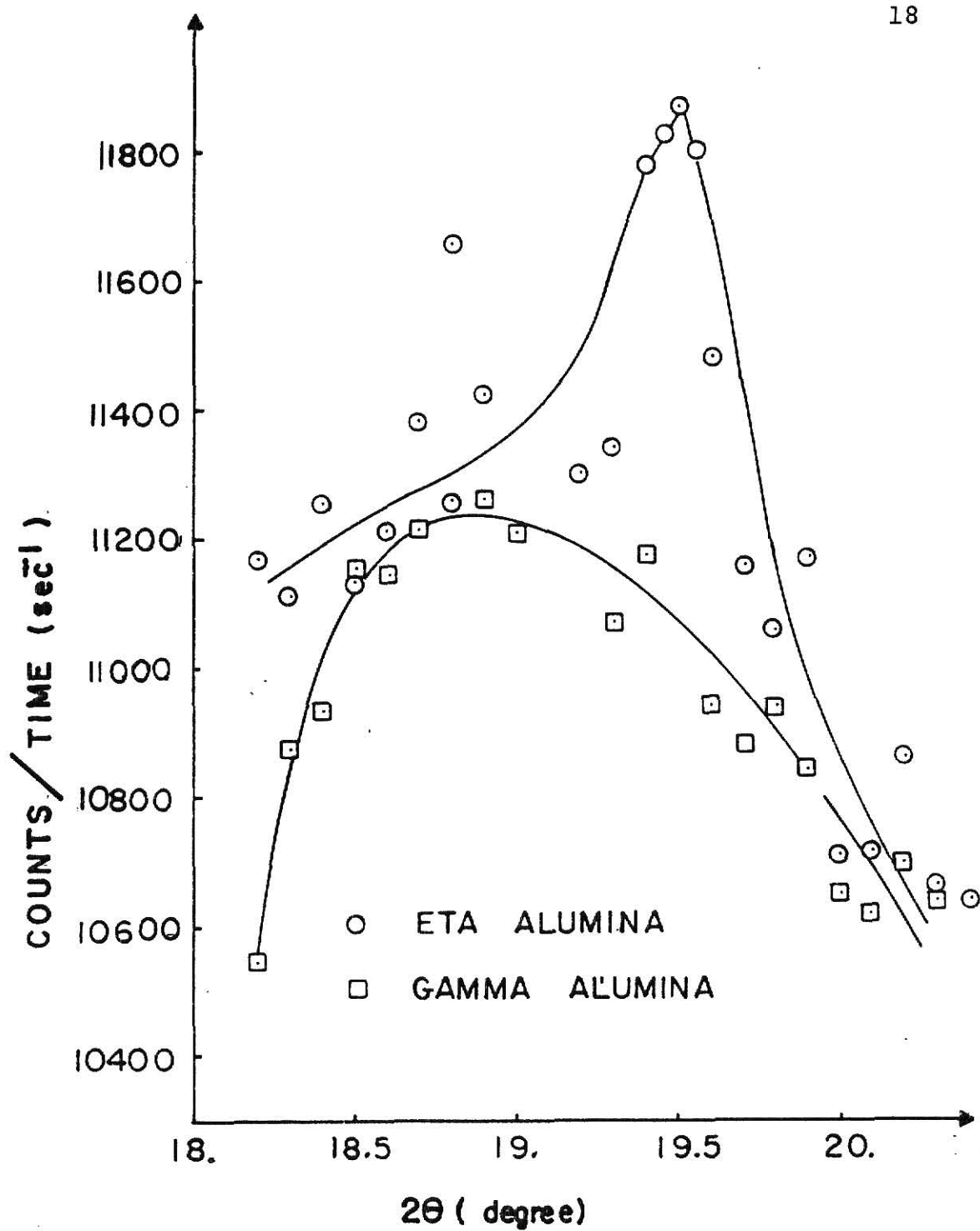
Figure 2.2. X-ray diffraction pattern of gamma and eta alumina.
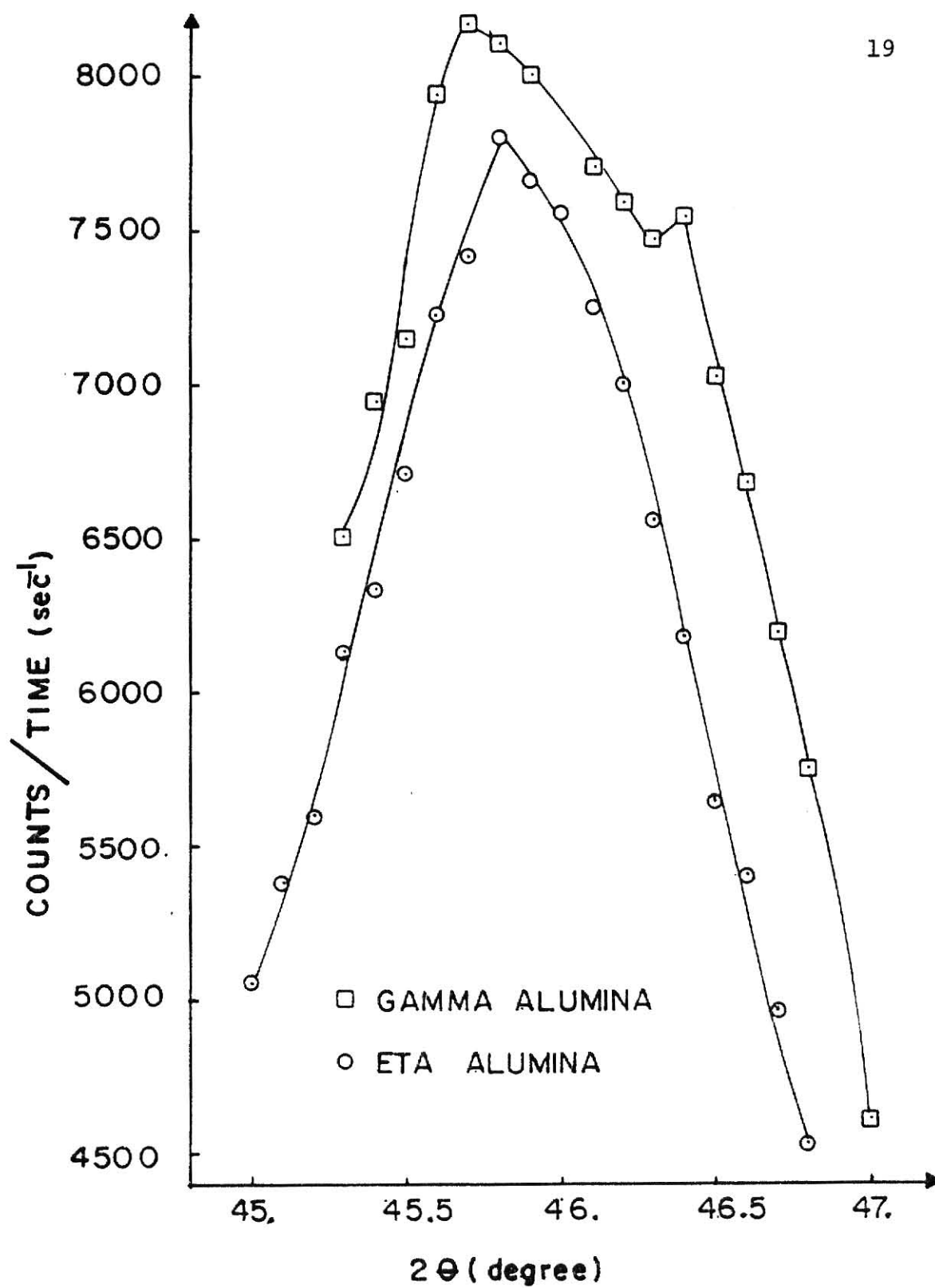
Figure 2.3. X-ray diffraction pattern of gamma and eta alumina.

Eta alumina is relatively easy to produce from pure bayerite. Most authors, Stumpf et al. (5), Wefers and Bell (6), agree with MacIver (7) about the thermal transformation of bayerite to eta alumina.

2.4 Gamma Alumina

Gamma alumina was prepared as follows:

The boehmite, prepared as the method above, was placed in an oven preheated to 500°C and kept there for 48 hours. The diffraction pattern is shown in Figure 1.6. The method is essentially that of MacIver (7).

A counting method was used to distinguish the eta and gamma forms of alumina. The sample F1A2 is gamma alumina according to the two criteria given above.

The literature on the preparation of gamma alumina is often contradictory. However, many believe that gamma alumina is formed by heating boehmite. According to Sato et al. (12) both crystalline boehmite and pseudoboehmite transform thermally to gamma alumina but at different temperatures. Crystalline boehmite transforms to gamma alumina at 520°C while pseudoboehmite transforms to gamma alumina at approximately 450°C. Gamma alumina also can be obtained by heating bayerite or gibbsite at a pressure greater than one atmosphere in moist air at a heating rate larger than 1°C per minute. Boehmite can be converted to gamma alumina under any calcination conditions according to Wefers and Bell (6). Fink (13) produced gamma alumina by calcination of boehmite in dry air at 600°C for 12 hours. Stumpf

(5) confirmed that both boehmite and gibbsite transform thermally to gamma alumina.

2.5 Gamma alumina with different physical properties

While the precipitation method was used to produce gamma alumina, the conditions at which the precipitation and calcinations were carried out are the major factors that influence the physical properties of the final product. "Pumping", calcination time and calcination temperature are three variables in this study.

In order to study these three effects, eight sets of experiments must be made according to the 2^k fractorial design of experiments method (Appendix A).

In the production of boehmite, after the pH reached 8.0, the precipitate was aged at 80°C in the mother liquor for 24 hours. 10 ml of concentrated (70 wt %) of nitric acid solution was added to lower the pH to 3.0. Then the pH of the mixture was brought up to 8.0 again by slowly adding 15 ml of concentrated solution of NH_4OH to the mixture. The process of lowering the pH and bringing it up again is called pumping. When nitric acid was added to the precipitated solution, the size of the large particles decreased and the small particles disappeared. As the pH decreased, the small particles were completely redissolved while large particles were partially redissolved. By slowly adding NH_4OH, precipitate was formed on the existing large particles. Thus, larger particles can be obtained by "pumping".

The pumped precipitated solution was then aged for 24 hours and filtered using a coarse filter paper and moderate vacuum. The solid was then washed with excess distilled water and dried at 120°C for 48 hours.

The final product gamma alumina, was obtained by calcinating two kinds of boehmite: one with pumping and one without pumping at two calcination temperatures and times as outlined in Table 2.1.

Table 2.1. Preparation conditions of gamma aluminas.

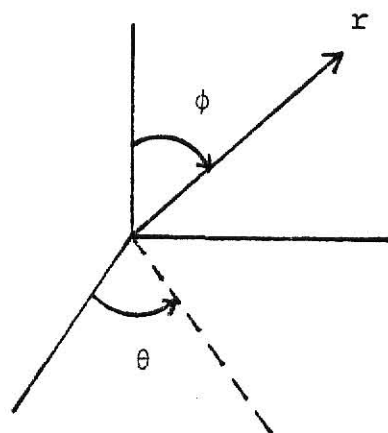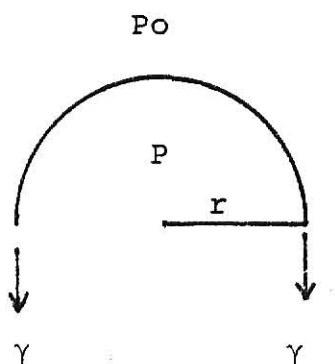| Sample	Pumping	Calcination temperature (°C)	Calcination time (hours)
F1A1	no	500	24
F1A2	no	500	48
F1B1	no	700	24
F1B2	no	700	48
FA1A1	yes	500	24
FA1A2	yes	500	48
FA1B1	yes	700	24
FA1B2	yes	700	48
F2A1*	no	500	24

*Sample aged for 96 hours.

PHYSICAL PROPERTIES

3.1 Background

The results of the surface area and pore size distribution measurements will be presented in this chapter as well as the nitrogen isotherms. A brief account of the ideas on which pore size measurements from adsorption-desorption isotherms are based will be given first.

Consider a liquid drop of radius r of a substance with surface tension γ. A force balance on a hemisphere of the drop is:

$$\int_{\varnothing=0}^{\pi/2} \int_{\varnothing=0}^{2\pi} Pr^2 \sin\varnothing \, d\varnothing \, d\theta = \int_{\varnothing=0}^{\pi/2} \int_{\theta=0}^{2\pi} Po \, r^2 \sin\varnothing \, d\varnothing \, d\theta + 2\pi r\gamma$$

Integration yields

$$P \pi r^2 = Po \pi r^2 + 2 \pi r \gamma$$

or

$$P - Po = \Delta P = 2 \gamma/r \tag{1}$$

Thus, because of surface tension, the pressure inside the drop is greater than that outside.

A more general derivation across an arbitrary surface results in

$$\Delta P = \gamma \left(\frac{1}{R_1} + \frac{1}{R_2} \right) \tag{2}$$

Where R_1 and R_2 are the radii of curvature of the surface. For a sphere, $R_1 = R_2 = r$ and equation (2) reduces to equation (1). Equation (2) is known as Young and Laplaces equation.

Application of equation (2) to a cylindrical liquid sur-face, $R_1 = r$ and $R_2 = \infty$, yields $\Delta P = \gamma/r$. Thus, for a given r, a cylindrical "drop" has a lower P than does a spherical one because the curvature of the cylindrical surface is less than that of the spherical surface.

Equation (2) can also be applied to meniscuses. Consider those shown in Figure 3.1. Here the surfaces are again spherical and cylindrical but this time they are concave rather than con-vex and the radii of curvature are negative. Thus, for the hemisphere, $R_1 = R_2 = -r$, and $\Delta P = -2\gamma/r$ and for the cylinder, $R_1 = -r$, $R_2 = \infty$, and $\Delta P = -\gamma/r$. Thus, when a liquid wets a solid and a concave meniscus is formed the pressure on the liquid side is less than the pressure on the vapor side. Liquid nitro-gen wets most solids and is typical of this behavior.
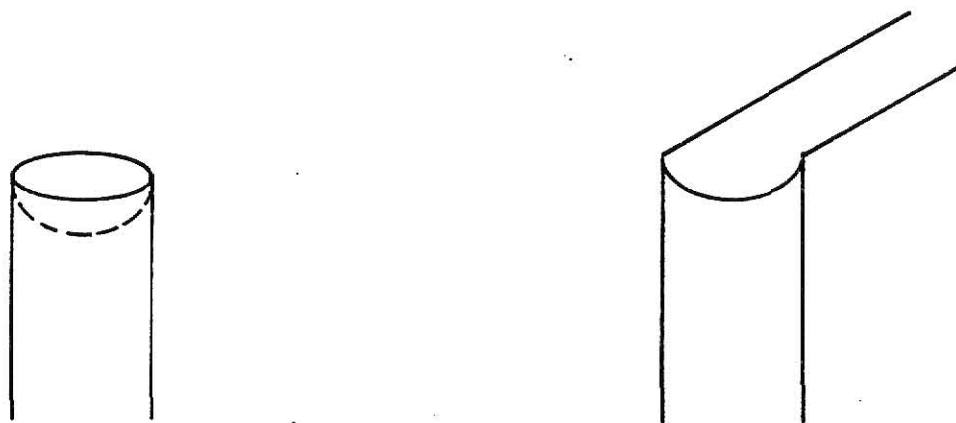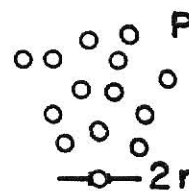
Figure 3.1.   Two kinds of meniscus.

$$\frac{\text{Vapor} \ P_0}{P_0}$$

(a)   (b)

Figure 3.2.   Vapor pressure across different
              surfaces.

Return now to liquid drops, it is desired to find the vapor pressure exerted by a drop of radius r. Let Po be the vapor pressure of a liquid in equilibrium with its vapor across a planar surface and let P be the vapor pressure of a liquid in equilibrium with its vapor when the liquid is composed of drops of radius r. The situation is shown schematically in Figure 3.2 P is unknown. The change of Gibbs free energy of the vapor on going from (a) to (b) is

$$G = \int_{Po}^{P} v \, dP$$

and the change in Gibbs free energy of the liquid is

$$\Delta G = \int_{Po}^{P + 2\gamma/r} v_1 \, dP$$

Equating the two changes in free energy, utilizing the ideal gas law for the vapor volume, and assuming the liquid specific volume is constant yields

$$R_g T \ln \left(\frac{P}{P_o} \right) = v_1 \left(P + \frac{2\gamma}{r} - P_o \right)$$

Because $2\gamma/r$ is much greater than $P - P_o$, this equation can be solved for P/P_o to yield

$$P/P_o = \exp \left(\frac{2 \, v_1 \, \gamma}{r \, R_g \, T} \right) \tag{3}$$

Equation (3) is known as the Kelvins equation. For an arbitrary surface the equation becomes

$$P/P_o = \exp \left(\frac{v_1}{R_g T} \left(\frac{1}{R_1} + \frac{1}{R_2} \right) \right) \tag{4}$$

Equation (4) is the basic equation for pore size measurement from adsorption-desorption isotherm data.

Consider a substance with cylindrical pores open at both ends and suppose it is immersed in nitrogen vapor initially at very low pressure. As the pressure increased, condensation occurs on the wall. The vapor pressure exerted by this condensate is

$$P = P_O \exp \left(\frac{-v_1 \gamma}{r R_g T} \right)$$

because $R_1 = -r$ and $R_2 = \infty$. Therefore, the smaller the pore the lower the vapor pressure of the first condensate that appears and thus the small pores will fill first.

Consider now the situation when the pressure is P_O and all pores are full of liquid. As the pressure is lowered, the liquid vaporizes and a meniscus with a hemispherical shape with $R_1 = R_2 = -r$ appears. The vapor pressure is thus

$$P = P_O \exp \left(\frac{-2v_1 \gamma}{r R_g T} \right)$$

and the larger pores will empty first as the pressure is decreased.

If all pores had the same radius r, then they would fill at the pressure

$$P = P_O \exp \left(\frac{-v_1 \gamma}{r R_g T} \right)$$

and empty at the pressure

$$P = P \exp \left(\frac{-2v_1 \gamma}{} \right)$$

giving rise to the familiar hysteresis in the curves of volume adsorbed versus pressure.

3.2 Isotherm and Hysteresis

Experimental isotherms fall into five principal forms as shown in Figure 3.3. Type I is the Langmuir type. These isotherms exhibit a limiting adsorption that presumably corresponds to a complete monolayer. Chemisorption isotherms are Type I. Type II, commonly called signoid or S shaped isotherms, are very common. They are typical of physical adsoprtion and correspond to multilayer adsorption. Surface area can be calculated using this isotherm in the relative pressure range from 0.05 to 0.30. Type III isotherms are relatively rare. This type of isotherm is observed when the heat of adsorption is equal to or less than the heat of liquification of the adsorbate. Types II and III exhibit an infinite amount of adsorption as the saturation pressure is approached. They represent multilayer adsoprtion on a flat surface or on a non-porous material. Types IV and V are essentially Types II and III except that the amount adsorbed does not approach infinity as the saturation pressure is increased. These types of isotherm usually show hysteresis effects and are observed only on porous materials.

There are five distinct types of hysteresis loops as shown in Figure 3.4.

Type A: Both adsorption and desortion branches are steep at intermediate relative pressure. This type of hysteresis is observed by cylindrically shaped capillaries which are open at
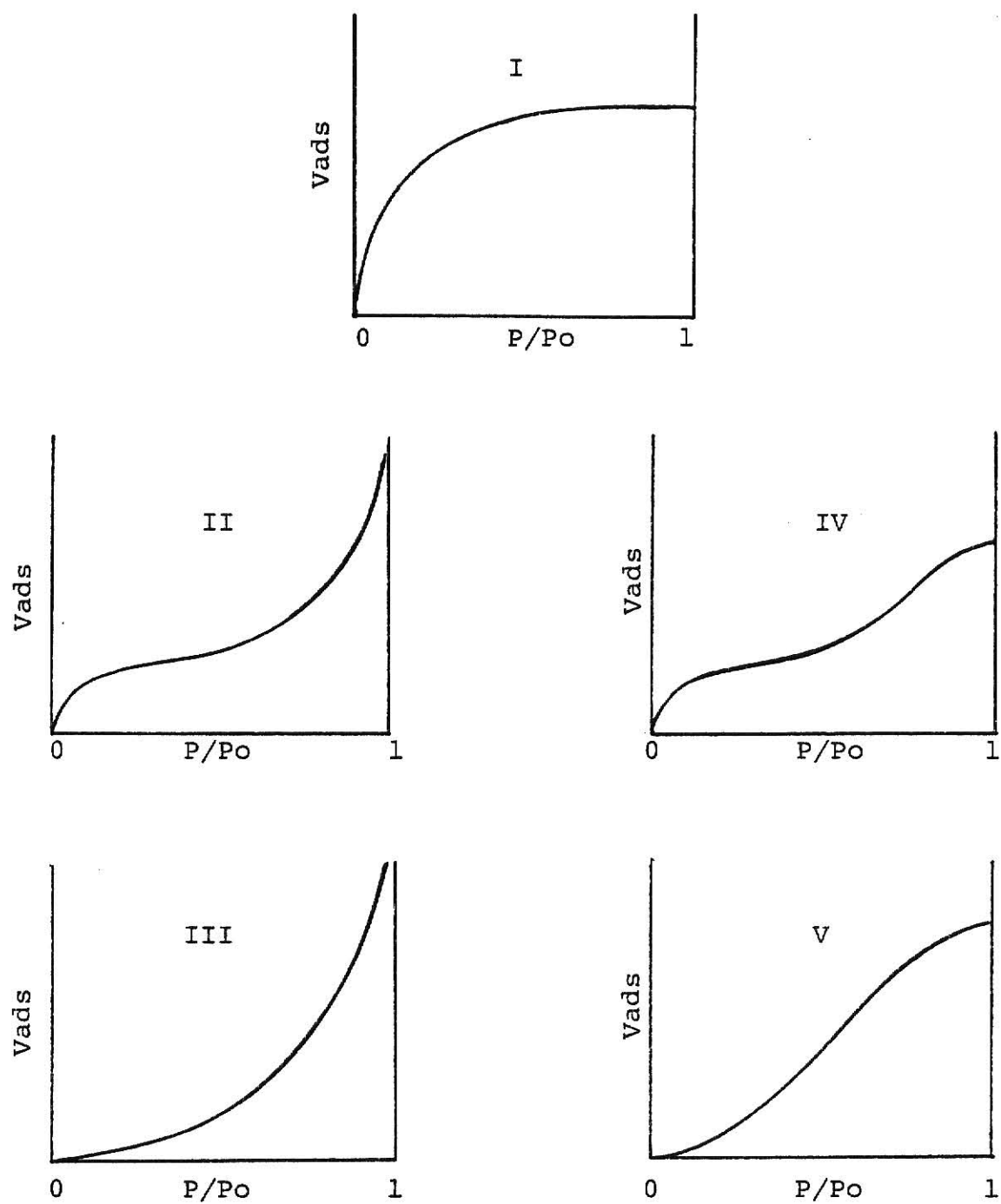
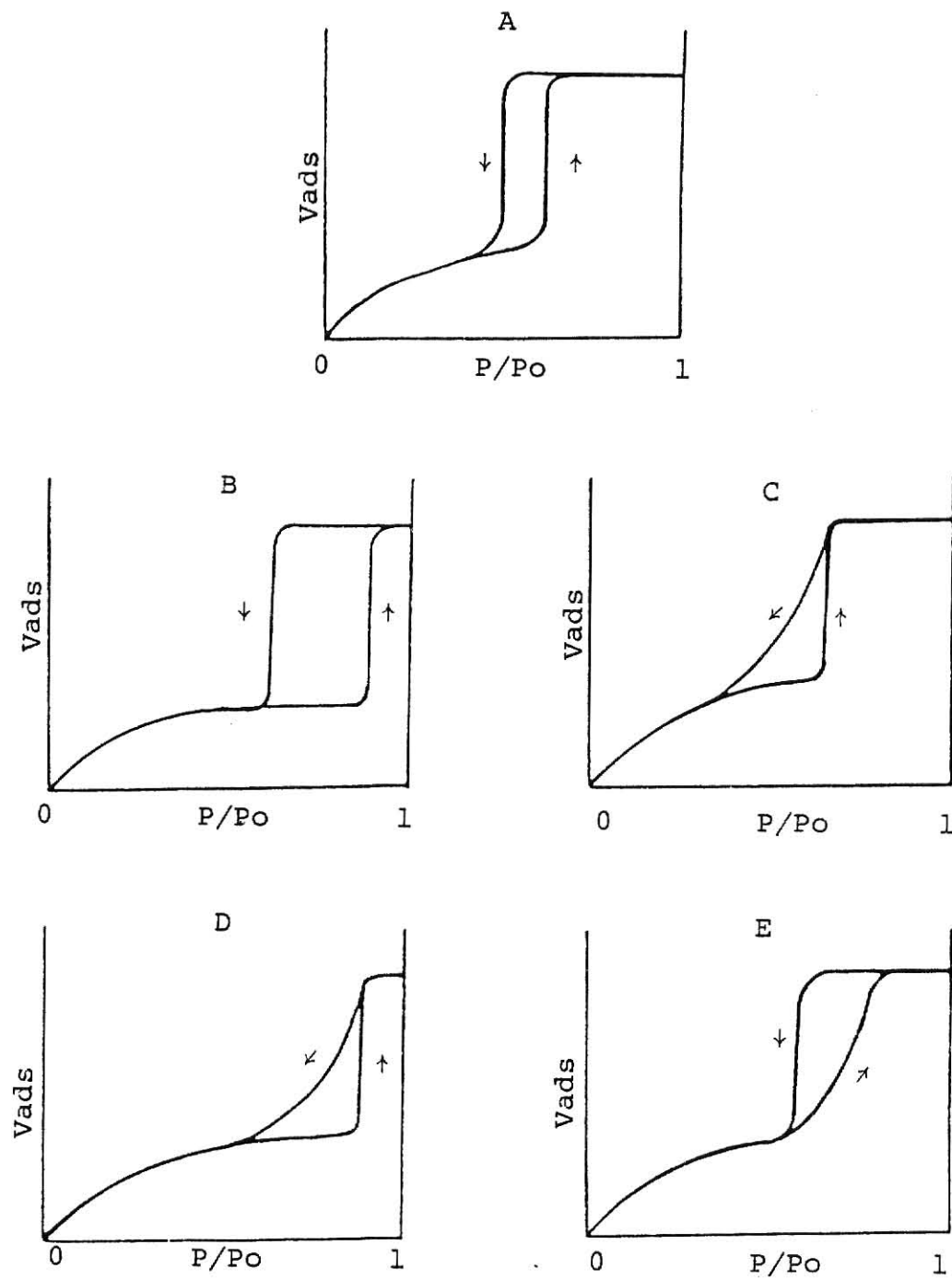Figure 3.3. Five types of isotherms.

Figure 3.4. Five types of hysteresis.

both ends. Other shapes such as, polygonal rather the circular cross sections, wide necked "ink bottles", tubular capillaries with one narrowed part, "ink bottles" with narrow and short necks, capillaries open at both ends with wide parts and narrow and short necks, and trough-shaped capillaries all give rise to the same type hysteresis. Type A hysteresis curves are frequently found in the literature.

Type B: The adsorption branch is steep at the saturation pressure while the desorption branch is steep at intermediate relative pressures. This type of hysteresis is formed by open slit shaped capillaries with parallel walls or capillaries with very wide bodies and narrow short necks. Quite a number of samples of this Type B hysteresis loop are found in the literature.

Type C: The adsorption branch is steep at intermediate relative pressures and the desorption branch is sloping. This type of hysteresis is relatively rare and is only observed for capillaries having continuously changing internal radius with wide part at the openings and for wedge-shaped capillaries with closed sides and open ends.

Type D: The adsorption branch is steep at saturation pressure while the desorption branch is sloping. This kind of hysteresis curve is rare.

Type E: The adsorption branch has a sloping character and the desorption branch is steep at intermediate relative pressures. Tubular or "ink bottle" capillaries with short

wide parts of various width gives rise to type E hysteresis. This type of hysteresis is frequently found.

If the capillaries are predominantly of one form, the conventional types of hysteresis mentioned above can be found. Experimental hysteresis loops might be formed by combining two or more types of hysteresis loops.

3.2.1 Pseudobeohmite

The isotherm of pseudoboehmite as shown in Figure 3.5 is type I which is referred to as the Langmuir isotherm. This kind of isotherm is observed in physical adsorption when the pores are very narrow and a monomolecular layer is enough to fill them. There is no hysteresis in this case.

3.2.2 Eta alumina

The isotherm of the one sample eta alumina shown in Figure 3.6 is type IV. This type of isotherm is observed for physical adsorption on highly porous adsorbents. The flattening of the isotherm at high pressure region occurs due to the capillary condensation.

Hysteresis starts at the relative pressure $P/P_o = 0.35$ and ends at the relative pressure $P/P_o = 0.92$. The experimental hysteresis is not one of the five conventional types of hysteresis (14) but rather appears to be a combination of two types: A and E. The hysteresis loop is slightly sloping because there is a distribution of various size cross sections.

Hysteresis of this type can be attributed primarily to
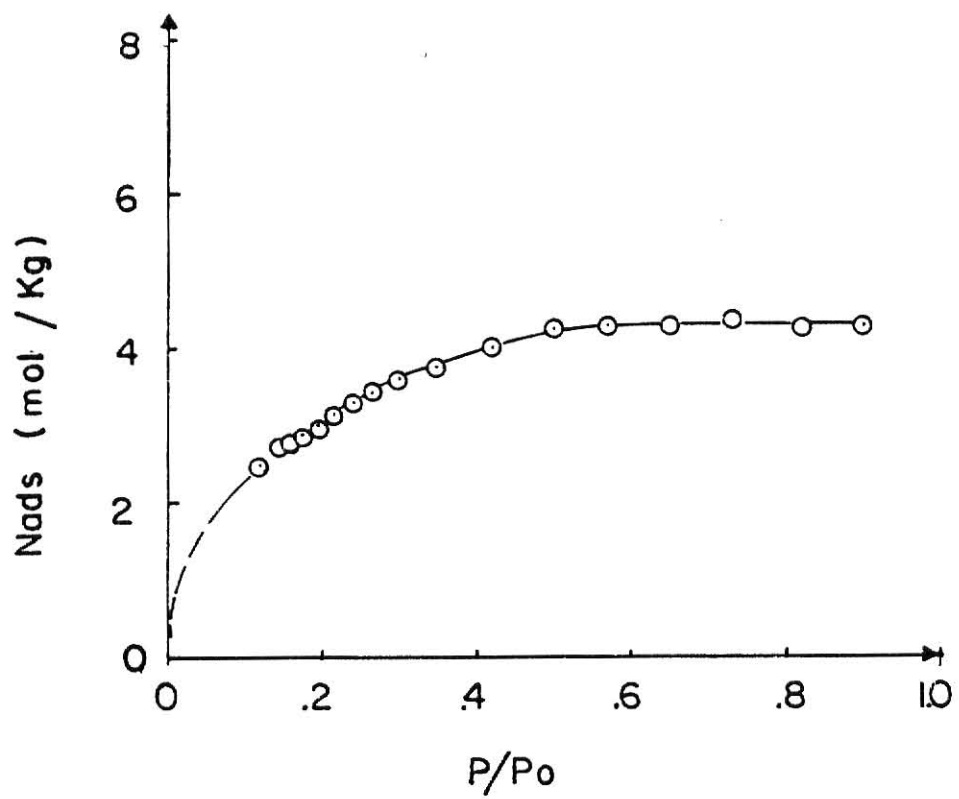
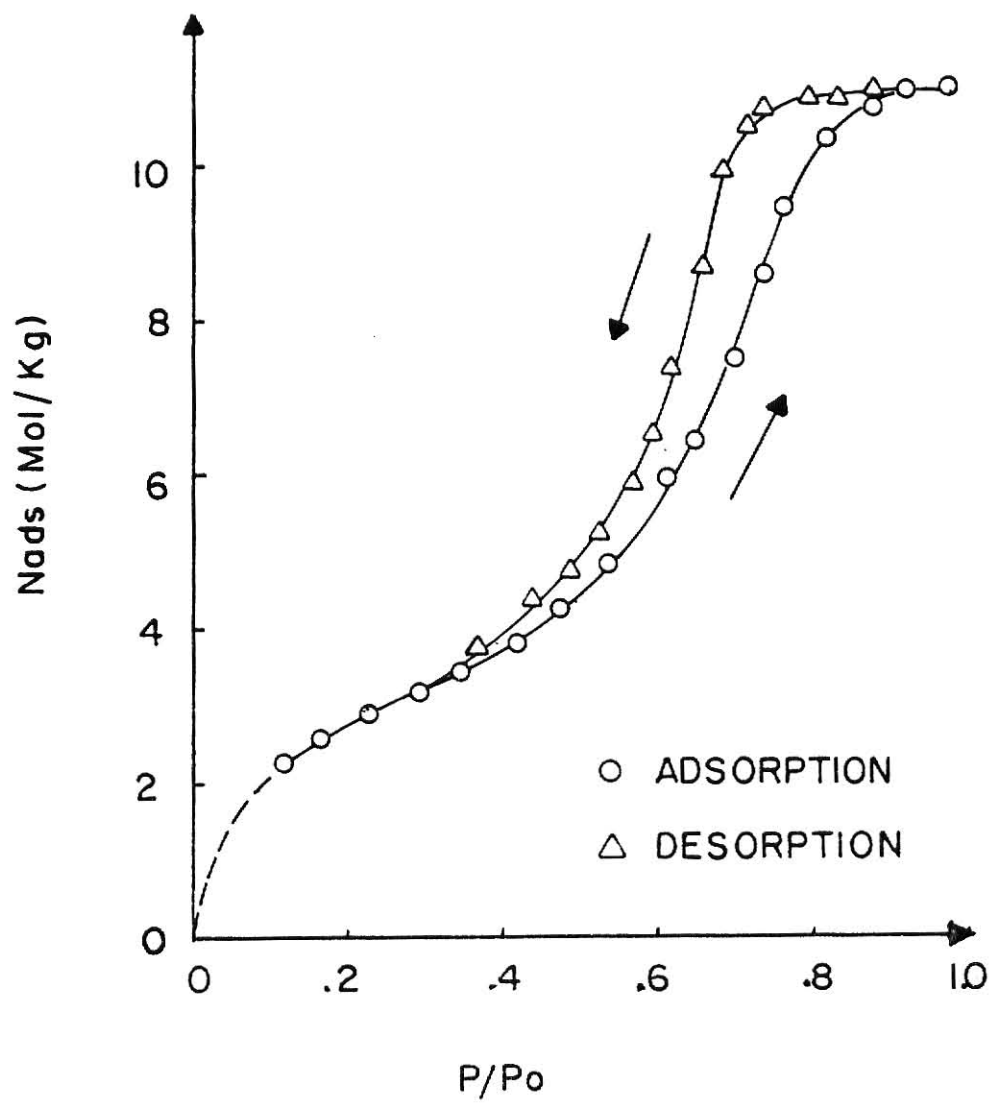Figure 3.5.   Isotherm of pseudoboehmite.

Figure 3.6.   Isotherm of eta alumina.

both ends. The pores in this material are believed to build up from more or less spherical particles and/or irregular polyhedral shapes. The radius of the cylinder of the wider part must be smaller than or equal to twice the narrow part.

In the adsorption branch, the pore is filled at a relative pressure corresponding to $2r_n$; but, during desorption the pore is emptied at relative pressure corresponding to the radii of the open ends r_n.

3.2.3 Gamma alumina

The isotherm of nine gamma aluminas shown in Figures 3.7 to 3.15 are very much alike except for FlAl. deBoer (14) states that the hysteresis loops maintain their character when the porous material is heated in a dry atmosphere. The sloping of the desorption branch is mainly due to the broad pore size distribution. The hysteresis can be interpreted by the same reasoning as given for eta alumina. The relative pressures at which hysteresis starts and ends for gamma alumina are listed in Table 3.1.

Longer calcination time and higher calcination temperature tend to start the hysteresis at a higher relative pressure even though the hysteresis ends at approximately the same relative pressure. Meanwhile pumping tends to lower the starting point for hysteresis. This implies that samples calcinated at longer time and at higher temperature develop more uniform cross sections as the pores are enlarged. Pumping creates more disorder

Table 3.1. Hysteresis of gamma aluminas

Sample	Pumping	Calcination temperature (°C)	Calcination time (hours)	Relative pressure at which hysteresis starts	ends
F1A1	no	500	24	0.65	0.88
F1A2	no	500	48	0.65	0.96
F1B1	no	700	24	0.62	0.99
F1B2	no	700	48	0.70	0.99
FA1A1	yes	500	24	0.60	0.99
FA1A2	yes	500	48	0.62	0.99
FA1B1	yes	700	24	0.64	0.99
FA1B2	yes	700	48	0.66	0.99
F2A1*	no	500	24	0.57	0.97

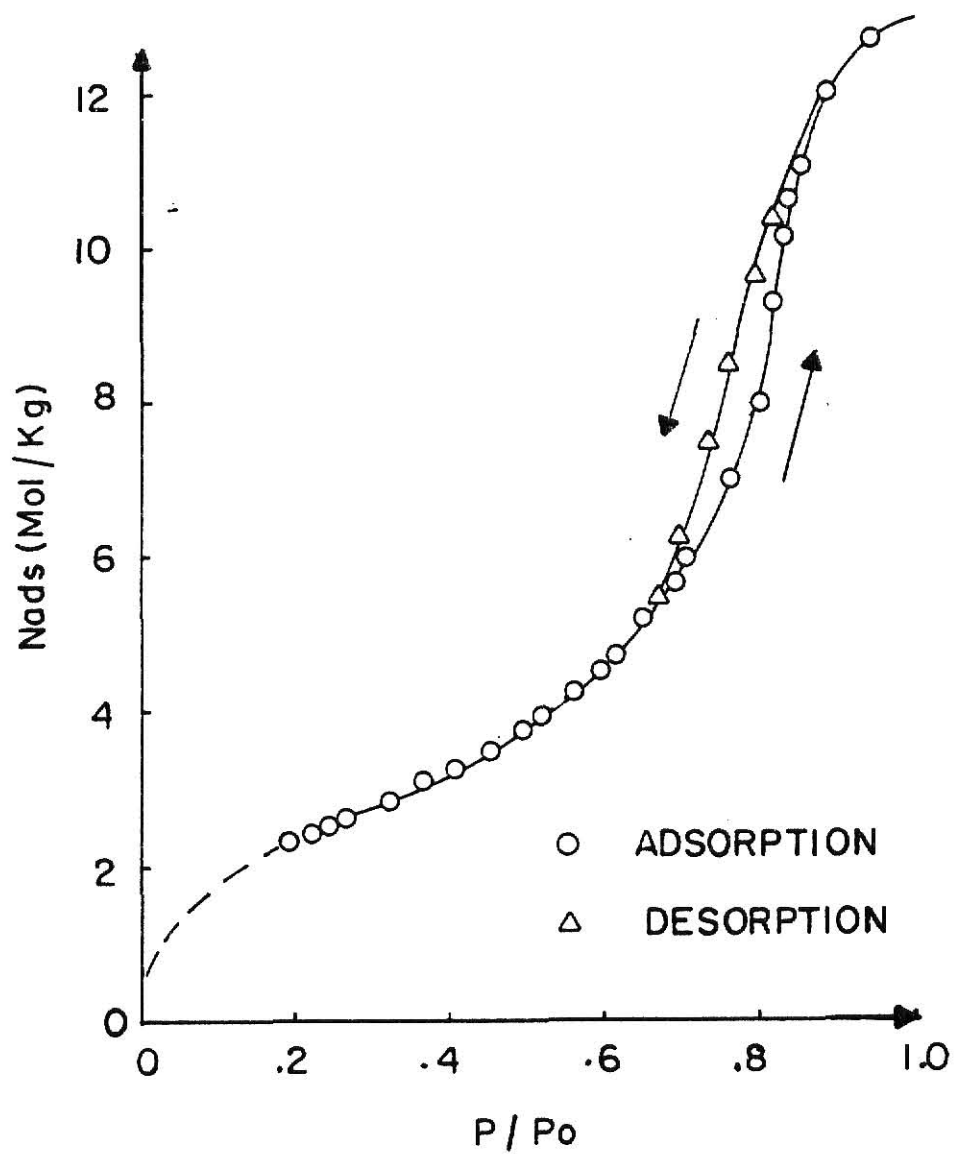*Sample aged for 96 hours.

Figure 3.7.   Isotherm of F1A1, a Gamma Alumina
              calcinated at 500°C for 24 hr without
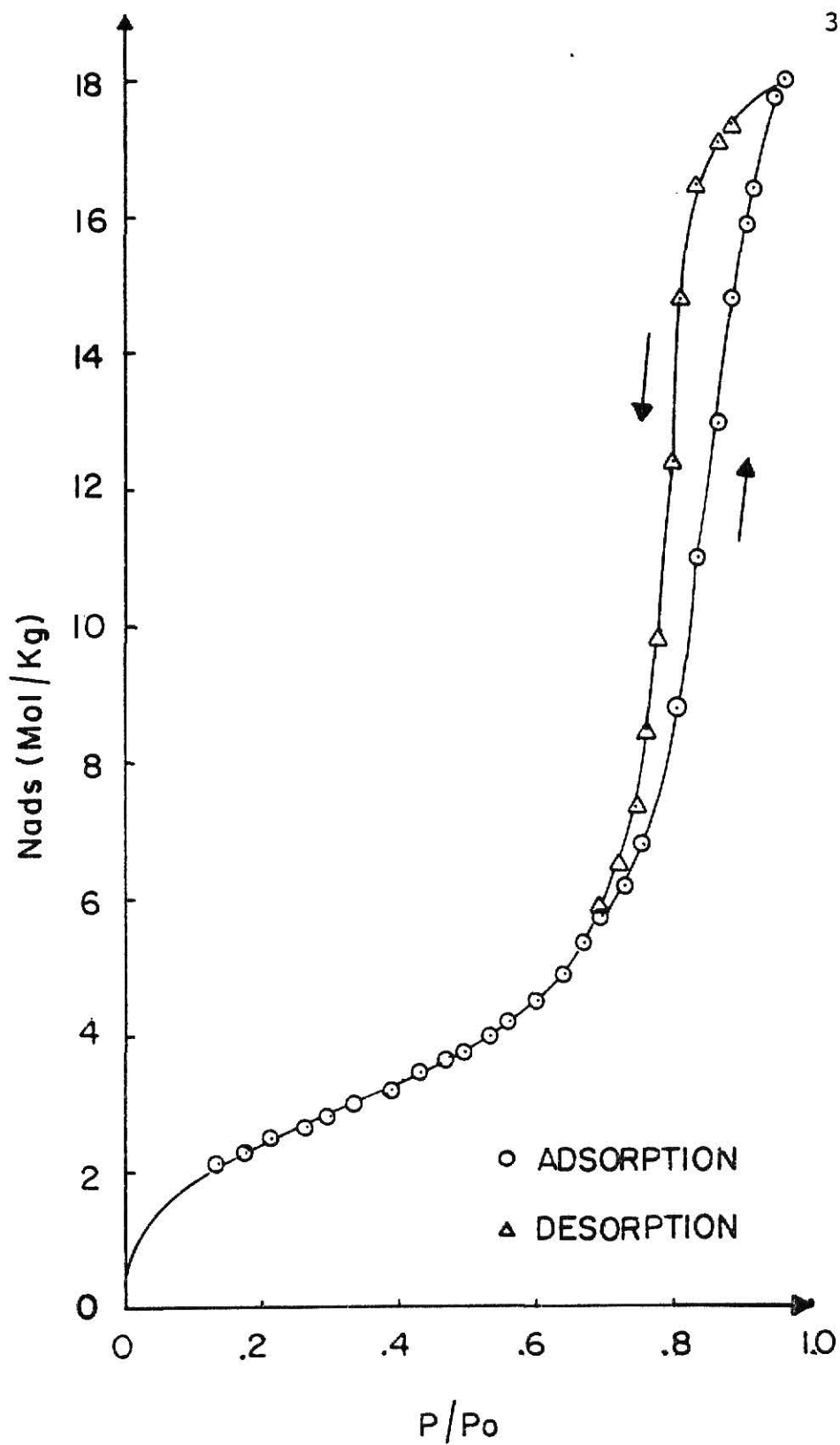   pumping.

Figure 3.8.   Isotherm of FlAl, a gamma alumina
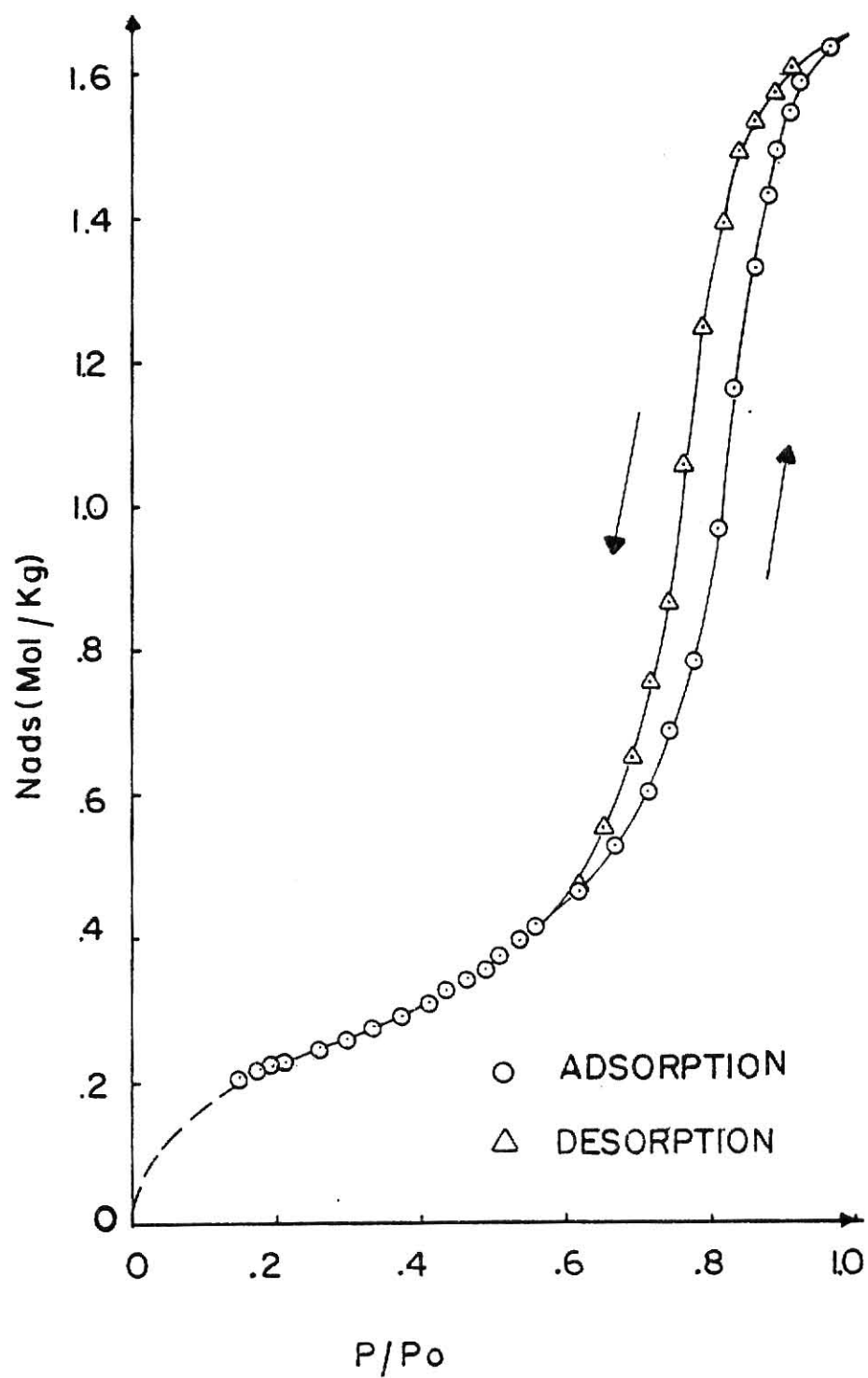calcinated at 500°C for 24 hr without
pumping.

Figure 3.9.   Isotherm of FlB1, a gamma alumina
              calcinated at 700°C for 24 hr
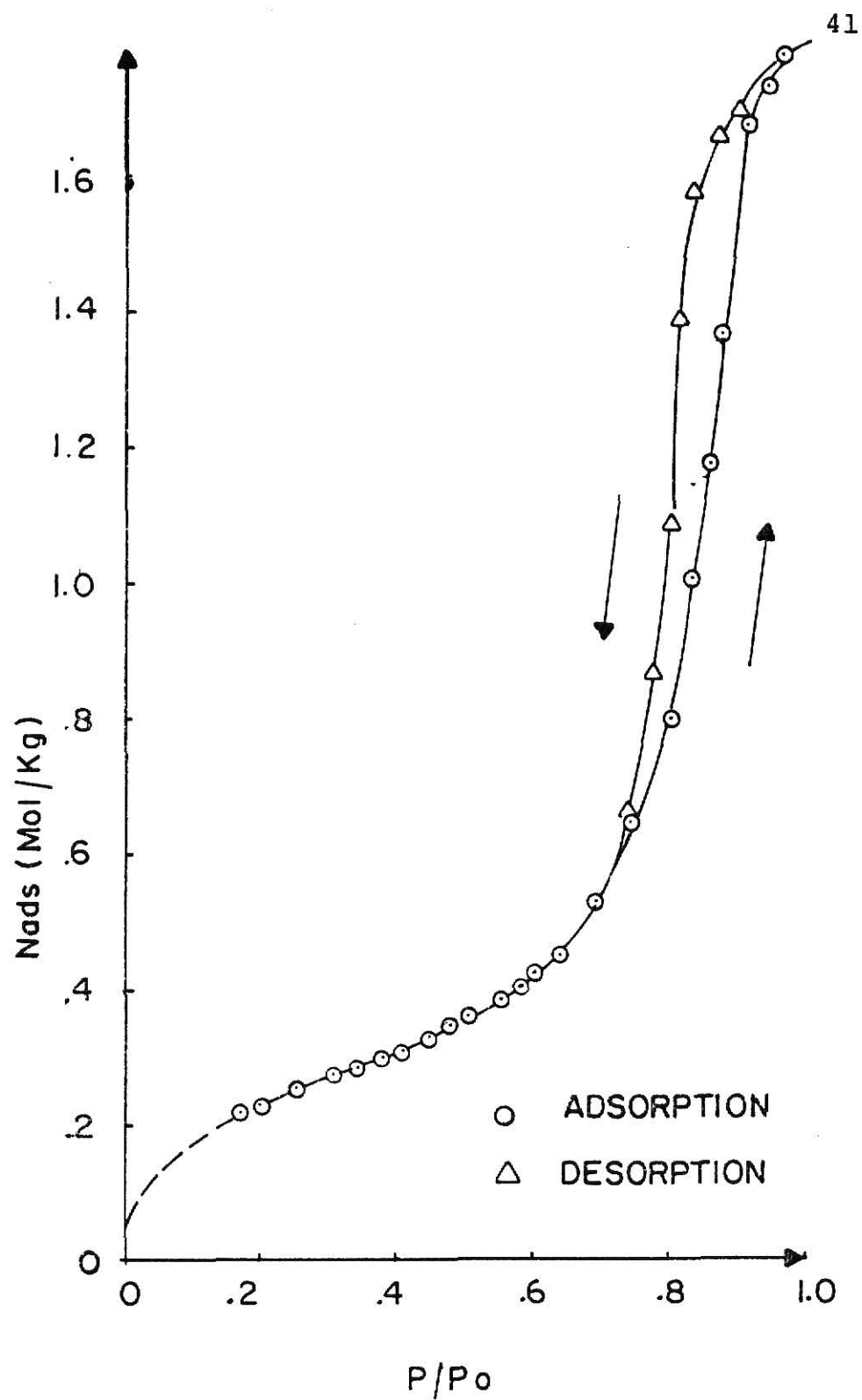   without pumping.

Figure 3.10. Isotherm of F1B1, a gamma alumina
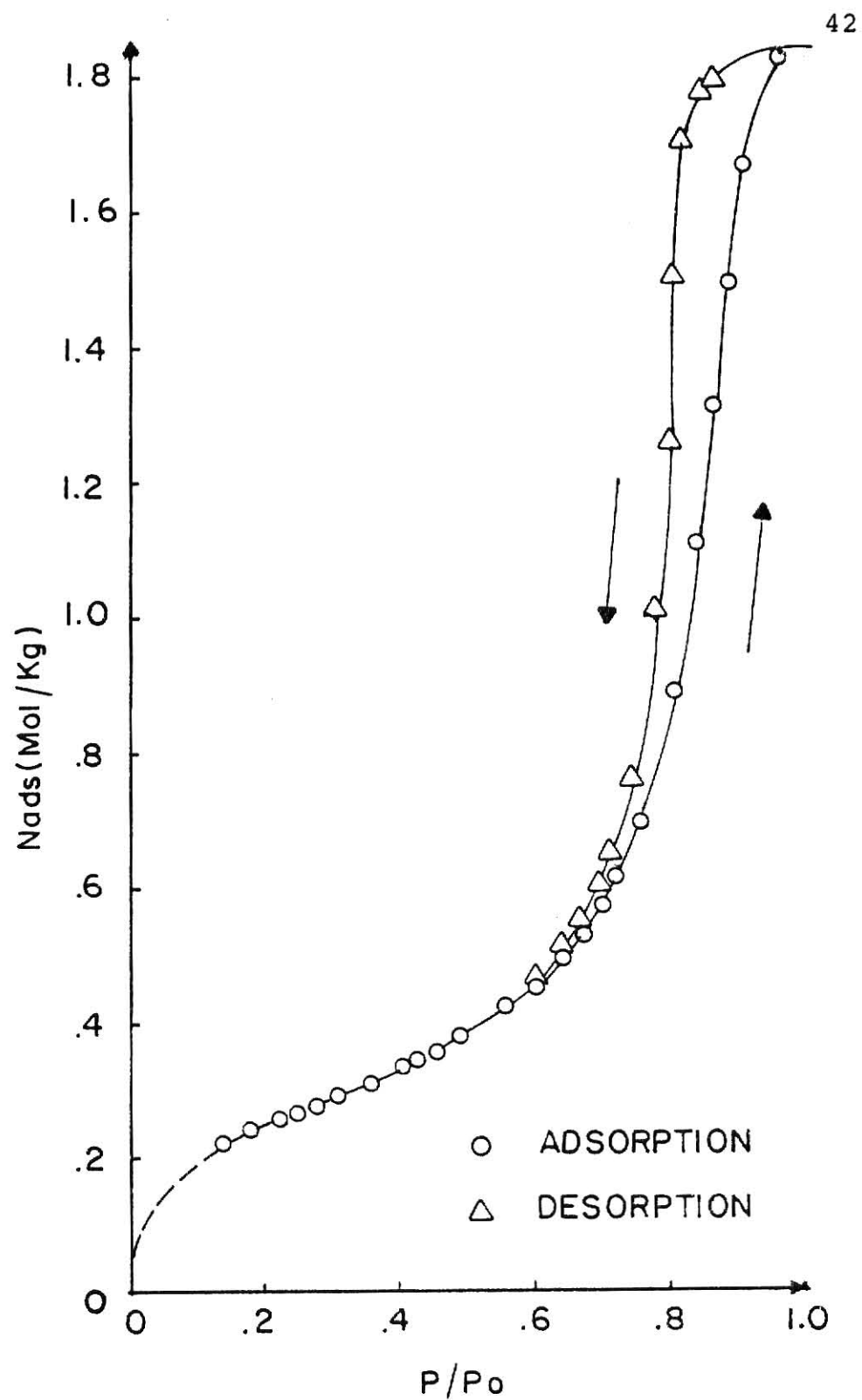calcinated at 700"C for 48 hr without
pumping.

Figure 3.11.   Isotherm of FAlAl, a gamma alumina
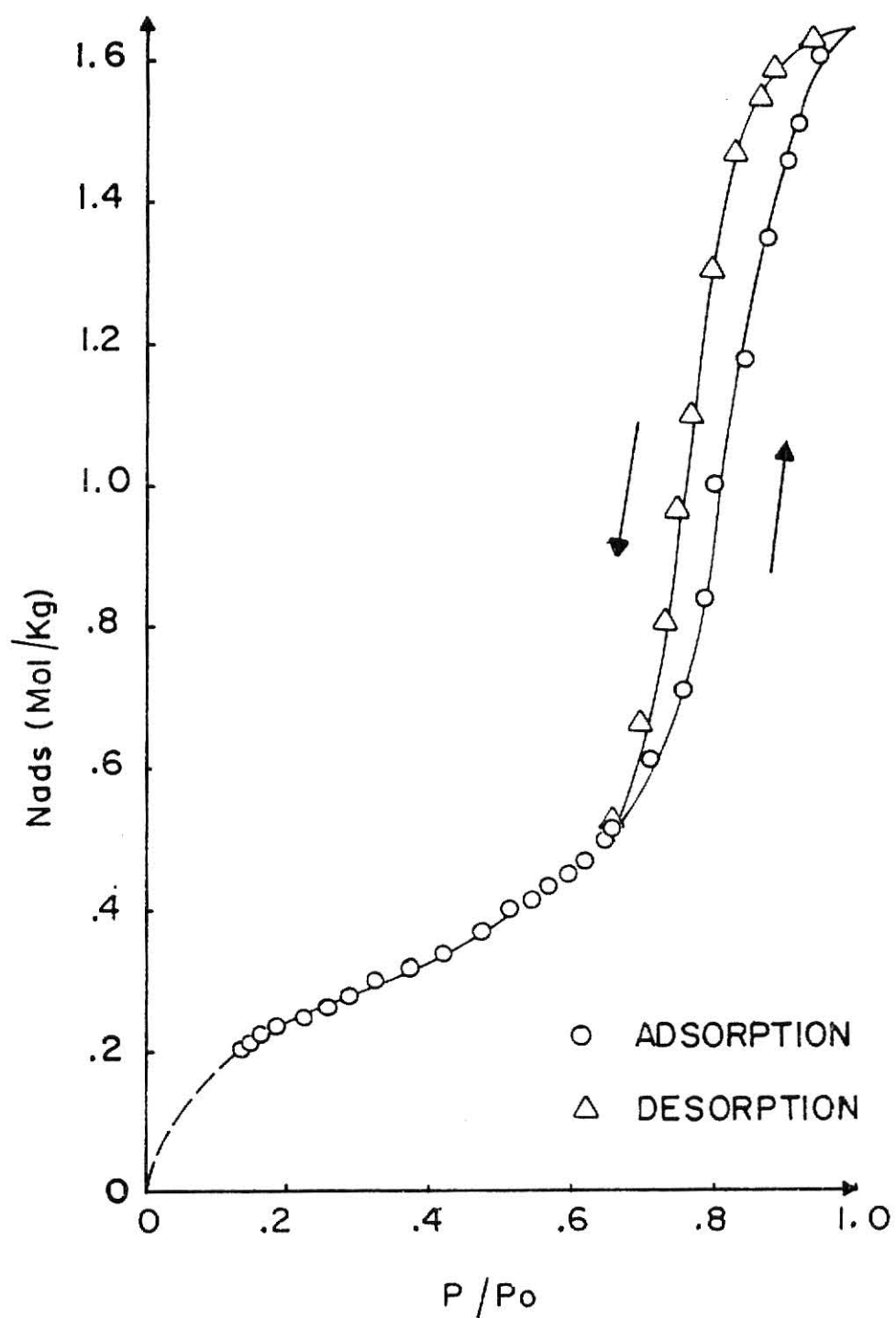calcinated at 500°C for 24 hr with
pumping.

Figure 3.12. Isotherm of FA1A2, a gamma alumina calcinated at 500°C for 48 hr with pumping.
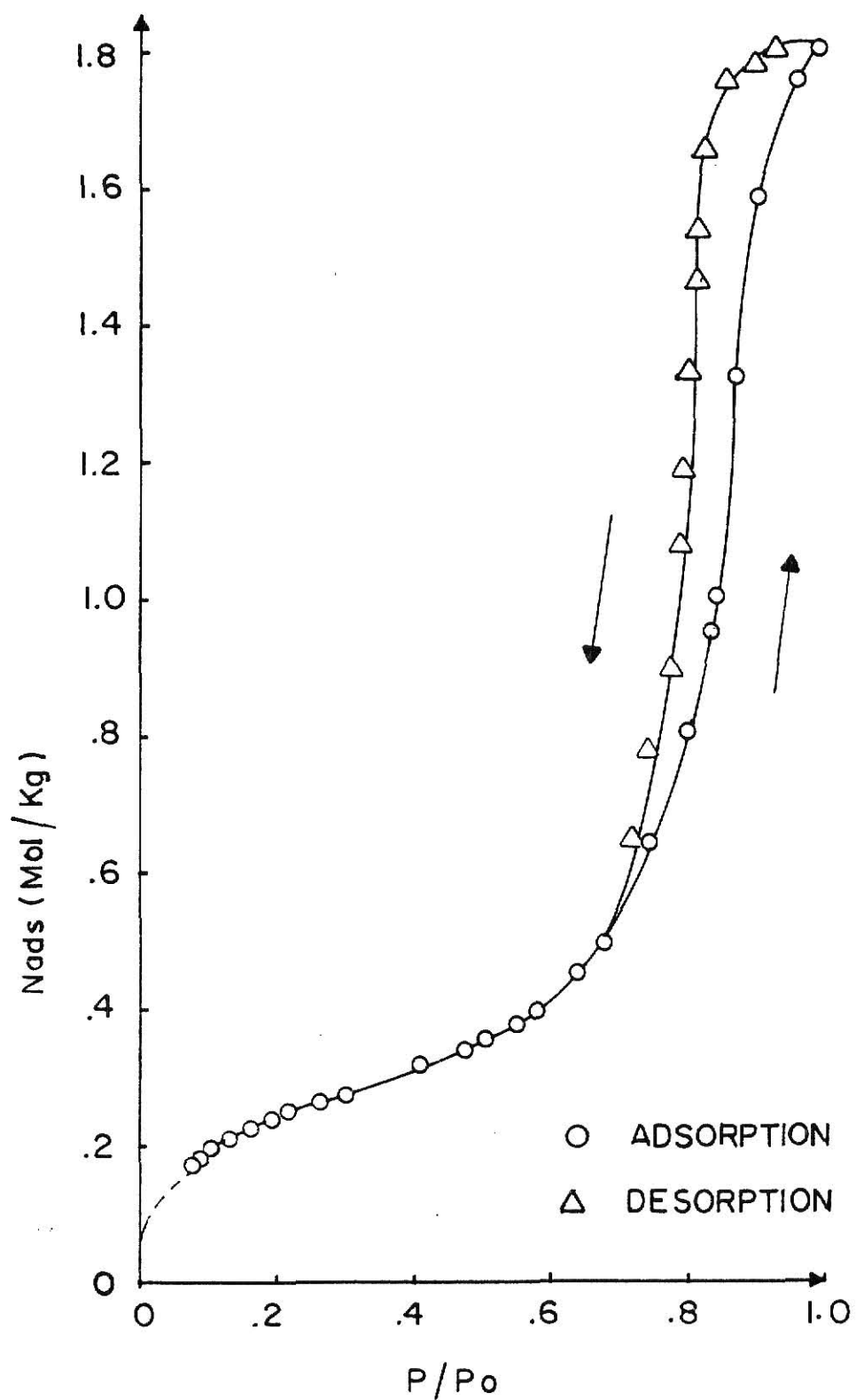
Figure 3.13. Isotherm of FA1B1, a gamma alumina calcinated at 700°C for 24 hr with pumping.
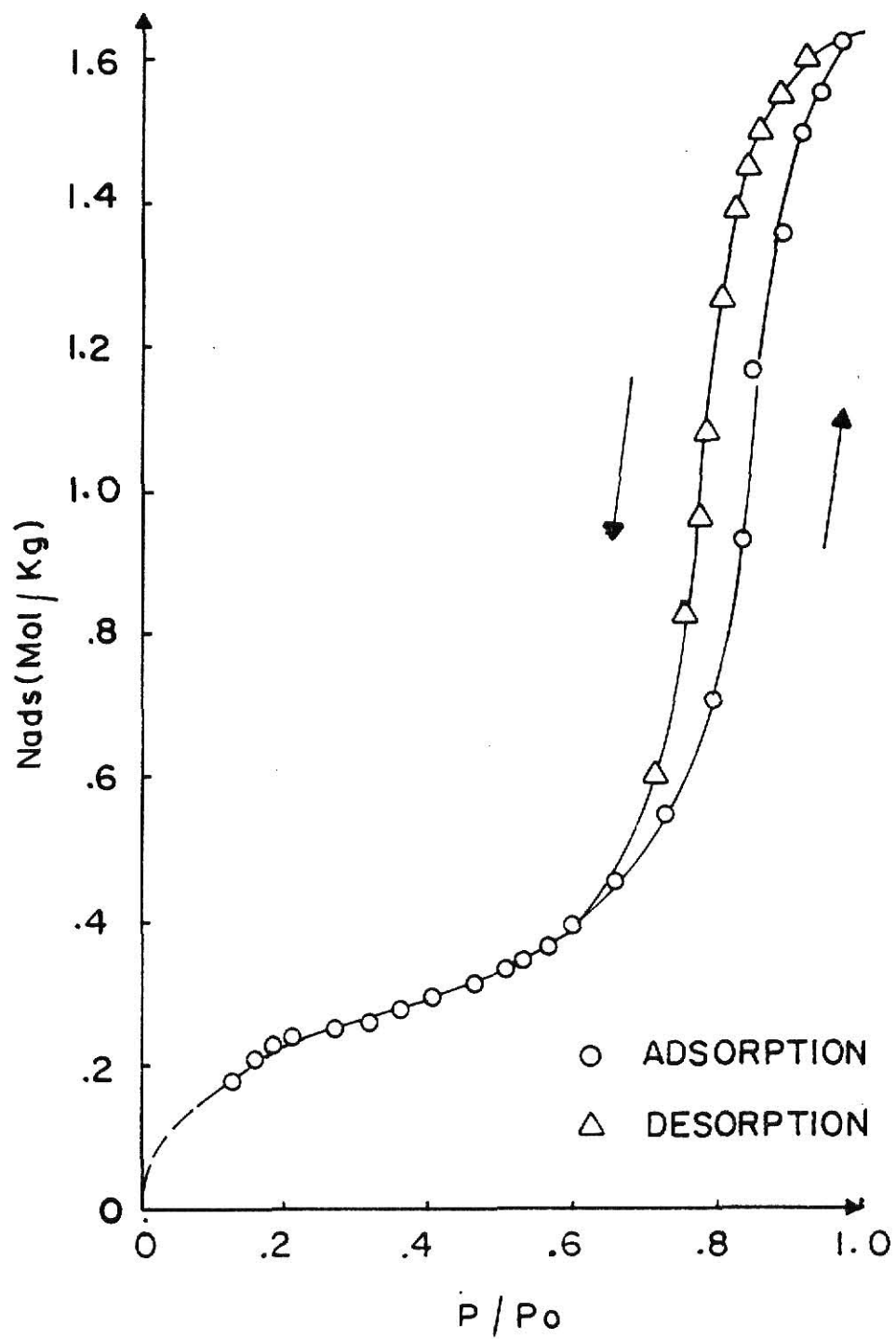
Figure 3.14. Isotherm of FA1B2, a gamma alumina
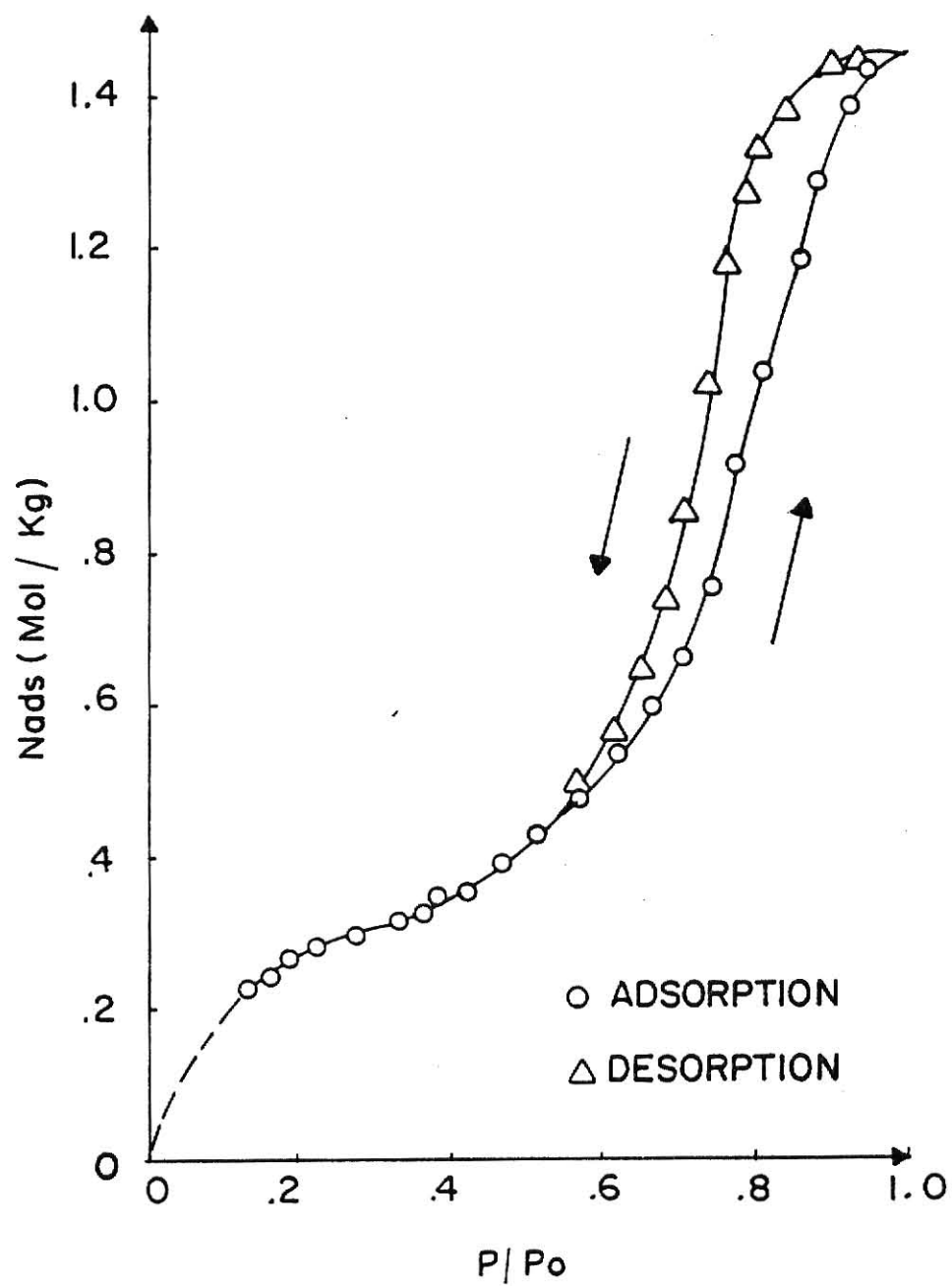calcinated at 700°C for 48 hr with
pumping.

Figure 3.15. Isotherm of F2Al, a gamma alumina aged
for 96 hr before calcinated at 500°C
for 24 hr without pumping.

and upon calcination, a larger variation in the cross section
of the pores develops.

3.3 Surface Area

Surface areas have been determined utilizing the BET
model. The final equation is

$$\frac{P}{v \, (P_O - P)} = \frac{1}{v_m \, C} + \frac{(C - 1) \, P}{v_m \, C \, P_O} \tag{5}$$

where v_m is the adsorbed volume corresponding to complete mono-
layer coverage and C is a constant. A derivation of this equa-
tion is given by Young and Crowell (15). A plot of $\frac{P}{v \, (P_O - P)}$
versus $\frac{P}{P_O}$ is a straight line with the slope

$$S = \frac{(C - 1)}{v_m \, C}$$

and Y intercept

$$I = \frac{1}{v_m \, C}$$

Eliminating C and solving for v_m yields

$$v_m = \frac{1}{S + I}$$

The BET model is for multilayer adsorption and assumes all
sites identical. The BET plot is usually applied to only a
limited range of the adsorption data, namely $0.05 \leqslant P/P_O \leqslant 0.35$.
Above $P/P_O = 0.35$ the model fails because of condensation in
the pores. Below $P/P_O = 0.05$ the model fails because the ad-
sorbed volume cannot be accurately determined. The BET plots
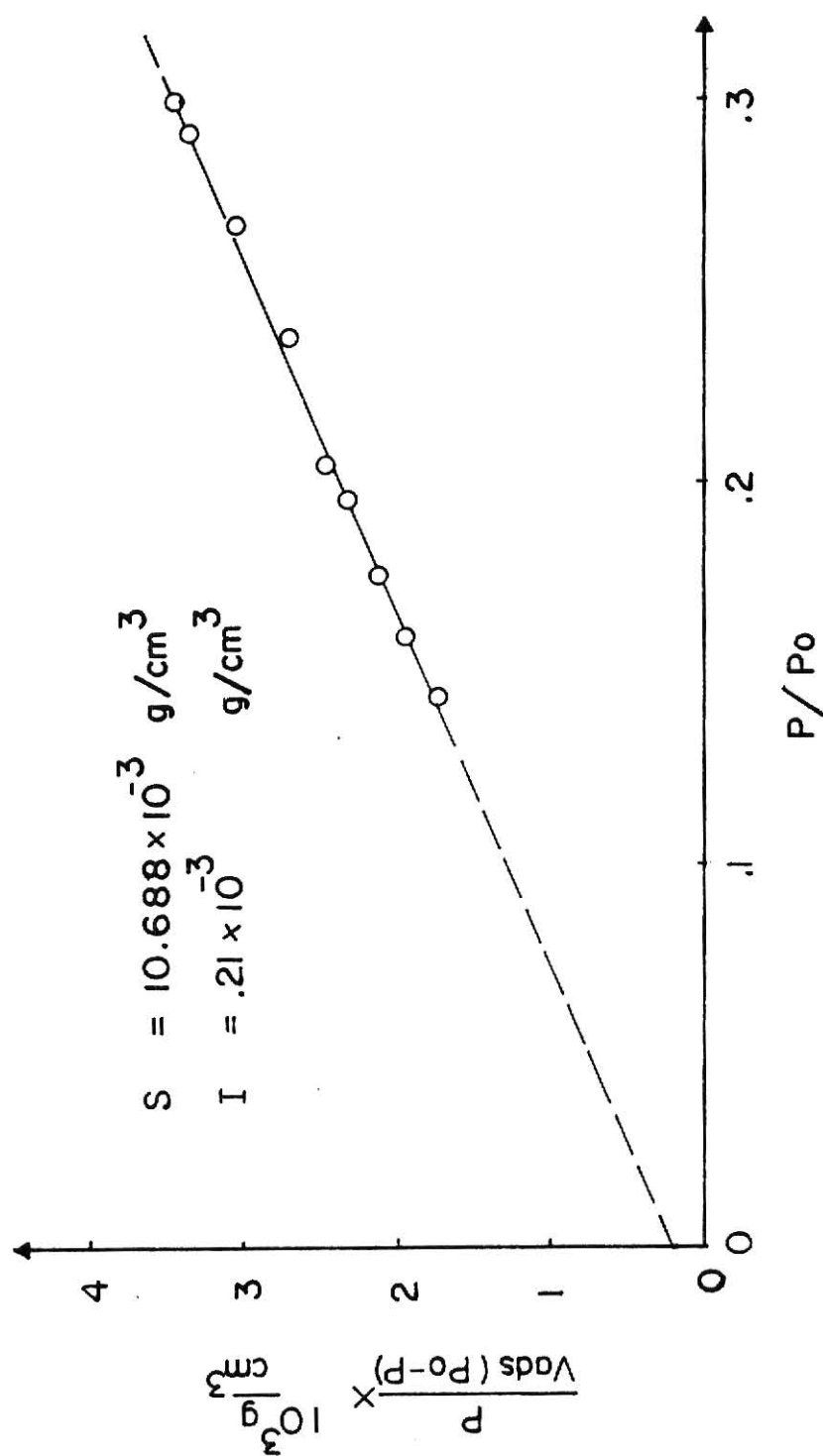
Figure 3.16. BET plot of pseudoboehmite.

49
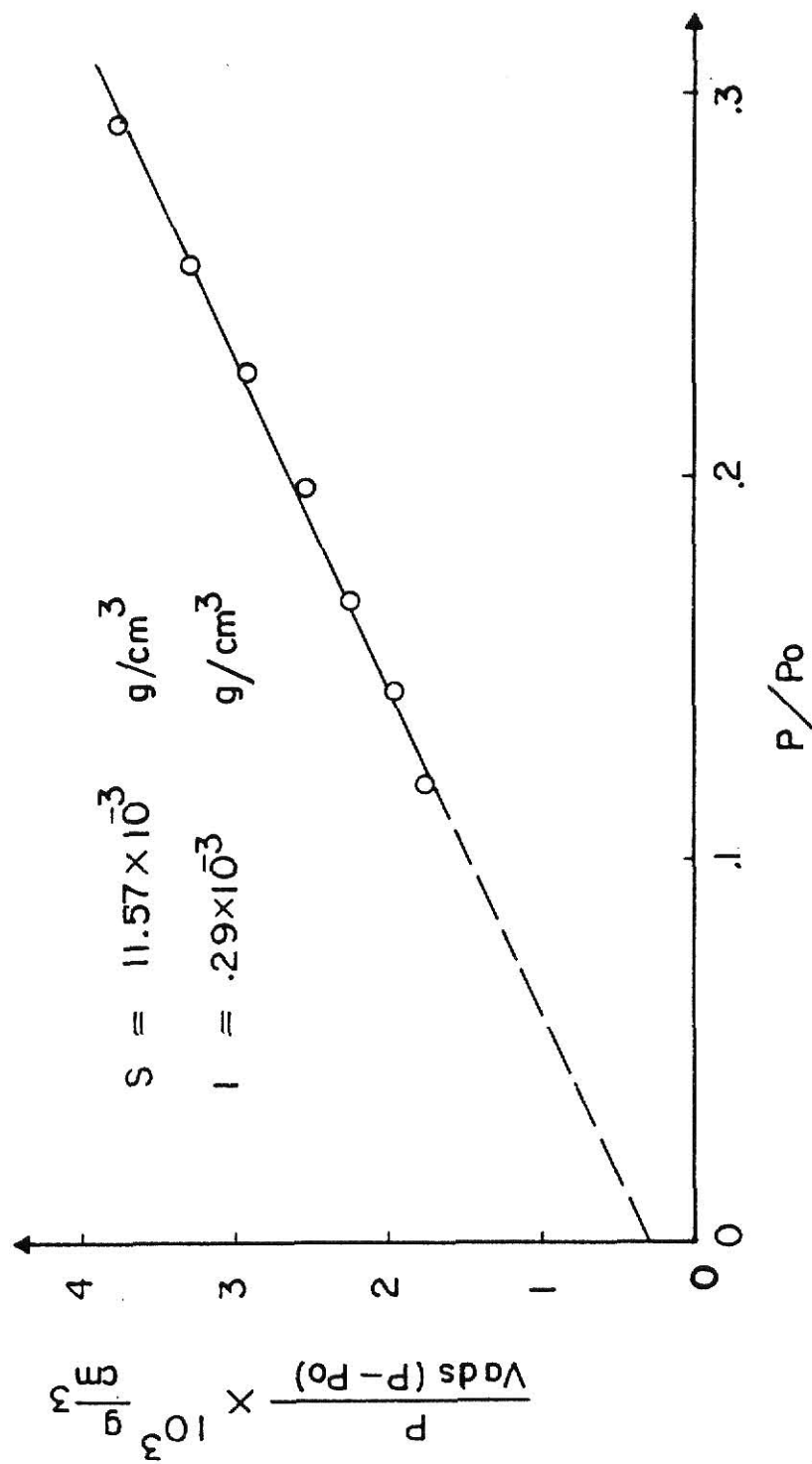
Figure 3.17. BET plot of eta alumina.

Figure 3.18. BET plot of F1Al, a gamma alumina calcinated at 500°C for 24 hr without pumping.

BET plot of F1A2, a gamma alumina calcinated at 500°C for 48 hr without pumping.

$$S = 14.39 \times 10^{-3} \frac{g}{cm^3}$$

$$I = .28 \times 10^{-3} \frac{g}{cm^3}$$

$$\frac{P}{V_{ads}(P_o \, P)} \times 10^3 \frac{g}{cm^3}$$

P/P_o

Figure 3.19.

Figure 3.20. BET plot of F1B1, a gamma alumina calcinated at 700°C for 24 hr without pumping.

Figure 3.21. BET plot of F1B2, a gamma alumina calcinated at 700°C for 48 hr without pumping.

$S = 13.59 \times 10^3 \quad \dfrac{g}{cm^3}$

$I = .23 \times 10^3 \quad \dfrac{g}{cm^3}$
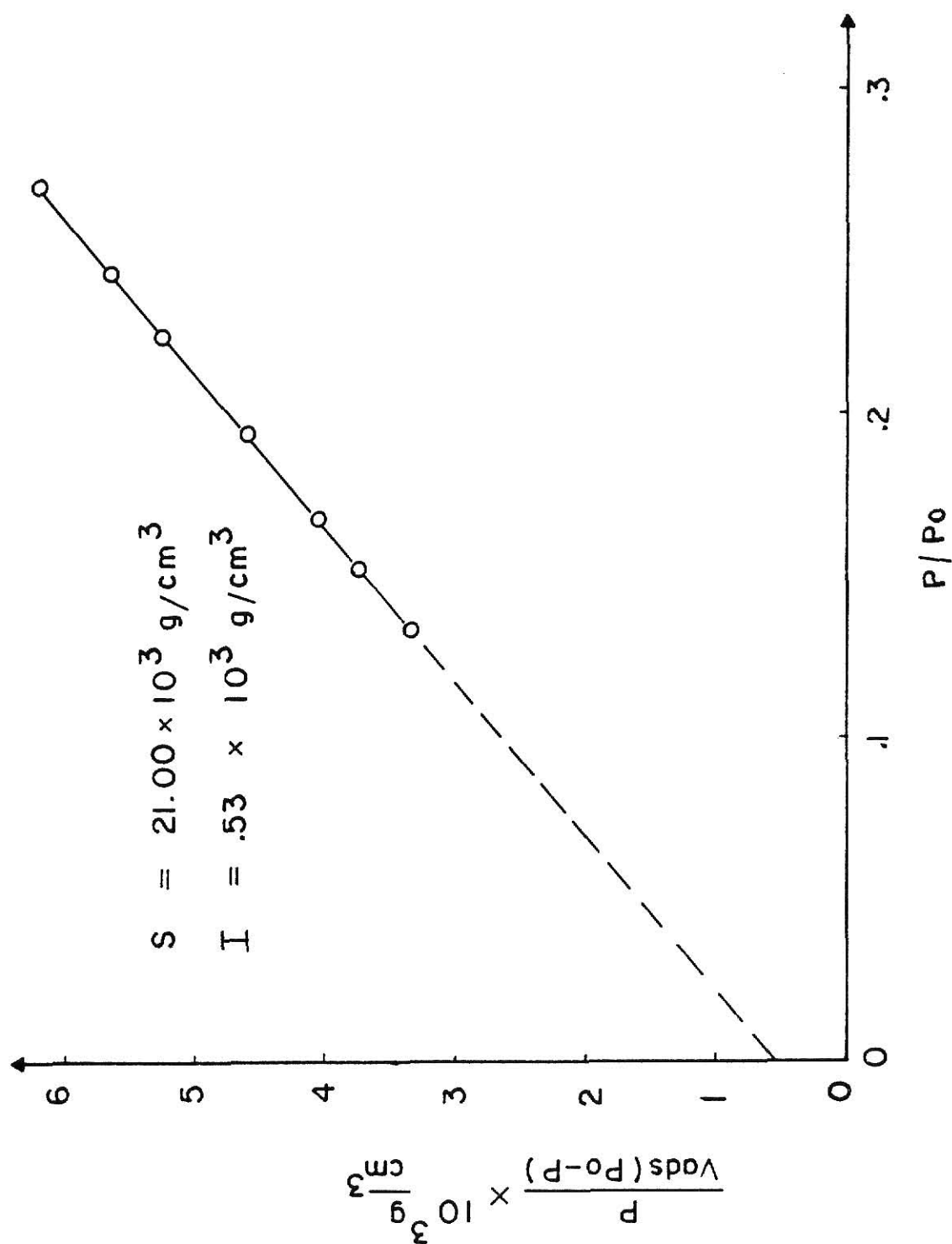
Figure 3.22. BET plot of FAlAl, a gamma alumina calcinated at 500°C for 24 hr with pumping.

Figure 3.23. BET plot of FA1A2, a gamma alumina calcinated at 500°C for 48 hr. with pumping.

$$S = 13.94 \times 10^{-3} \quad \frac{g}{cm^3}$$

$$I = .20 \times 10^{-3} \quad \frac{g}{cm^3}$$

Figure 3.24. BET plot of FAlB1, a gamma alumina calcinated at 700°C for 24 hr with pumping.

$$S = 14.98 \times 10^{\bar{3}} \quad g/cm^3$$

$$I = .25 \times 10^{\bar{3}} \quad g/cm^3$$

P/Po
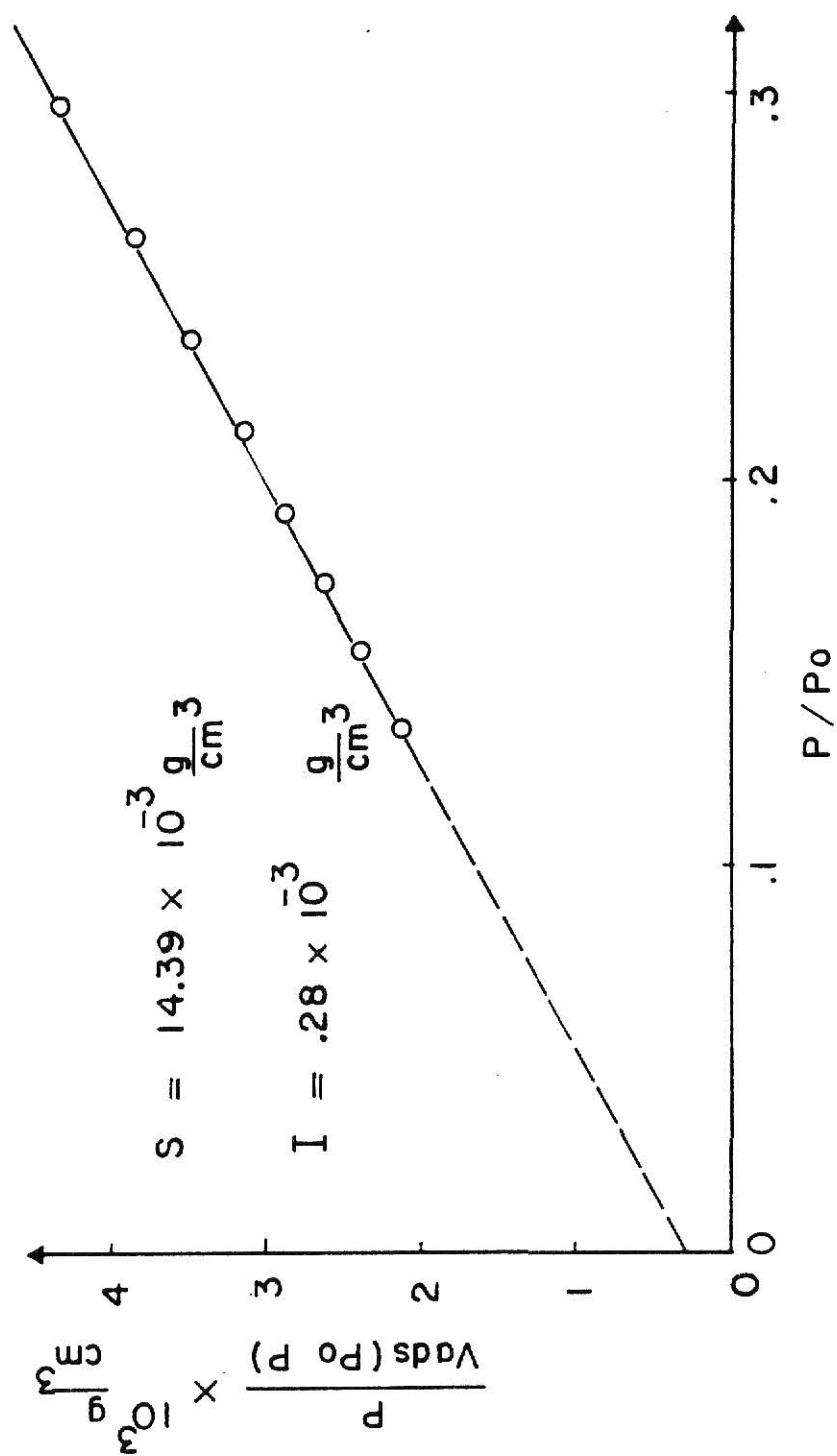
$$\frac{P}{Vad's \, (P_o-P)} \times 10^3 \, \frac{g}{cm^3}$$
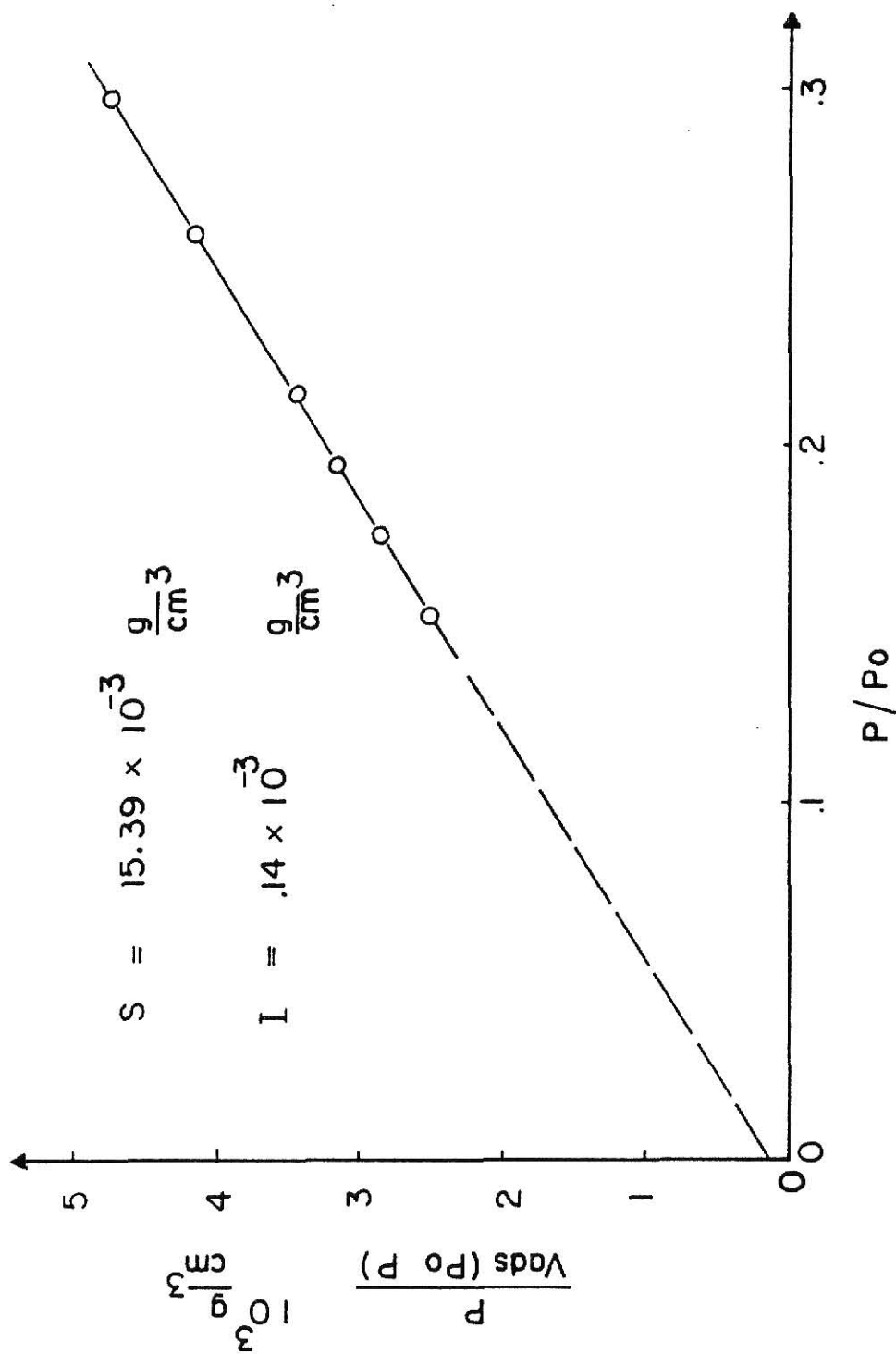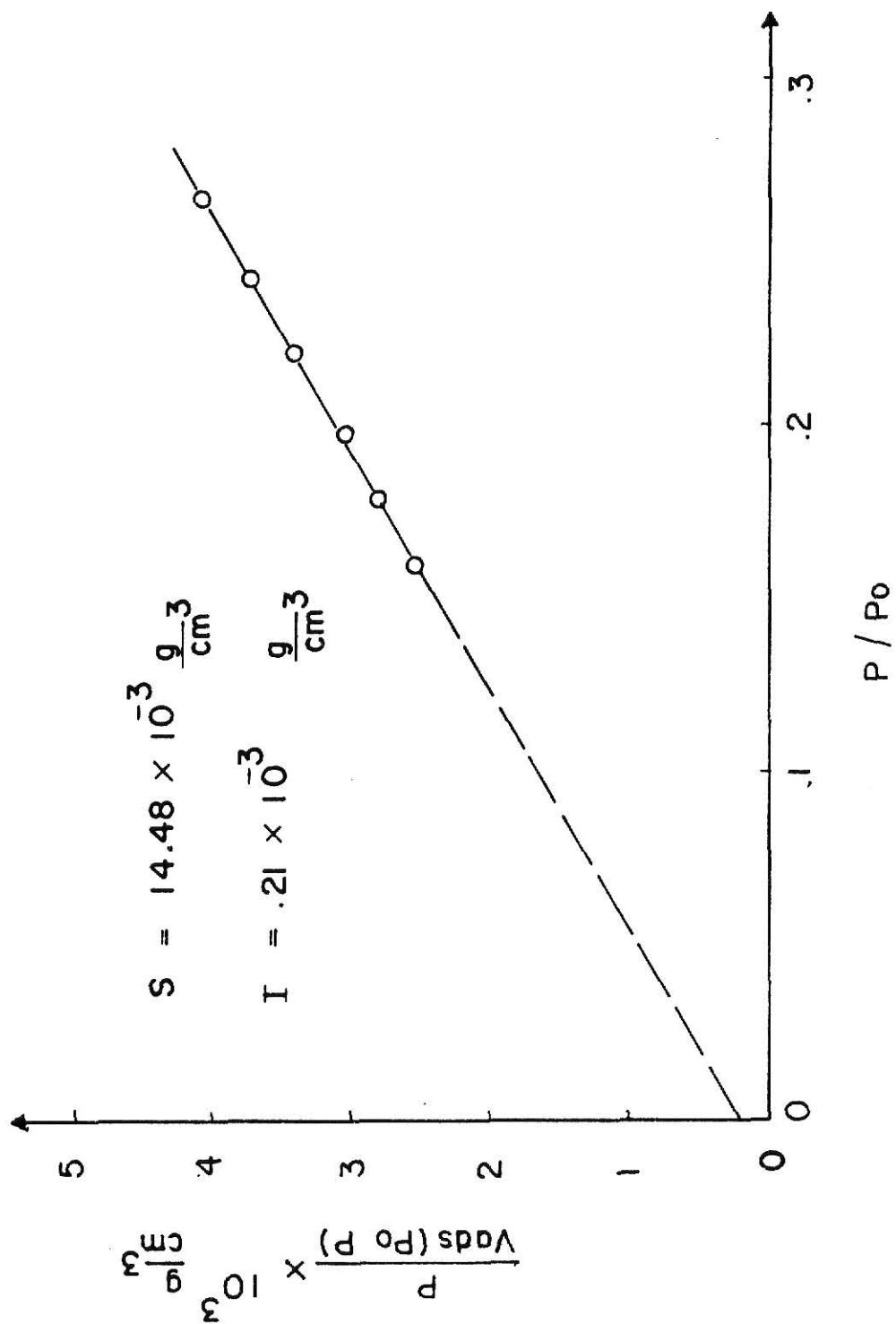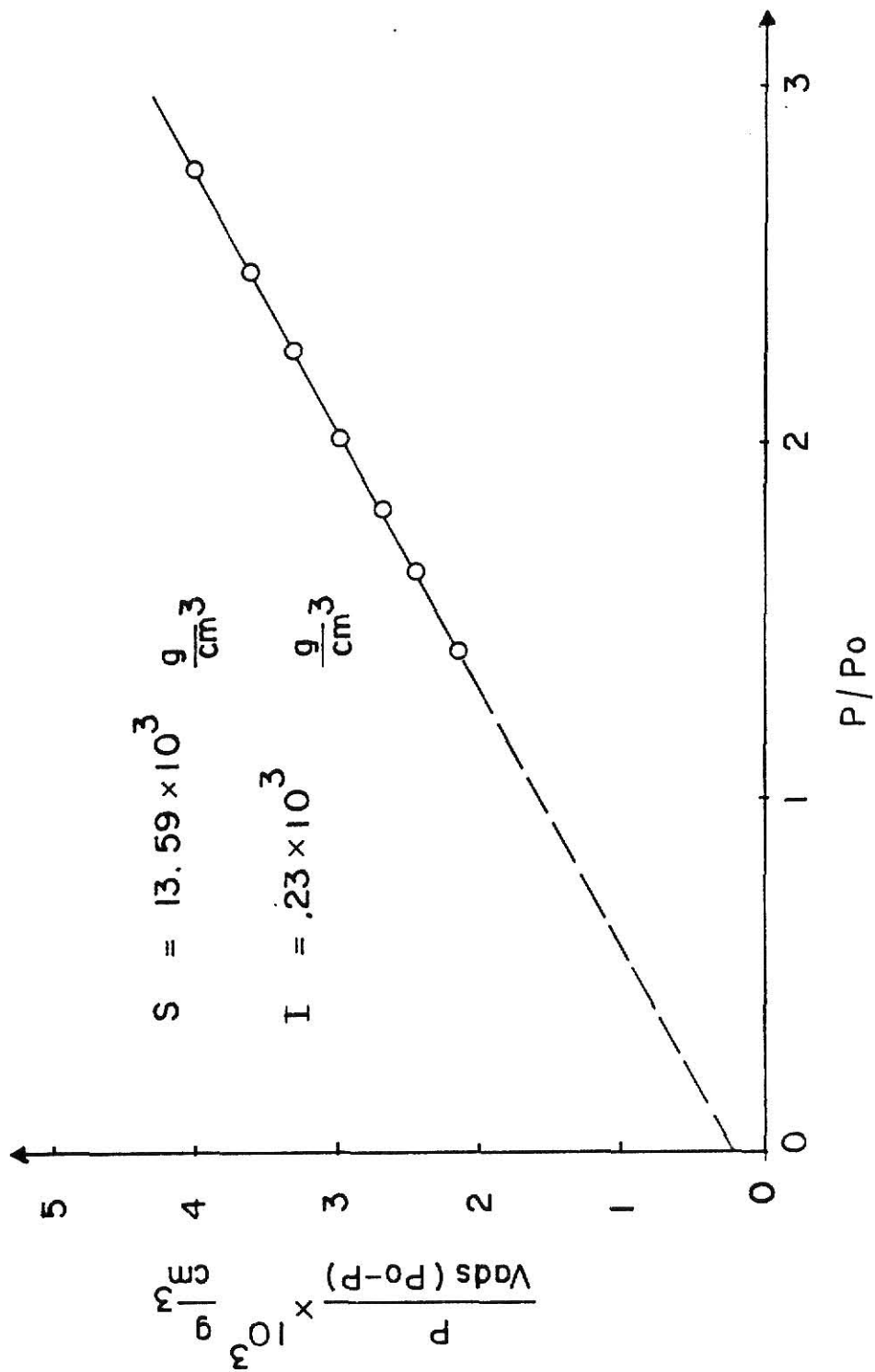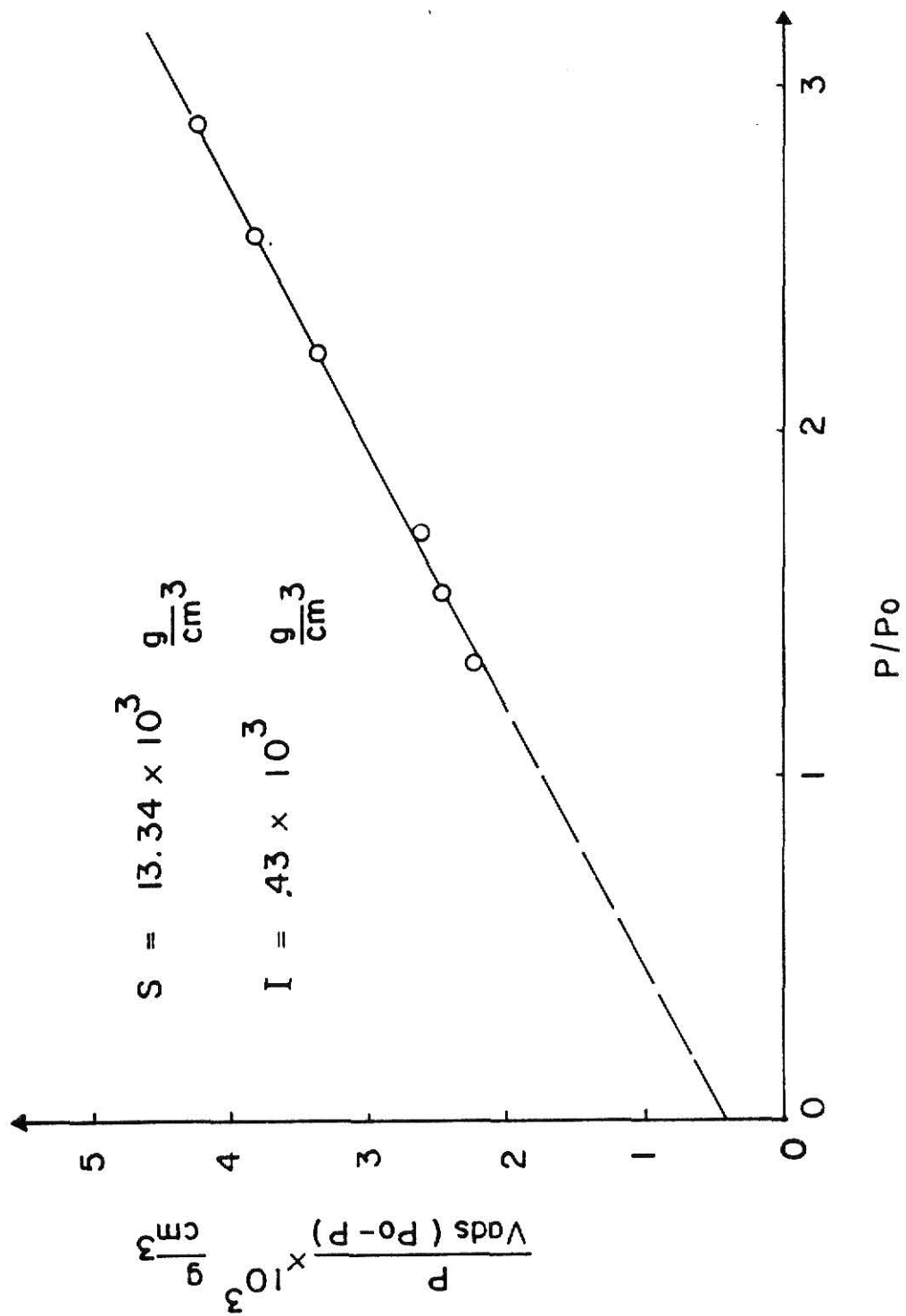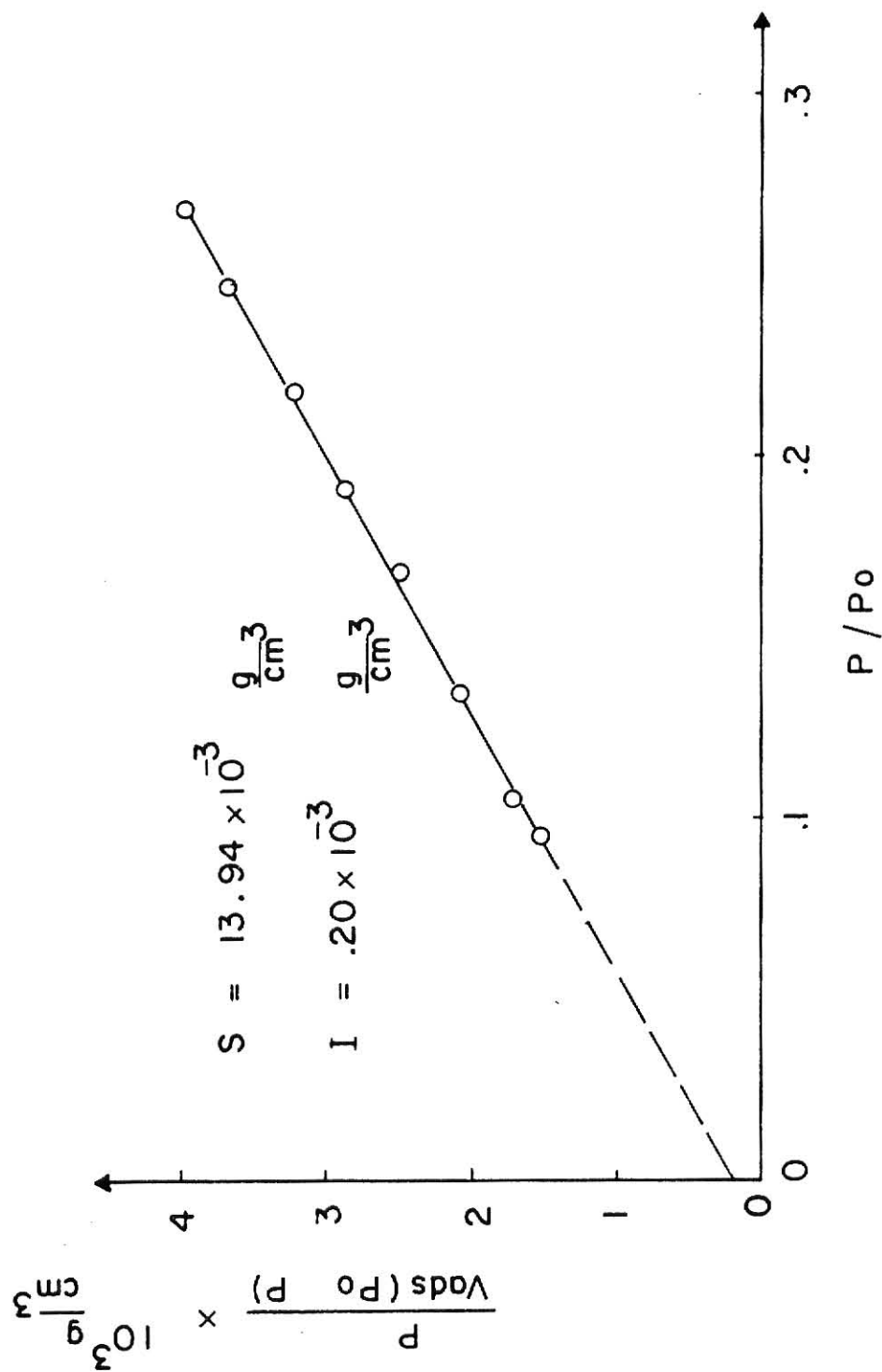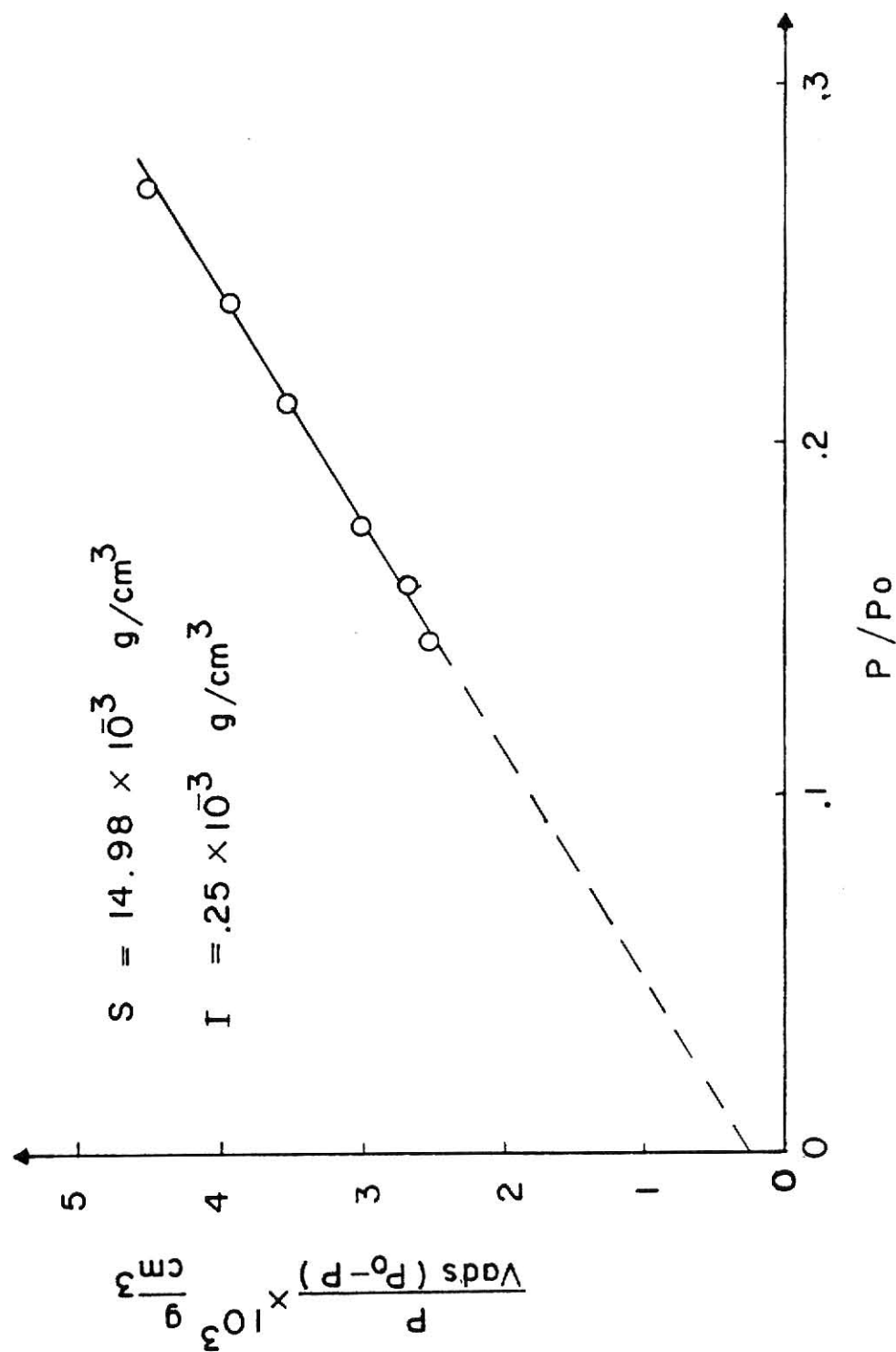
Figure 3.25. BET plot of FA1B2, a gamma alumina calcinated at 700°C for 48 hr with pumping.
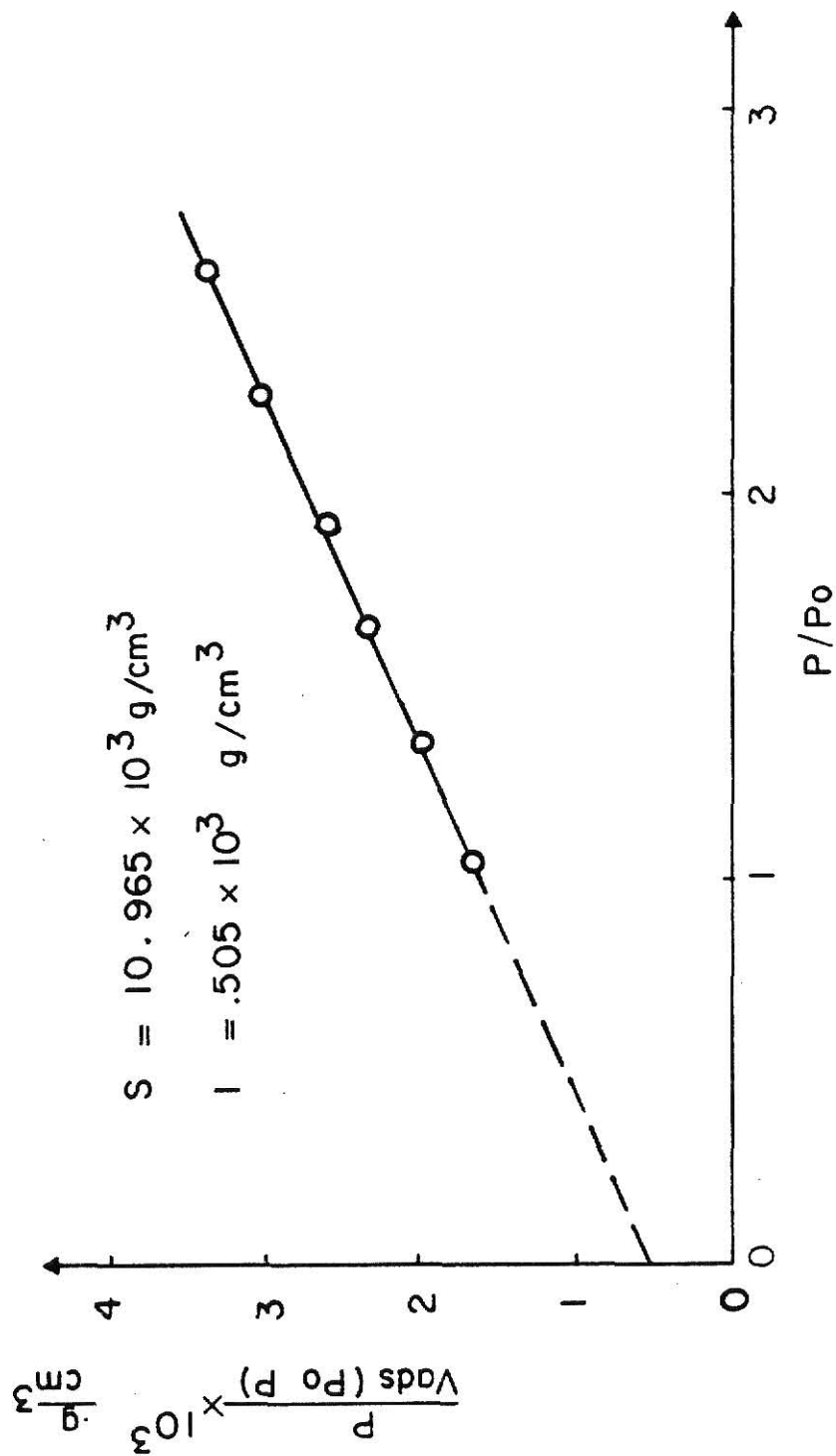
Figure 3.26. BET plot of F2Al, a gamma alumina aged at 80°C for 96 hr before calcinated at 500°C for 24 hr without pumping.

Once v_m has been determined, the number of molecules corresponding to monolayer coverage can be calculated and then using the area per adsorbed molecule the surface area can be calculated. For nitrogen at liquid nitrogen temperature, the area per adsorbed molecule is 16.2 $\overset{o}{A}^2$ which corresponds to 4.37 cm^2 of surface per cm^3 (STP) adsorbed. The surface area results from this work are shown in Table 3.2.

3.4 Pore size distribution

Obtaining pore size distribution from actual volume adsorbed versus pressure data is somewhat more complicated than described in 3.1. The problem is that multilayer adsorption is occurring as well as condensation. Thus the total volume adsorbed for a given increase in pressure cannot be attributed solely to condensation in a particular pore size. Similarly, when the pressure is lowered not all of the desorbed volume can be attributed to vaporization from a particular pore size. There is additional desorption of the multilayers from pores where vaporization had occurred at higher pressure.

The approach used here was developed by Lippens et al (16). The Kelvin equation for cylindrical pores can be written

$$\ln x = \ln \left(\frac{P}{P_o} \right) = \frac{-2v_1\gamma}{R_g\, r_k} \tag{6}$$

v_1 is the molecular volume of the adsorbed liquid nitrogen, T is the boiling temperature of liquid nitrogen, R_g is the gas constant, γ is surface tension of liquid nitrogen, and r_k is called the Kelvin radius. Substituting the properties of liquid

Table 3.2. Surface area of different aluminas

Sample	Pumping	Calcination temperature (°C)	Calcination time (hours)	Surface area (m^2/g)
Pseudo-boehmite				399
Eta alumina				368
F1A1	no	500	24	203
F1A2	no	500	48	298
F1B1	no	700	24	181
F1B2	no	700	48	297
FA1A1	yes	500	24	316
FA1A2	yes	500	48	317
FA1B1	yes	700	24	309
FA1B2	yes	700	48	387
F2A1*	no	500	24	381

*Sample aged for 96 hours.

nitrogen: $\gamma = 8.72$ dynes/cm; $v_1 = 34.68$ cm^3/gmole. The equation (6) can be written as

$$r_k = - \frac{7.2748 \times 10^{-6}}{T \ln x} \quad cm$$

However, at each relative pressure the wall film remaining contains n layers. Thus, the real radius, denoted by r_p is the summation of the Kelvin radius and the thickness of the adsorbed layers, t.

$$r_p = r_k + t$$

The computation begins with the sample at equilibrium at pressure P_1 near P_o, the vapor pressure of liquid nitrogen. Let i denote the ith step. $x_i + \Delta x$ and $x_i - \Delta x$ are the upper and lower relative pressures of this increment; $t(x_i + \Delta x)$ and $t(x_i - \Delta x)$ are respective thicknesses of the adsorbed layers; and $r_p(x_i + \Delta x)$ and $r_p(x_i - \Delta x)$ are respective radii; $\Delta S(x_i)$ is the surface area of pores not filled with liquid nitrogen, and bars denote average value over the increment in question.

For all desorption increments after the first , the desorption volume increment comes from two different sources: 1) pores that empty as pressure decreases, and 2) the decrease in film thickness of pores that were already empty. As the pressure decreases from $x_i + \Delta x$ to $x_i - \Delta x$, all liquid nitrogen but the $t(x_i - \Delta x)$ layers is evaporated to give a volume equal to

$$(r_{pi} - t(x_i - \Delta x)) \, S(x_i)$$

The volume that comes from the decrease of the thickness of the adsorbed layer in the pores, which have already emptied at a higher pressure than $x_i + \Delta x$, is equal to

$$(t(x_i + \Delta x) - t(x_i - \Delta x)) \quad \Sigma \Delta S(x_{i-1})$$

Thus the adsorbed volume increment can be written

$$X_i = X(x_i + \Delta x) - X(x_i - \Delta x)$$

$$= (\overline{r}_{pi} - t(x_i - \Delta x)) \, S(x_i)$$

$$+ (t(x_i + \Delta x) - t(x_i - \Delta x)) \, \Sigma \Delta S(x_{i-1}) \qquad (8)$$

This equation contains two unknown variables $S(x_i)$ and $\Sigma \Delta S(x_{i-1})$. However, since $\Delta S(x_1) = 0$, $S(x_2)$ can be obtained from equation (8). The volume of liquid nitrogen in the pores at any pressure $x_i - \Delta x$ is then defined as

$$X(x_i - \Delta x) = V(x_i - \Delta x) + \Sigma \Delta S(x_i) \, t(x_i - \Delta x)$$

where

$$V(x_i - \Delta x) = \text{pore volume of pores corresponding} \\ \text{to pressure less than } x_i - \Delta x$$

Thus the corrected pore volume at any point can be calculated using the equation

$$V(x_i - \Delta x) = X(x_i - \Delta x) - t(x_i - \Delta x) \, \Sigma \Delta S(x_i).$$

The pore size distribution curve can be obtained by differentiating the plot of pore volume versus radius.

In this study, the value of the thickness of the adsorbed layers given by Lippens and deBoer (16) are used to calculate

pore volume. These values as a function of relative pressure are shown in Figure 3.27.

A computer program was written to calculate the corrected cumulative pore volume and pore size distribution. The inputs are the amount of nitrogen adsorbed and the thickness of adsorbed layers at several relative pressures. The output are the corrected cumulative pore volume at several pore radii and the pore size distribution.

The computer program is shown on the following pages. The important symbols are

DENSL = density of liquid nitrogen at one atmosphere

CONST = 0.13746×10^6

TEMP = liquid nitrogen boiling point

FRX(I) = relative pressure

ADS(I) = mole N_2 adsorbed at FRX(I)

T(I) = thickness of adsorbed layers at FRX(I)

AVERP(I) = mean real radius between FRX(I-1) and FRX(I)

VOLPOR(I) = pore volume at FRX(I)

Z(I) = d VOLPOR(I)/ d AVERP(I)

The pore size distribution of the sample pseudoboehmite, eta alumina and nine gamma alumina prepared by different conditions were calculated in this study. The results are shown in Figure 3.28 to 3.38. A summary of surface areas, pore volumes and pore sizes is shown in Table 3.3.

3.5 Discussion

Emphasis in this work has been primarily on the effects of temperature of calcination, time of calcination and of

```
      DIMENSION FRX(50),ADS(50),T(50),X(50),RK(50),RP(50),VOLPOR(50),
     *SUMS(50),SUDEV(50),DELTX(50),AVERP(50),DELTS(50),DELTV(50),
     *GNAVR(50),ANAVR(50),Z(50),
      READ,DENSL,CONST
      READ,TEMP,N
      I=0
    1 I=I+1
      READ,FRX(I),ADS(I),T(I)
      X(I)=ADS(I)*DENSL
      RK(I)=0.-1./CONST/TEMP/ALOG(FRX(I))
      T(I)=T(I)*.1E-9
      RP(I)=RK(I)+T(I)
      IF(I-1)2,2,3
    2 VOLPOR(I)=X(I)
      AVERP(I)=(RP(I)+RP(I-1))/2.
      GNAVR(I)=ALOG(AVERP(I))
      ANAVR(I)=ALOG(AVERP(I)/.1E-9)
      DELTS(I)=(DELTX(I)-(T(I-1)-T(I))*SUMS(I-1))/(AVERP(I)-T(I))
      SUMS(I)=SUMS(I-1)+DELTS(I)
      VOLPOR(I)=X(I)-SUMS(I)*T(I)
      IF(I-N)1,30,30
   30 CALL DGT3(GNAVR,VOLPOR,Z,N,IER)
      DO 60 I=1,N
      WRITE(6,50) AVERP(I),VOLPOR(I),Z(I),ANAVR(I)
   50 FORMAT('0',4(3X,E13.6))
   60 CONTINUE
      STOP
      END

      SUBROUTINE DGT3(X,Y,Z,NDIM,IER)
      DIMENSION X(50),Y(50),Z(50)
      IER=-1
      IF(NDIM-3)8,1,1
    1 A=X(1)
      B=Y(1)
      I=2
      DY2=X(2)-A
      IF(DY2)2,9,2
    2 DY2=(Y(2)-B)/DY2
      DC 6 I=3,NDIM
      A=X(I)-A
      IF(A)3,9,3
    3 A=(Y(I)-B)/A
      B=X(I)-X(I-1)
      IF(B)4,9,4
    4 DY1=DY2
      DY2-(Y(I)-Y(I-1))/B
      DY3=A
      A=X(I-1)
      B=Y(I-1
      IF(I-3)5,5,6
```

```
5 Z(I)=DY1+DY3-DY2
6 Z(I-1)=DY1+DY2-DY3
  IER=0
  I=NDIM
7 Z(I)=DY2+DY3-DY1
8 RETURN
9 IER=1
  I=I-1
  IF(I-2)8,8,7
  END
```

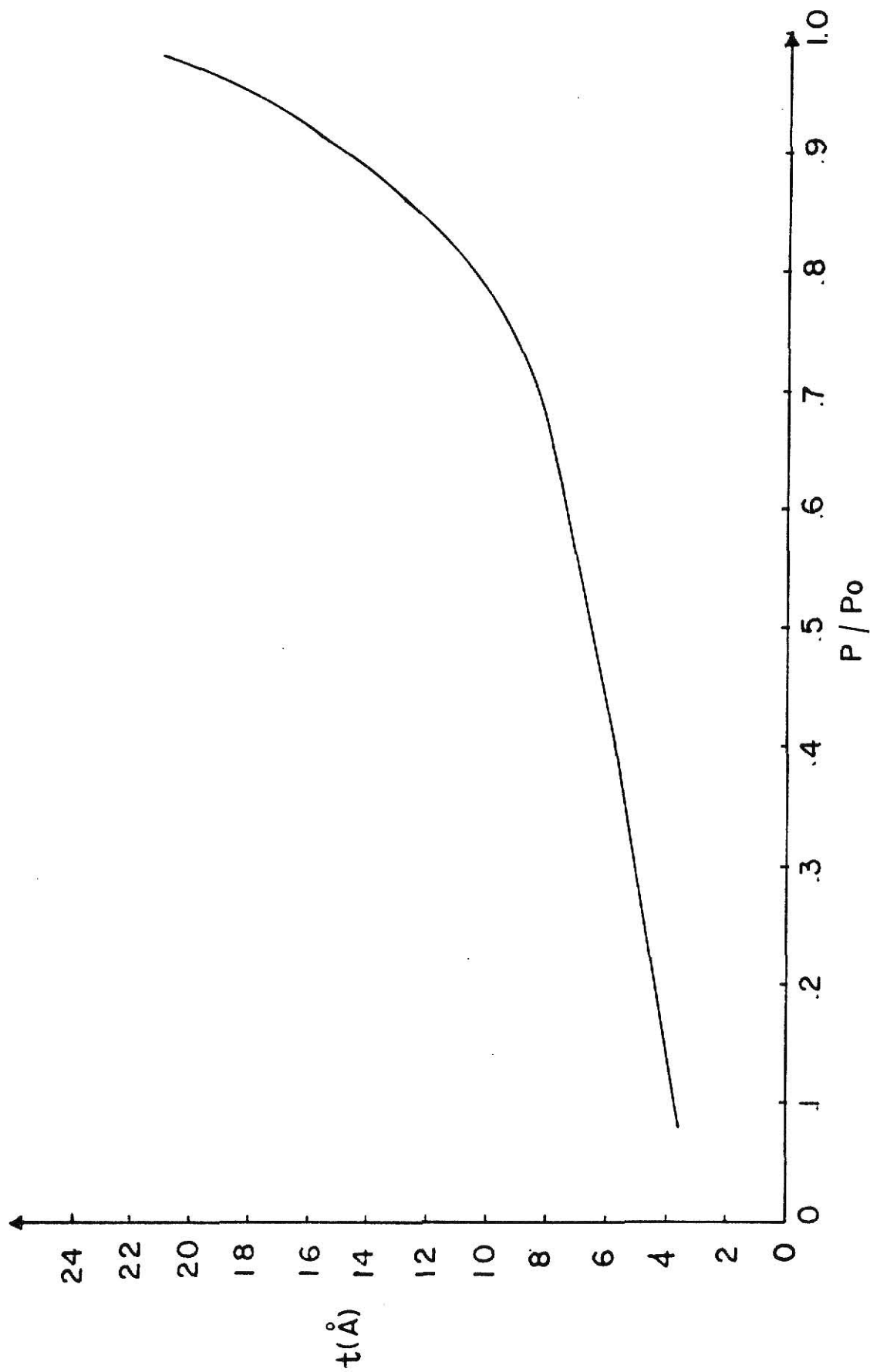Figure 3.27. Thickness of the adsorbed layer as a function of relative pressure.
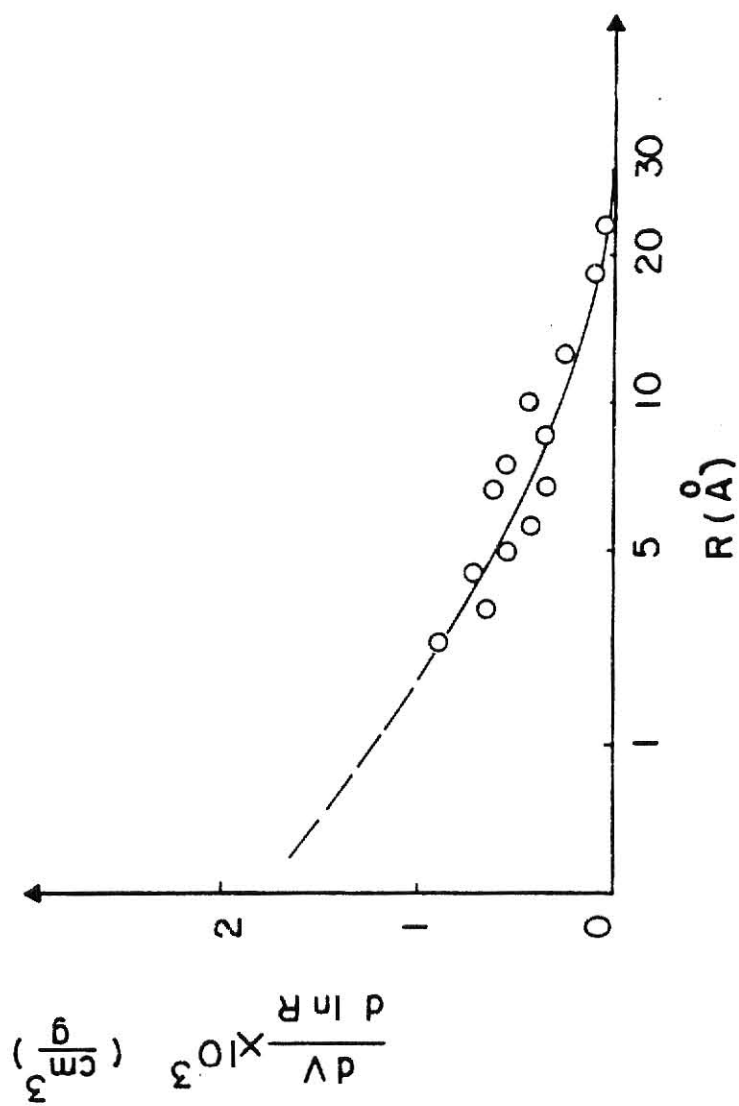
Figure 3.28. Pore size distribution of pseudoboehmite.
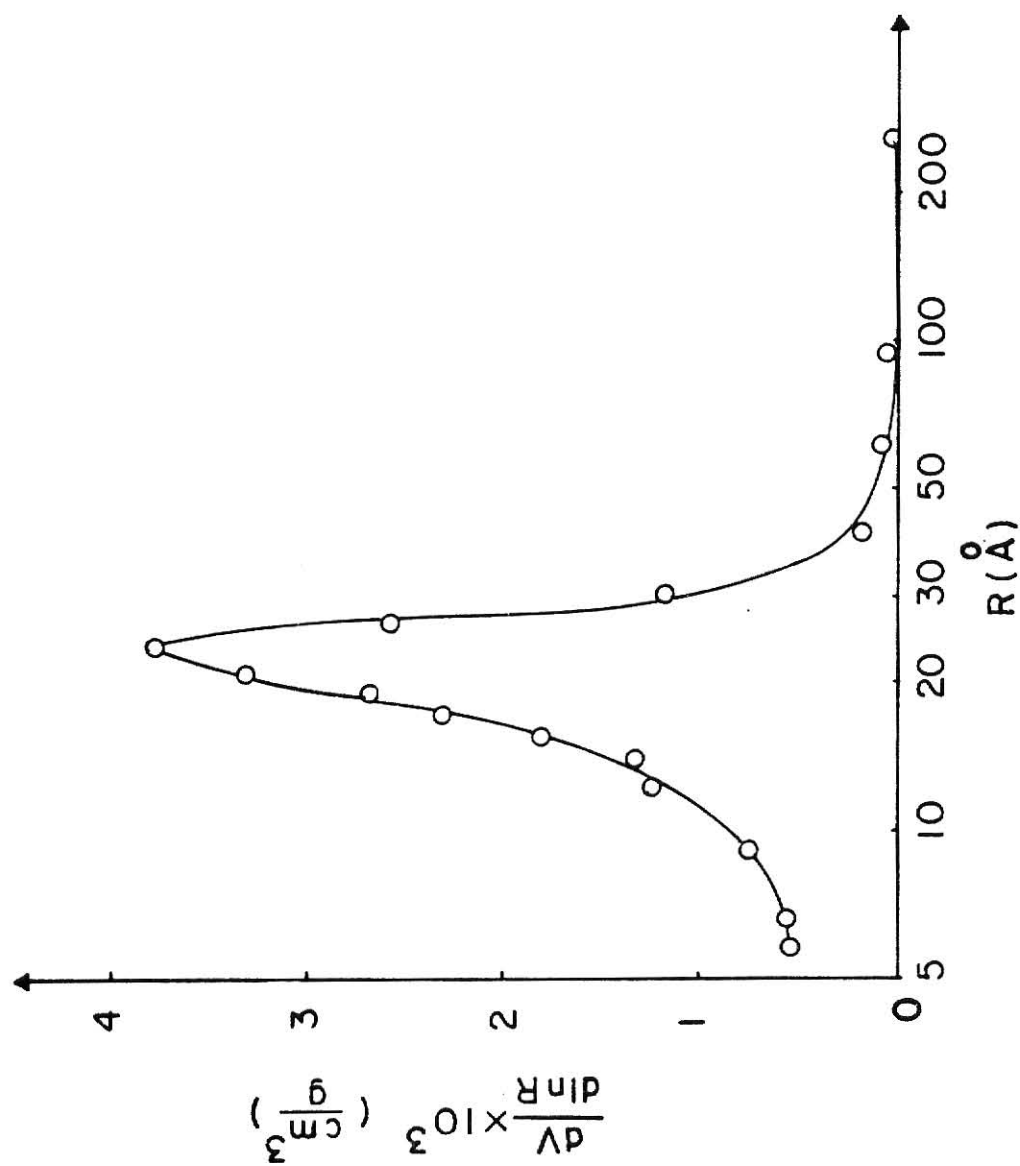
Figure 3.29. Pore size distribution of eta alumina.

Figure 3.30. Pore size distribution of FlAl, a gamma alumina calcinated at 500°C for 24 hr. without pumping.

Figure 3.31. Pore size distribution of F1A2, a gamma alumina calcinated at 500°C for 48 hr without pumping.

Figure 3.32. Pore size distribution of FlBl, a gamma alumina calcinated at 700°C for· 24 hr without pumping.

Figure 3.33. Pore size distribution of F1B2, a gamma alumina calcinated at 700°C for 48 hr without pumping.
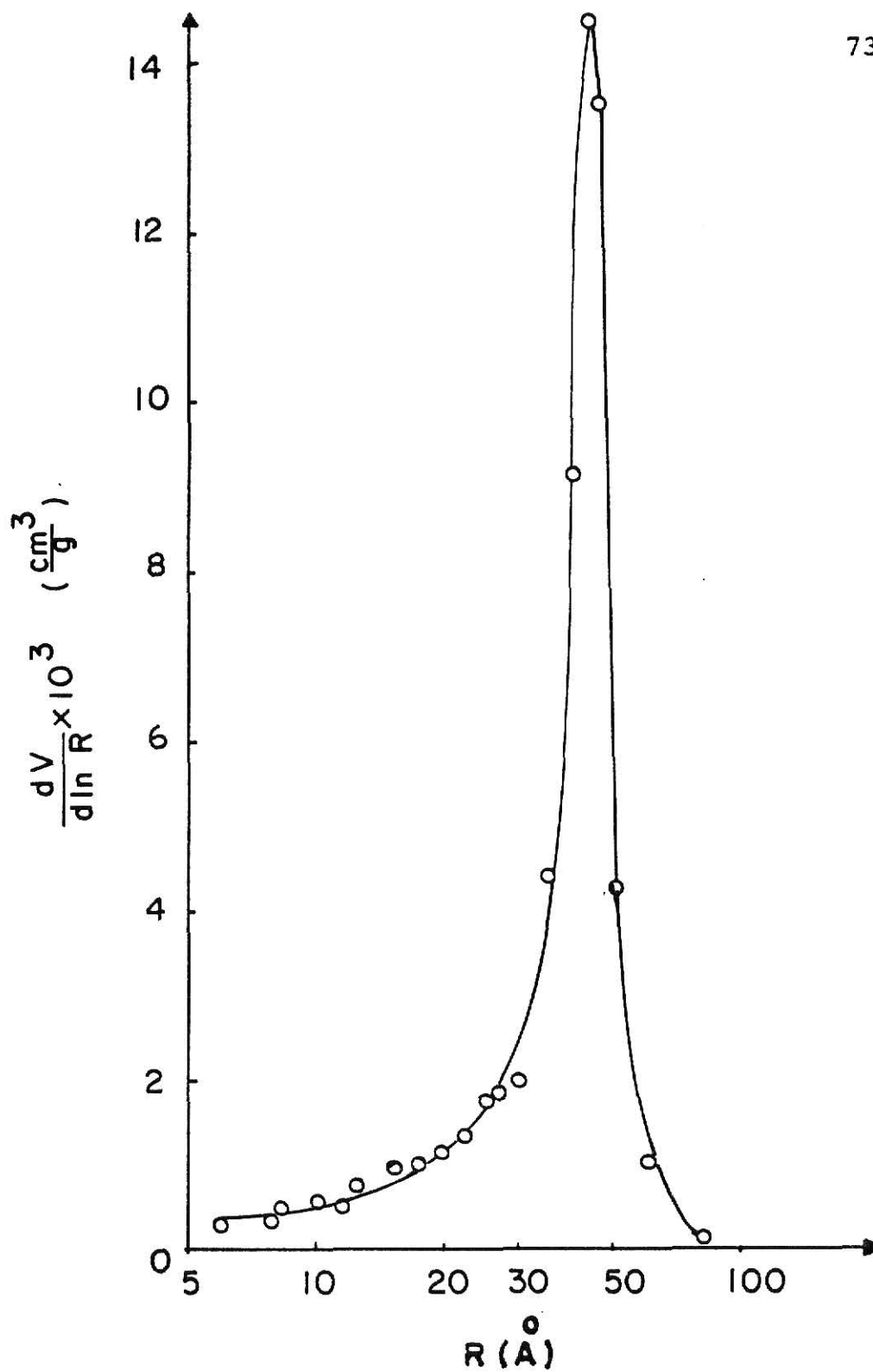
Figure 3.34.   Pore size distribution of FAlAl, a gamma
alumina calcinated at 500°C for 24 hr
with pumping.
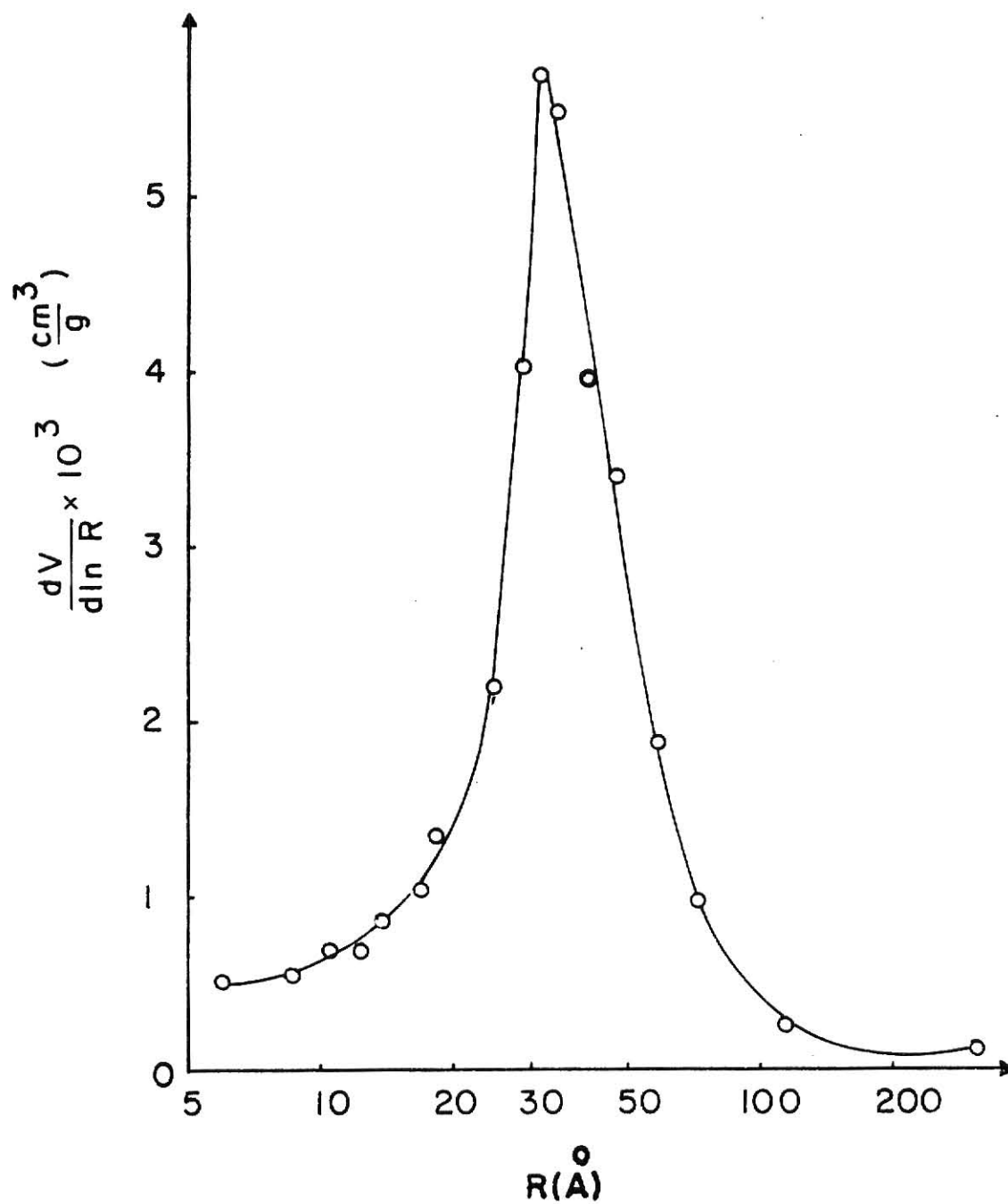
Figure 3.35. Pore size distribution of FA1A2, a gamma alumina calcinated at 500°C for 48 hr with pumping.
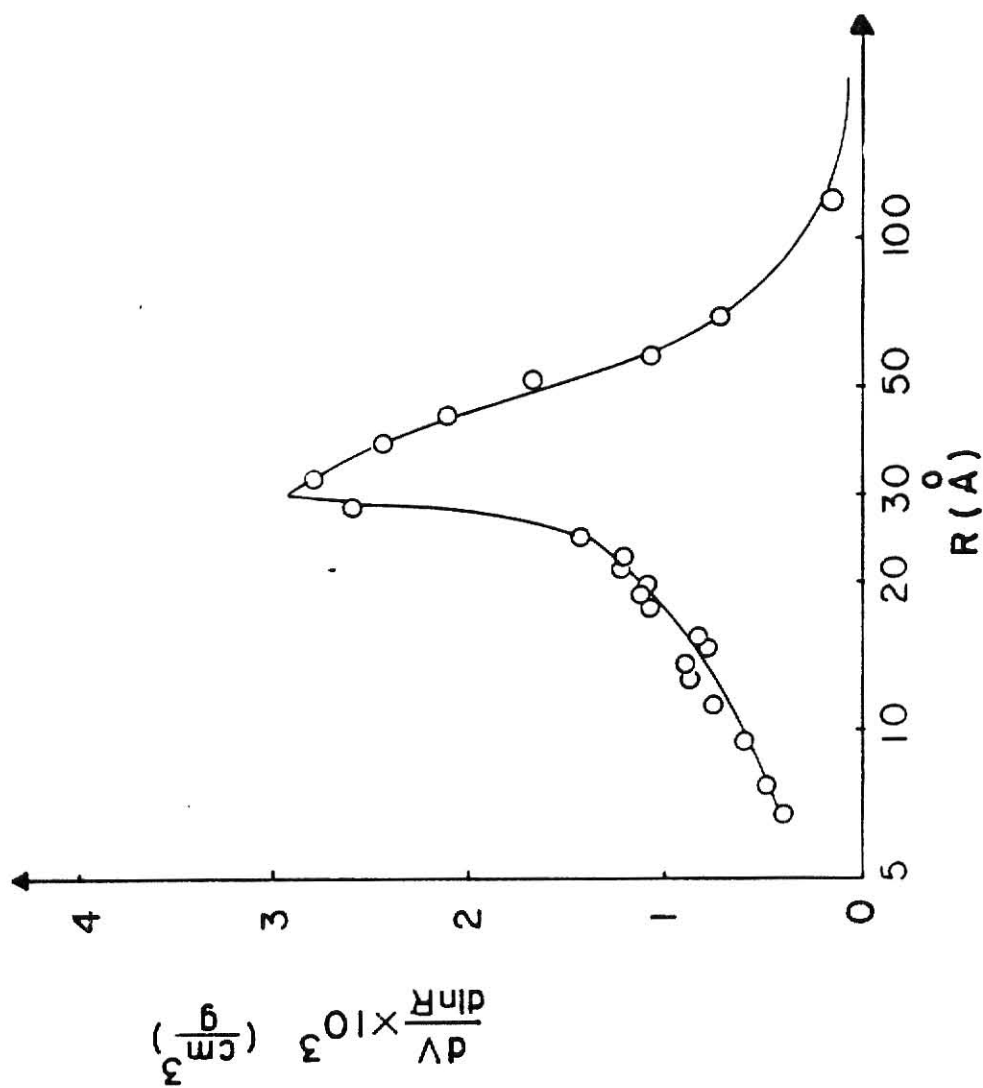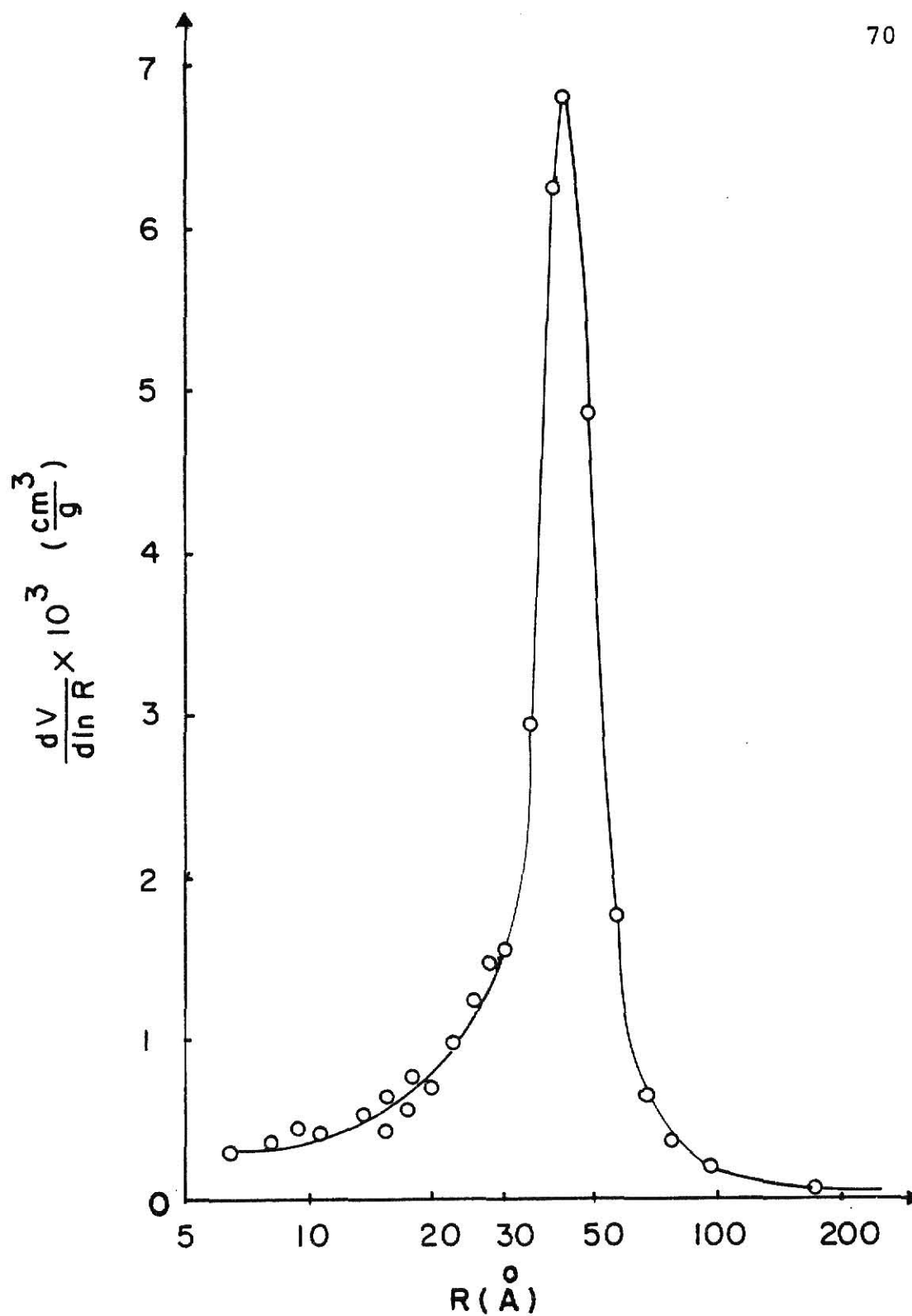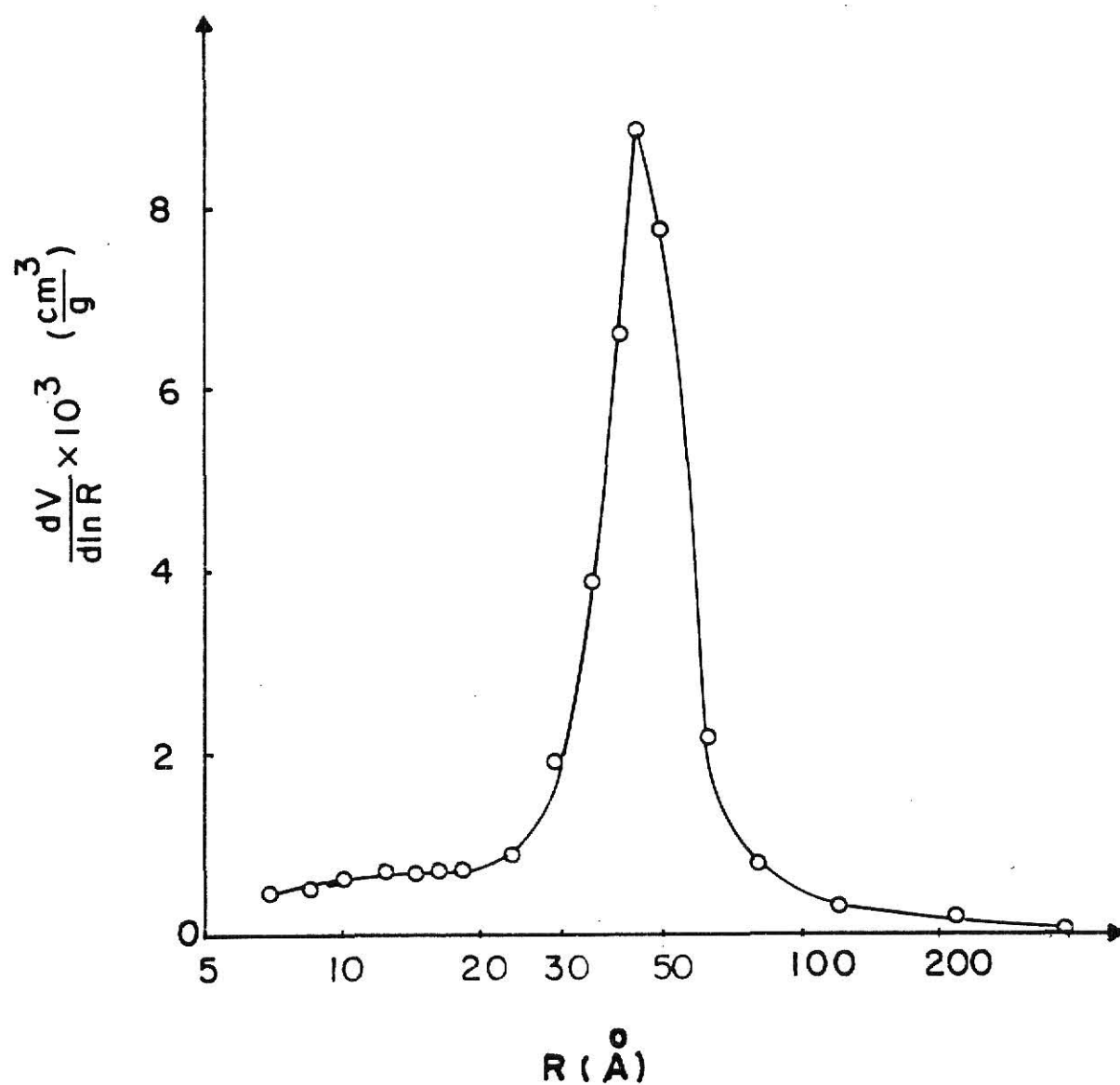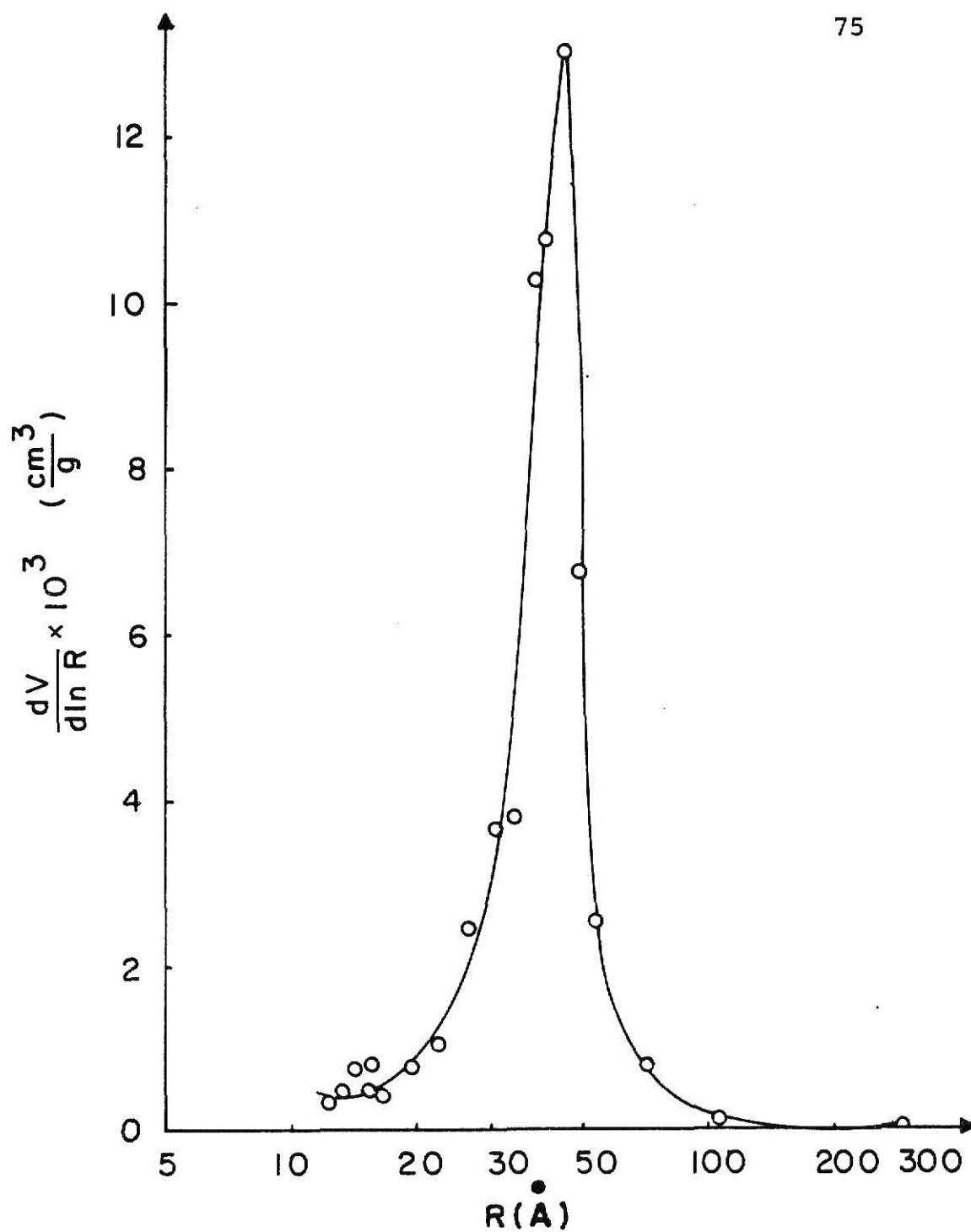
Figure 3.36.   Pore size distribution of FAlBl, a gamma
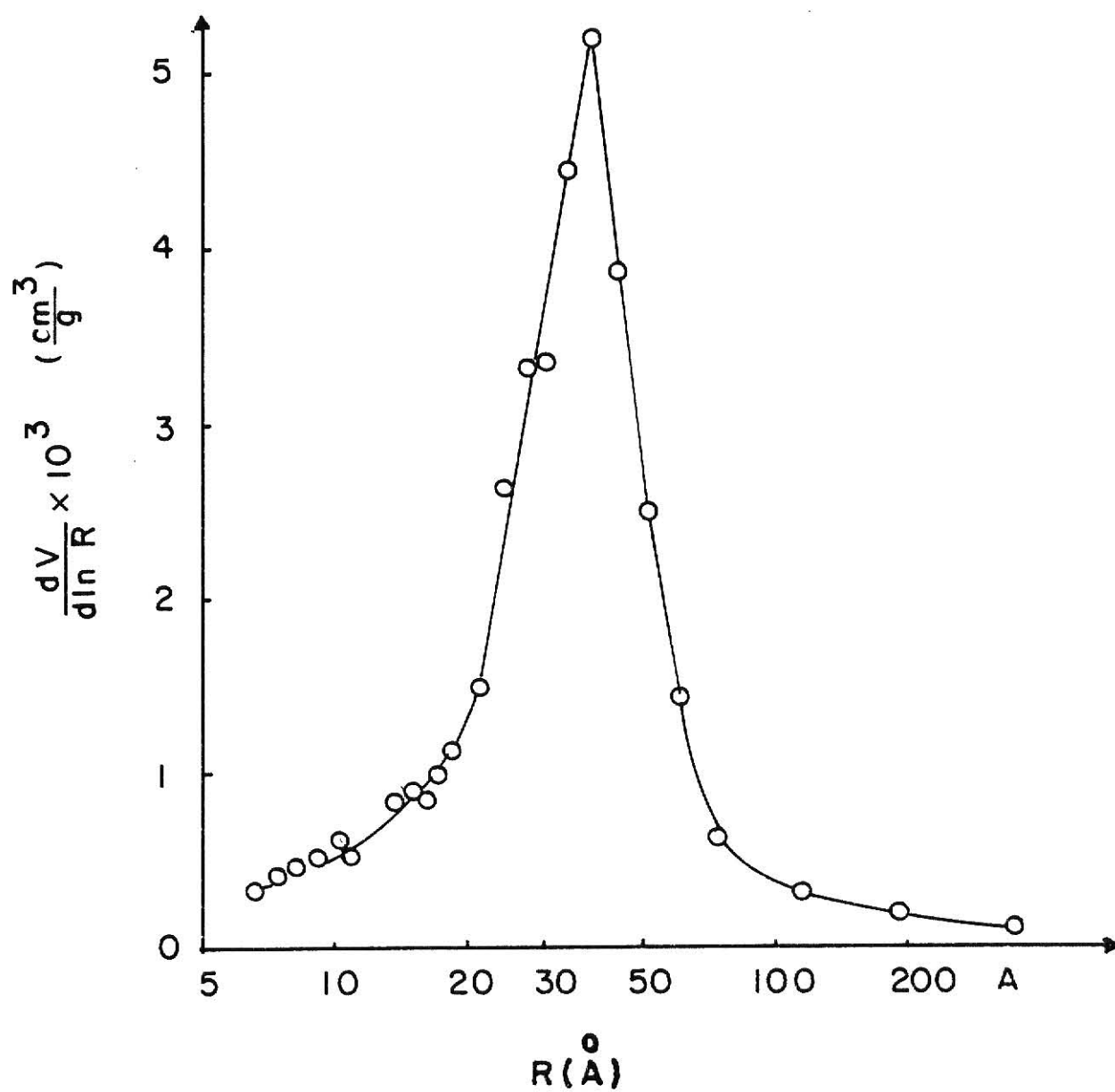alumina calcinated at 700°C for 24 hr
with pumping.
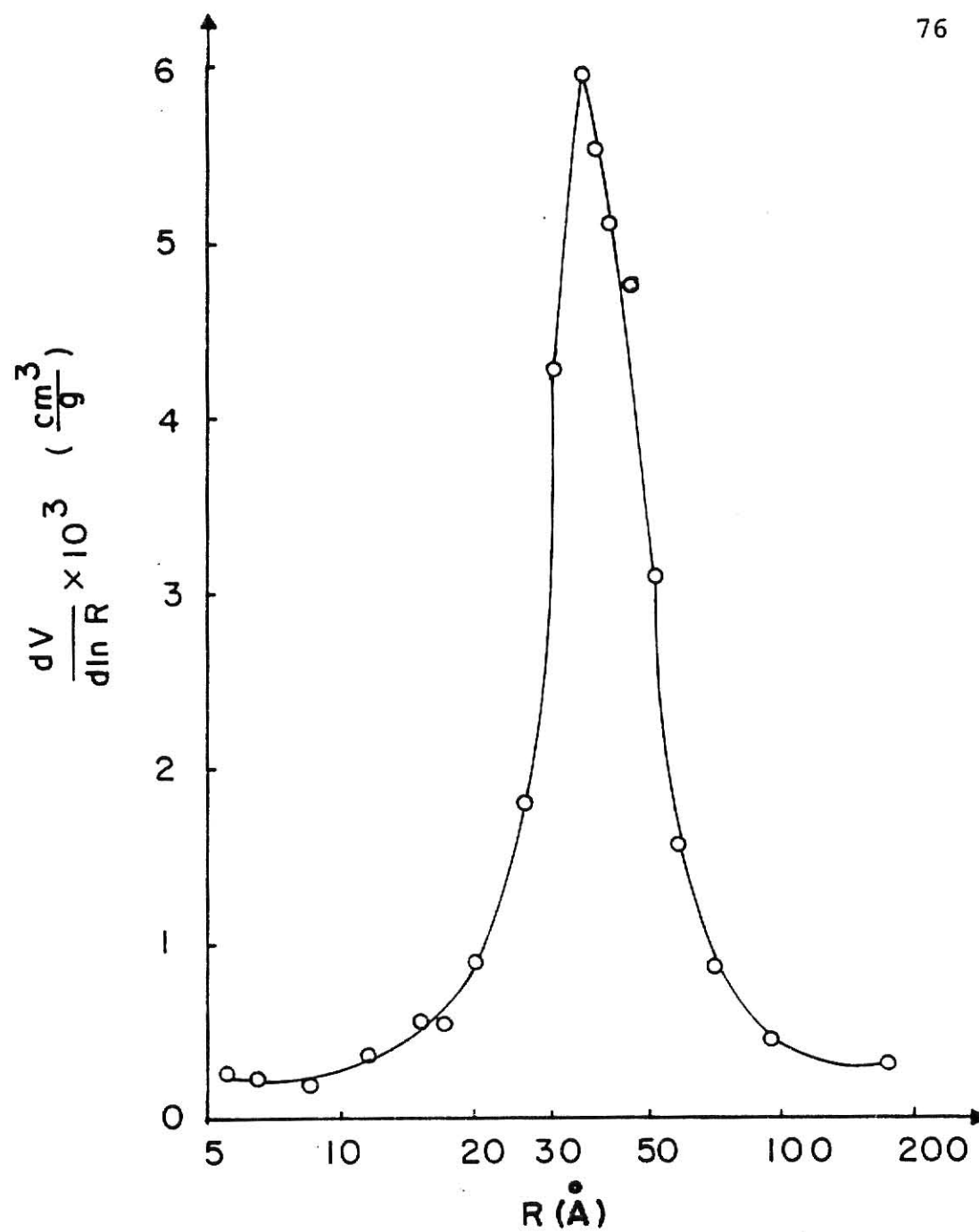
Figure 3.37.   Pore size distribution of FA1B2, a gamma alumina calcinated at 700°C for 48 hours with pumping.
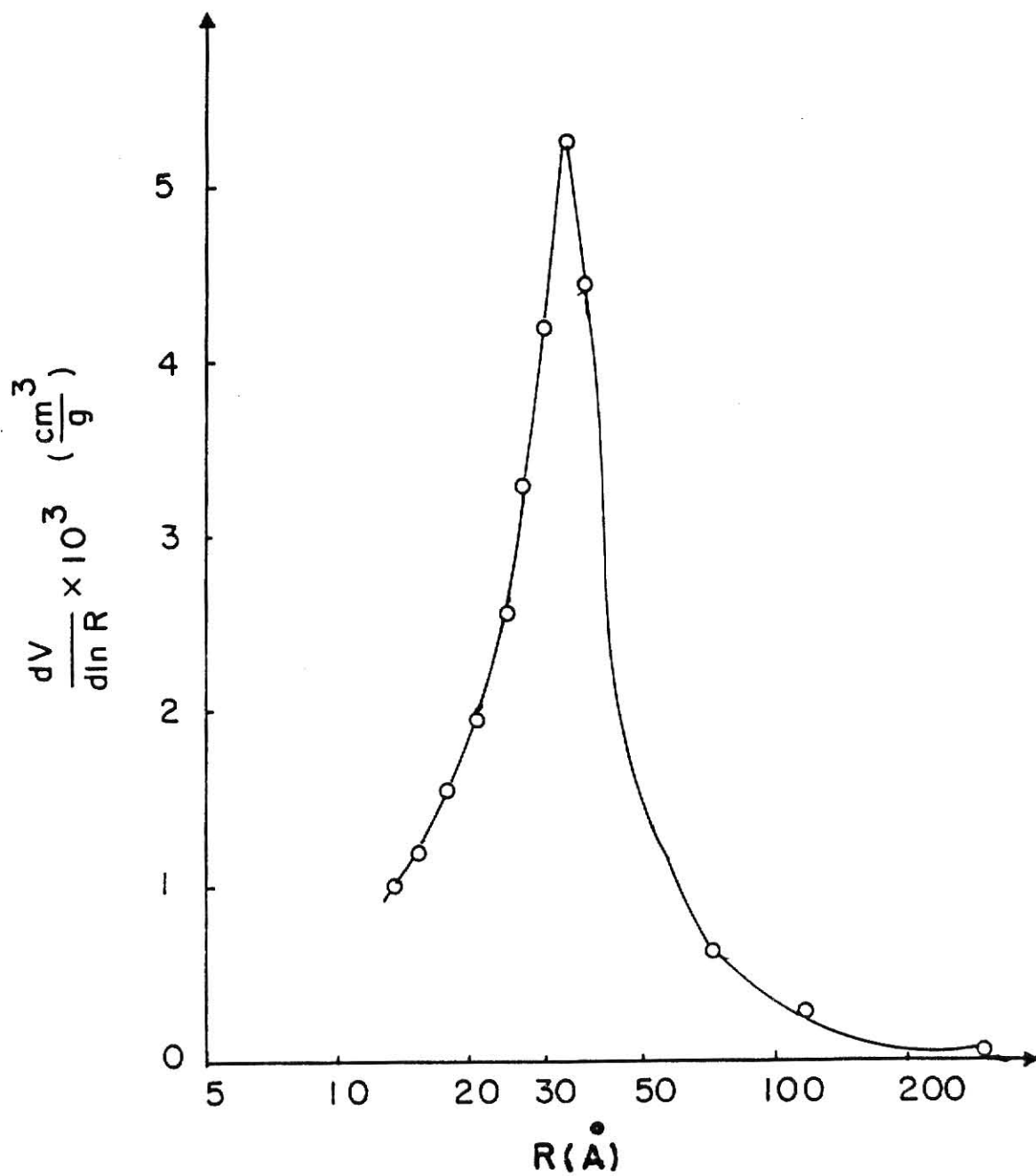
Figure 3.38. Pore size distribution of F2Al, a gamma alumina aged at 80°C for 96 hours before calcinated at 500°C for 24 hours without pumping.

Table 3.3. Pore volume and pore radius of
           different aluminas

Sample	Pumping	Calcination temperature (°C)	Calcination time (hours)	Total Pore Volume (cm^3/g)	Pore Radius (Å)
Pseudo-boehmite				0.147	–
Eta alumina				0.384	24.0
F1A1	no	500	24	0.444	30.0
F1A2	no	500	48	0.656	42.5
F1B1	no	700	24	0.574	37.5
F1B2	no	700	48	0.621	44.5
FA1A1	yes	500	24	0.639	44.0
FA1A2	yes	500	48	0.572	32.0
FA1B1	yes	700	24	0.631	44.0
FA1B2	yes	700	48	0.576	37.5
F2A1*	no	500	24	0.509	33.5

*Sample aged for 96 hours.

"pumping" on gamma alumina. In the course of preparing gamma alumina, pseudoboehmite was produced. In addition, one sample of eta alumina was prepared.

3.5.1 Pseudoboehmite

One of the characteristics of pseudoboehmite is a very small crystallite size. The small crystallites size is the reason for the broad peaks of the X-ray diffraction pattern of pseudoboehmite as shown in Figure 1.4 of Chapter 1. As the material is dehydrated, since most pores are generated at grain boundaries, the small crystallites give rise to small pores and to high surface area (398 m^2/g). As shown in Figure 3.28 the adsorbed volume is low and nearly all of the adsorbed volume should be attributed to pores less than 10 Å.

The finding of the broad peaks of the diffraction pattern of pseudoboehmite are in agreement with the findings of Lippens and Steggarda (8). They have reported surface areas for pseudo-boehmite between 395 and 605 m^2/g.

3.5.2 Eta alumina

The one sample of eta alumina which was prepared had a surface of 369 m^2/g and an average pore size of 24 Å (Figure 3.29). This surface area is high relative to gamma and the pore size is low. Eta alumina results from the dehydration of the trihydrate, $Al_2O_3 \cdot 3H_2O$, bayerite, while gamma alumina results from the dehydration of the monohydrate, $Al_2O_3 \cdot H_2O$, boehmite. Thus, to achieve comparable levels of dehydration three times the number of oxygen atoms will have been driven

from the bayerite compared to the boehmite. It is suspected that this extra oxygen atom removal results in eta alumina having smaller crystallites than gamma alumina and also smaller pores and larger surface area. The small pore size and the sharpness of the pore size distribution curve (indicating most pores are of the same size) are in agreement with the results of MacIver et al. (7).

3.5.3 Gamma alumina

Turning now to the principle results of this work, namely those dealing with gamma alumina. As mentioned previously, gamma alumina is produced by dehydration of pseudoboehmite which has a layered structure. As water is removed, pores are formed primarily between some of the layers. As additional water is driven from the layers, additional pores are formed and the layers become thinner causing the original pores to become larger. This mechanism explains the increasing pore size and surface area as calcination time is increased as shown by runs F1A1 and F1A2 at a calcination temperature of 500°C and runs F1B1 and F1B2 at a calcination temperature of 700°C. Presumably additional data for longer calcination time would show a slowing of the increases and then a relatively stable surface area and pore size which would decrease only very slowly.

It should be recalled that eta and gamma alumina are used at reactor temperatures up to 600°C. Comparing the data at 500 and 700°C, both with and without pumping (runs F1A1 and

F1B1, runs F1A2 and F1B2, runs FA1A1 and FA1B1, and runs FA1A2 and FA1B2) shows that over this range, temperature of calcination is not particularly important. The comparisons were made at 24 and 48 hours and it may be that a temperature effect would have been seen at shorter times with the higher temperature causing the material to "open up" faster. It is also expected that any ultimate loss of surface area would occur sooner at 700°C than at 500°C.

"Pumping" is a variable that has not been previously investigated. The results show that for a calcination time of 24 hours, pumping results in increased pore volume and increased pore size with little change in surface area, but decreased pore volume and decreased pore size (runs FA1A1 and FA1A2, and runs FA1B1 and FA1B2) with increasing calcination time.

Explanation of these results can only be speculative. The idea of pumping is that as the original precipitate is redissolved, the small particles will be dissolved first leaving the large particles as nucleation sites when the pH is again raised. An explanation of the above results can be found by using the idea that "pumping" results in essentially the desired outcome but that the grain boundaries created by nucleation on existing particles are different than the grain boundaries in the original particle or in that part of the new particle which is not in contact with the original particle. The difference could be due, for example, to more occluded water where nucleation occurs on the original particle.

The proposed mechanism is then that in the early stages of dehydration large pores are formed at the grain boundary between the original and the new particles. However, as dehydration continues these pores collapse as the material tends toward its final state. This mechanism explains the decrease in pore volume and pore size with calcination time of the samples which have been "pumped" (runs FA1A1 and FA1A2, and runs FA1B1 and FA1B2).

The mechanism leaves unanswered the question of how pumping results in an increase of surface area over those samples which have not been "pumped". There are many parameters in the "pumping" process, for example, the rate of dissolving the original particles, the time allowed at the low pH and the rate of raising the pH. All of these could have an effect on the particle size distribution. It is easy to visualize a bimodal particle size distribution resulting from the pumping operation. If the parameters chosen in this work have resulted in one set of very small particles (new particles that were formed as the pH was lowered but not on the original particles) and a set of larger particles, the increase in surface area caused by the "pumping" and the apparent decrease in ultimate pore size would result.

3.6 Recommendations for Future Work

Adsorption experiments with a static system are very tedious and time consuming and the number of runs that can be

made is limited. In this work a start has been made on the variation of properties of gamma alumina. Similar studies are needed on eta alumina.

Even the data on gamma alumina is very limited and should be extended. For future experiments, runs with longer calcination time should be made. The calcination times of the non-pumping runs which have been made have not been long enough to show the steady state surface area and pore volume which should exist.

The work on "pumping" must be considered very preliminary and there are many variables that should be examined. Among them are the time allowed at high pH, the rate of lowering the pH, the rate of raising the pH and the aging time after pumping.

One run, F2Al, had an aging time at 80°C of 96 hours before calcination. Except for aging time this run was identical with F1Al. The increased aging time appears to have dramatically increased surface area and to have somewhat increased pore volume and pore size of the calcinated product. The effect of aging time should be further investigated.

ACKNOWLEDGMENTS

REFERENCES

1. Belding, W. A. and Warfield, W. C., "Controlling the
    Properties of Catalyst Substrates using Alumina", Kaiser
    Aluminum and Chemical Corporation, Pleasanton, p 1, 1982.

2. Satterfield, C. N., "Heterogeneous Catalysis in Practice",
    McGraw-Hill, New York, p 87, 1980.

3. Gates, B. C., et al., "Chemistry of Catalytic Processes",
    McGraw-Hill, New York, p 249, 1979.

4. Kotanigawa, T., et al., App. Catal. 1:185 (1981).

5. Stumpf, H. C., et al., I & E. C. 42:1398 (1950).

6. Wefers, K. and Bell, G. M., "Oxides and Hydroxides of
    Aluminum", Alcoa Research Laboratories, Technical paper 19.

7. MacIver, D. S., et al., J. of Catal. 2:485 (1963).

8. Lippins, B. C. and Steggerda, J. J. in "Physical and
    Chemical Aspects of Adsorbents and Catalysts", edited by
    Lisen, B. G., Academic Press, New York, p 171, 1970.

9. Schmäh, H., Z. Naturforscher 1:322 (1946).

10. Oomes, L. E. et al., in "Reactivity of solids" edited by
    J. H. deBoer, Elsevier Publishing, New York, p 317, 1961.

11. van Norstrand, R. E., "X-ray Studies of Activated Aluminas.
    I. Eta and Gamma Aluminas", American Chemical Society,
    Dallas Meeting, April 8-13, p 43, 1956.

12. Sato, T. et al. Thermal Analysis, Int. 6th Conf.,
    Bayreuth, p 181 (1980).

13. Fink, P., Rue Romain de Chinie 14:811 (1969).

14. deBoer, J. H., "Structure and Properties of Porous
    Materials", edited by D. H. Everett and F. S. Stone,
    Butterworths Scientific Publications, London, p 68, 19 .

15. Young, D. M. and Crowell, A. D., "Physical Adsorption of
    Gaseous", Butterworths, London, p 148, 1962.

16. Lippens, B. C., et al., J. of Catal. 3:32 (1964).

APPENDIX A

2^k fractorial design

Many experiments require a study of the effects of two
or more variables. Using the classical statistical approach,
the effect of each variable will be known at only one arbi-
trarily chosen level of other variables. Additional experi-
ments at other levels are needed in order to analyze the effect
of variables. In the classical method, as a rule of thumb,
$N = 16 \, \sigma^2/\Delta^2$ experiments at each level are needed to detect a
real effect of magnitude Δ when the standard deviation of a
single observation is σ. Thus, the total number of experiments
required for a thorough investigation of several variables
could become very large.

The total experimental effort can be greatly reduced through
the use of fractorial design. With this method a large number
of variables can be thoroughly studied for the price of study-
ing just one variable.

The 2^k fractorial design is particularly useful in the
early stage of experimental work, when there are likely to be
many factors to be investigated. A 2^k fractorial design per-
mits all combinations of two versions of each of k variables
be performed with the smallest number of experiments. As there
are only two levels for each factor, the responses are assumed

to be a linear over the rage of the factor level chosen in the case of continuous variables and a step function in the case of qualitative variables. For a continuous variable, the two levels then become the upper and lower value of that variable; while for a qualitative variable, the two levels represent the presence and absence of that variable.

By using 2 fractorial design, only 4, 8, 16, . . experiments are needed to study the effect of 2, 3, 4, . . . variables, respectively. The upper level or the presence of the variable is most commonly denoted by (+); and the lower level or the absence of the variable is denoted by (-). The list of experimental runs making up the design is called the design matrix. The design matrix for a 2^3 fractorial is displayed in Table A.1.

X1	X2	X3
-	-	-
+	-	-
-	+	-
+	+	-
-	-	+
+	-	+
-	+	+
+	+	+

Table A.1. The design matrix for 2^3 fractorial design

On the assumption that the individual observations are uncorrelated and have equal variance, the 2^k fractorial design has 2^k-1 effects:

$$k \quad \text{main effects}$$

$$\frac{k(k-1)}{2} \quad \text{2 factor interaction effects}$$

$$\frac{k(k-1)(k-2)}{3 \times 2} \quad \text{3 factor interaction effects}$$

$$\frac{k(k-1)(k-2)..(k-h-1)}{h!} \quad \text{h factor interaction effects}$$

In this work, three variables in the preparation of gamma alumina were studied. Thus, 2^3 fractorial design was used. Let X1 be the calcinating time, X2 the calcinating temperature and X3 the presence or absence of pumping.

The effect of changing the calcinating time from 24 hours to 48 hours is estimated by

$$\overline{Y}_+ - \overline{Y}_-$$

where $\overline{Y}_+$ is the average response at longer time and $\overline{Y}_-$ is the average response at shorter time over the levels of the other factors. This estimate is called the main effect of calcinating time, i.e., "X1 main effect". Similarly, the estimate effect of changing the calcinating temperature from 500°C to 700°C also can be calculated by using the equation above where $\overline{Y}_+$ and $\overline{Y}_-$ refer respectively to the average response at the high and lower level of calcinating temperature to give "X2 main effect". The "X3 main effect" is due to the absence or presence of pumping.

In addition to providing independent estimates of the main effects, the 2^k fractorial design also provides an independent estimate of the "interaction" effects of two or more variables. The 2^k fractorial arrangement allows one to determine whether the effect of one variable is acting independent of the other variables.

In 2^3, there are 3 main effects: X1, X2 and X3, and 3 two factor interaction effects: X1X2, X1X3 and X2X3, and 1 three factor interaction effect: X1X2X3. X1X2 interaction effect occurs when the response of changing the calcinating time from 24 hours to 48 hours is different at two different levels of calcinating temperature: 500°C and 700°C. Calcinating time and pumping combine to produce the X1X3 interaction effect while calcinating temperature and pumping give the X2X3 interaction effect. Calcinating time, calcinating temperature and pumping might interact together to form a three factor interaction effect.

The coefficient of all 2^3 fractorial design effects are shown in Table 7.

A.1 Specific surface area

The interesting effects are X1, X2, X3, X1X2, X2X3 and X1X2X3 effects. The regression equation is then defined as

Surface area = 276.09 - 1.98(t-36) - 0.747(T-600)

+ 62.6(p-.5) - 2.413(t-36)(p-.5)

+ 0.317(T-600)(p-.5) + 2.285x10^{-3}(t-36)(T-600)(p-.5)

where t = calcination time in hours;

    T = calcination temperature in °C

    p ≡ pumping = 1 for pumping

                  = 0 for non-pumping

A.2 Pore volume

All the effects seem to carry the same weight. The governing equation then contains all the effects.

$$
\begin{aligned}
\text{Pore volume} = {} & .5891 + 1.421 \times 10^{-3}(t-36) + 0.1135 \times 10^{-3}(T-600) \\
& + .0309(p-.5) + 8.016 \times 10^{-6}(t-24)(T-600) \\
& + 3.9677 \times 10^{-3}(t-36)(p-.5) \\
& + .1213 \times 10^{-3}(T-600)(p-.5) \\
& + 9.1925 \times 10^{-6}(t-36)(T-600)(p-.5)
\end{aligned}
$$

A.3 Pore size

X2, X1X3 and X1X2X3 effects are of interest in this case.

$$
\begin{aligned}
\text{Pore radius} = {} & 39.0 + .0188(T-600) - .3958(t-36)(p-.5) \\
& + .5729 \times 10^{-3}(T-600)(t-36)(p-.5)
\end{aligned}
$$

Table A.2. 2^3 effects

	X1	X2	X3	X1X2	X1X3	X2X3	X1X2X3
	−	−	−	+	+	+	−
	+	−	−	−	−	+	+
	−	+	−	−	+	−	+
	+	+	−	+	−	−	−
	−	−	+	+	−	−	+
	+	−	+	−	+	−	−
	−	+	+	−	−	+	−
	+	+	+	+	+	+	+
Surface area	47.51	−14.94	62.60	0.77	57.92	63.55	10.97
Pore volume	.0341	.0227	.0309	.0384	.0952	.0242	.0441
Pore radius	0.25	3.75	−0.75	0	−9.50	−1.00	2.75

PREPARATION AND CHARACTERISTICS OF ALUMINAS

by

KIM-OANH THI NGUYEN

B.S., Kansas State University, 1981

AN ABSTRACT OF A MASTER'S THESIS

submitted in partial fulfillment of the

requirements for the degree

MASTER OF SCIENCE

Department of Chemical Engineering

KANSAS STATE UNIVERSITY
Manhattan, Kansas

1983

ABSTRACT

The objective of this work was to prepare gamma alumina
with different physical properties namely: surface area, pore
volume and pore size distribution. Pseudoboehmite, bayerite,
eta and gamma alumina were identified by X-ray diffraction.
Surface area, pore volume and pore size distribution have been
determined by physical adsorption using a static glass apparatus
with nitrogen as the adsorbent. The methods used to produce
pseudoboehmite, bayerite, eta and gamma alumina are given. Ad-
sorption isotherms, surfaces areas, pore volumes and pore size
distributions of pseudoboehmite, eta alumina and nine samples
of gamma alumina produced by different conditions of "pumping",
calcination times and calcination temperatures are given. The
hysteresises found in the adsorption-desorption studies are
explained. Some explanations on the effect of "pumping", cal-
cination time and calcination temperature on surface area, pore
volume and pore size distribution are given.